Durham University

# Durham E-Theses

## *The theory of auger recombination in quantum well heterostructures*

Smith, Colin

**How to cite:**

Smith, Colin (1985) *The theory of auger recombination in quantum well heterostructures*, Durham theses, Durham University. Available at Durham E-Theses Online: http://etheses.dur.ac.uk/6805/

**Use policy**

The full-text may be used and/or reproduced, and given to third parties in any format or medium, without prior permission or charge, for personal research or study, educational, or not-for-profit purposes provided that:

- a full bibliographic reference is made to the original source
- a link is made to the metadata record in Durham E-Theses
- the full-text is not changed in any way

The full-text must not be sold in any format or medium without the formal permission of the copyright holders.

Please consult the full Durham E-Theses policy for further details.

Academic Support Office, The Palatine Centre, Durham University, Stockton Road, Durham, DH1 3LE
e-mail: e-theses.admin@durham.ac.uk Tel: +44 0191 334 6107
http://etheses.dur.ac.uk

To my wife Angela

and my parents Joan

and Benny

# The Theory of Auger Recombination in Quantum Well Heterostructures

by

Colin Smith

Presented for the Degree of Doctor of Philosophy

at Durham University in 1985

The copyright of this thesis rests with the author.
No quotation from it should be published without
his prior written consent and information derived
from it should be acknowledged.

17 JUL 1985

**ABSTRACT**

This thesis is concerned with calculations of the Auger recombination rate in direct gap semiconductors. It is composed of two parts: in the first and major part, the calculation of the CHCC Auger recombination process in a model of a quantum well heterostructure is considered; and in the second part, the overlap integrals between the cell periodic parts of the conduction band and heavy hole band Bloch functions are calculated using a 15-band full zone empirical K.p method. These overlap integrals are important factors in determining the Auger rate involving the recombination of electrons with heavy holes.

The calculation of the quantum well CHCC Auger recombination rate differs from the bulk CHCC Auger calculations because carriers trapped in quantum wells reside within sub-bands associated with different bound states of the wells. The quantum well CHCC Auger recombination rate is thus calculated by considering all the possible intra and inter-sub-band carrier transitions (Hereafter referred to as bound-bound transitions ). Processes in which the excited electron starts in a bound state of the well but makes a transition to an unbound state are also considered, and it is shown that although these 'bound-unbound' transitions have customarily been ignored, they can make a significant contribution to the Auger rate. Simple physical descriptions are then used to explain the relative importance of the processes, and numerical results are presented for the Auger rate in 1.3 μm and 1.55 μm InGaAsP/InP quantum well systems. In these alloys it is found that the quantum well and bulk Auger rates are very similar for the same carrier concentrations, and similar approximations.

In the second part of this thesis conventional approximations for estimating conduction band - heavy hole band overlap integrals are tested using a 15 band full zone empirical K.p method. It is found that conventional estimates based on effective mass sum rules overestimate the modulus squared of the overlap integrals by at least an order of magnitude. Initial calculations with the wavevectors in the (001) direction, where the discrepancy is much larger, showing that the usual assumptions as to the dominant terms that appear in effective mass rules, are incorrect. Also shown is the underestimation of the overlap integrals by the 4 band K.p method. Finally the significance of the results is discussed.

**ACKNOWLEDGEMENTS**

I would like to thank:

My wife Angela for her patience, understanding, and support.

R A Abram for stimulating my interest in Auger recombination and supporting this with many useful suggestions.

M G Burt for his clear insight into many problems and illuminating expositions.

N J Doran and K J Blow for the kind use of their computing facilities at the British Telecom Research Laboratories, Martlesham Heath.

S Brand for many useful discussions

and the SERC and British Telecom for financial support.

## FORWORD

Chapter one tries to put the calculation of quantum well Auger recombination into perspective. It introduces Auger recombination and then briefly reports the low threshold current and temperature sensitivity of quantum well lasers.

Chapter two examines the various types of Auger recombination which may take place in a quantum well heterostructure and the model which is used to describe Auger recombination in this thesis. It also sets up the basic elements of the formalism.

Chapters three and four give a detailed development of the theory describing the quantum well model.

Chapter five presents the full numerical results for both the bound-bound and bound-unbound processes and discusses their interpretation in terms of simple physical models. The results are then compared with the calculations of other workers for both the bulk and quantum well systems.

Chapter six is independent of the main body of work, the calculations reported there being largely completed during a twelve week spell at the British Telecom Research Laboratories, Martlesham Heath. It is mainly computational in nature, and deals with the overlap integrals between the cell periodic parts of the Bloch wavefunctions, these integrals being of interest in both the bulk and the quantum well calculation of Auger rates.

INDEX PAGE NO

APPENDICES

## CHAPTER 1 - AN INTRODUCTION TO AUGER RECOMBINATION AND SEMICONDUCTOR LASERS

This chapter introduces Auger recombination in a quantum well (QW) heterostructure. First Auger recombination in a bulk semiconductor is discussed qualitatively, and its dependence on carrier concentration, temperature, and band gap is indicated. Lasing in a double heterostructure (DH) laser is then briefly reviewed, and the functional dependences of Auger recombination referred to above are used to explain why this form of recombination has been proposed as a possible reason for the high temperature, temperature sensitivity of the threshold current in long wavelength DH lasers. The various Auger processes suggested to account for the high temperature threshold current behaviour are then listed. Finally the QW laser is examined using the concepts introduced during the discussion of the DH laser, and the reasons for investigating Auger recombination in QW heterostructure are made apparent.

## 1.1 AUGER RECOMBINATION IN BULK SEMICONDUCTORS

Auger recombination is one of a number of non-radiative processes by which a conduction band electron and valence band hole can recombine. In Auger recombination the energy produced during the recombination is given to a third carrier, and the process may be accompanied by the creation or annihilation of a phonon. Auger recombination may proceed directly with an interband transition or indirectly via an intermediate state such as a trap or exciton.

In this thesis we shall be concerned mainly with the direct process, not involving a phonon, in which two conduction band electrons collide, with one being promoted, and the other recombining with a heavy hole (the so called CHCC process (ref 1.1)). This process is illustrated in figure 1.1 along with other direct processes such as the so called CHSH process.

The dependences of these direct processes on a) carrier concentration and b) temperature and band gap are discussed next.

For definiteness the direct CHCC process, not involving a phonon, is initially considered. After applying momentum and energy conservation to the collision and assuming non-degenerate carrier concentrations thermalised within bands, the rate of the illustrated 'forward' process

FIGURE 1.1

This figure shows schematically a selection of the direct band to band Auger processes not involving phonons. It also introduces the state notation 1, 1´, 2 and 2´ which will be used later.

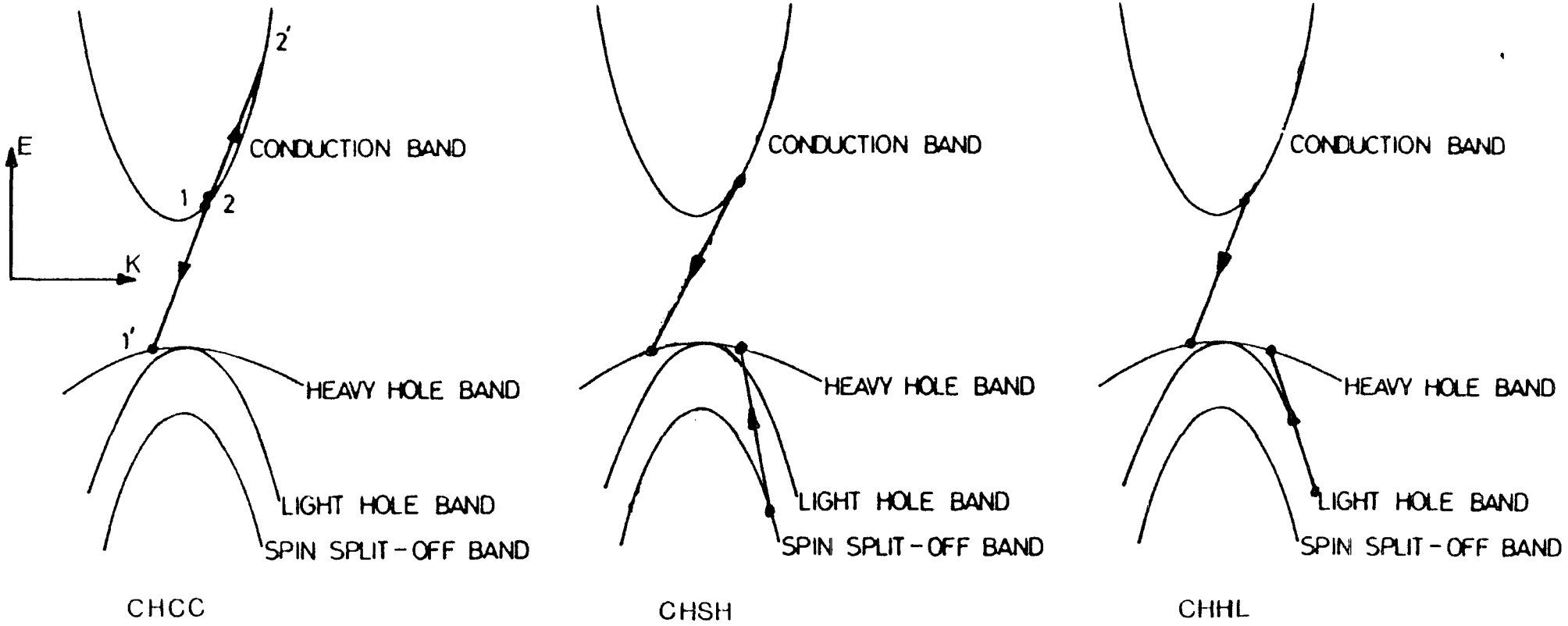

(Auger recombination) is found to depend upon the square of the conduction band electron concentration n multiplied by the heavy hole concentration p. This is physically reasonable since two electrons collide and a hole must be present for recombination to occur. From the rate for the forward process must be subtracted the rate of the reverse process (impact ionization) to give the net rate at which electrons are removed from the conduction band. But since under high excitation conditions, such as those found in a laser, the forward process greatly dominates the reverse process, the net rate of recombination will depend on $n^2p$ provided it is assumed that non-degenerate statistics are still valid, and any screening effects of the extra electrons are neglected. Similarly for alternative Auger processes, such as the CHSH process (see figure 1.1), where the energy of the recombination is given to a valence band electron, the rate at which electrons are removed from the conduction band depends on $np^2$.

Comparing these carrier concentration dependences with that of radiative recombination under non-degenerate conditions (ie np) it is seen that the relative importance of Auger recombination increases with carrier concentrations. The Auger recombination rate itself increasing as the cube of the carrier concentration in excited, undoped materials with equal concentrations of electrons and holes.

The major part of the band gap and temperature dependences of the CHCC Auger recombination rate R may be understood by considering the probability of the dominant forward process occurring. This is proportional to the probability of the initial states containing electrons, multiplied by the probability of the final states being unoccupied by electrons. Assuming again non-degenerate statistics and carrier thermalisation

$$R \propto e^{-(E_1 - \mu_c)/x_B T} \; e^{-(E_2 - \mu_c)/x_B T} \; e^{(E_{1'} - \mu_v)/x_B T_c} \qquad 1.1$$

where the energy subscripts correspond to the state notation introduced in figure 1.1, the zero of energy is taken as the bottom of the conduction band, $T_c$ is the carrier temperature, $x_B$ is Boltzmann constant, $\mu_c$ and $\mu_v$ are the conduction and valence quasi-fermi levels respectively, and the probability of the promoted or Auger state being empty is taken as one since it is usually a considerable energy from the band edge. Now maximising the above subject to energy and momentum conservation, and assuming parabolic bands gives

$$E_1 = E_2 = -\mu(E_1' + E_g) \qquad 1.2$$

where $E_g$ is the band gap and $\mu$ is the ratio of the conduction band effective mass to the valence band effective mass. It follows

$$R \propto n^2 p \exp\left(-\frac{\mu}{1+\mu}\,\frac{E_g}{x_B T}\right) \qquad 1.3$$

More generally, other processes such as the CHSH processes give

$$R \alpha \exp \left( - \alpha \frac{\Delta E}{x_B T_c} \right) \qquad 1.4$$

where $\Delta E$ is the separation between the band extremities of the bands in which the initial states for the forward process reside, minus the separation between the band extremities of the bands in which the final states of the forward process reside, and $\alpha$ is a function of the effective masses of the carriers involved. For a more detailed treatment of these matters the reader is referred to, for example, reference 1.2.

FIGURE 1.2

a) A simplified stylised diagram of the DH laser in the form of a Fabry-Perot Cavity

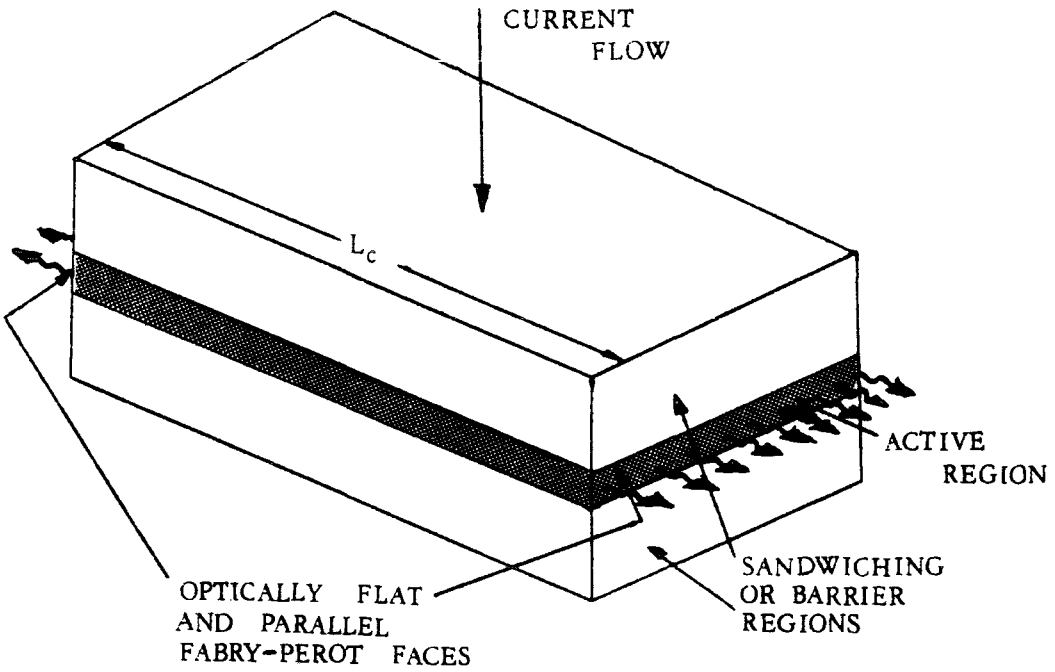


b) The conduction ($E_c$) and valence ($E_v$) edges for a stylised graded DH laser under forward bias.

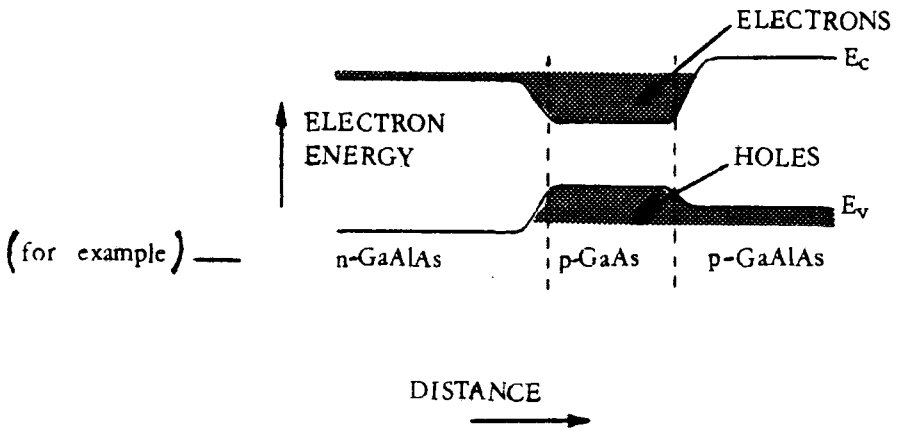

## 1.2 THE SEMICONDUCTOR DOUBLE HETEROSTRUCTURE LASER

### 1.2.1 LASING IN A DH LASER

In this section lasing in a DH laser is briefly reviewed, the opportunity being taken to define those quantities which will be used later in discussing QW lasers. For a fuller discussion the reference is made to 1.3 and 1.4.

A diagram of the physical structure of a DH laser is shown in figure 1.2. For lasing to occur, the increase in the number of photons in the system due to the predominance of stimulated emission over fundamental adsorption must be greater than or equal to the photon losses from the system. The factors controlling the photon population are now discussed, and it is shown how the threshold condition (defined as the condition where lasing just occurs) is brought about in a DH laser.

The tendency of the number of photons in the system to increase may be expressed as the product of two quantities, the optical gain and the optical confinement factor. The optical gain g (an expression for which is given later in section 1.3.1), is defined, for a given frequency, as the incremental increase in photon flux per unit flux. It depends on both the density of states for the bands in which the involved carriers reside, and the amount of population inversion. The dependence on population inversion entering the expression for the gain through a statistical factor which weights the transitions.

The optical confinement factor $\Gamma$ is defined as the ratio of the number of photons in the active region of the laser (ie the region in which lasing takes place) divided by the total number of photons in both the active and surrounding cladding regions. It depends upon the device geometry.

The losses within the active region of the system are due to 1) incomplete confinement, 2) incomplete reflection at the Fabry-Perot faces, and 3) optical dissipation losses. The optical dissipation losses can be further categorised into a) free carrier absorption, which depends upon the number of free carriers present, b) scattering losses which are due to irregularities in the boundaries between different layers of the laser, and c) intervalence band absorption which depends upon valence band structure, the density of states for the valence bands and their probability of occupancy. Later for reference purposes, items 2) and 3) will jointly be referred to as cavity losses.

Requiring that a light wave makes a complete transversal of the Fabry-Perot cavity (see figure 1.2) without attentuation (ie that the photon losses are exactly balanced by the increase due to the predominance of stimulated emission over fundamental absorption) gives the standard threshold equation

$$R_1 R_2 \, e^{(g\Gamma - \Gamma\alpha_A - (1-\Gamma)\alpha_c)L_c} = 1 \qquad 1.5$$

where $\alpha_A$ represents the losses of the active region, $\alpha_c$ represents the losses in the sandwiching region, Lc is the length of the Fabry-Perot cavity, and $R_1$ and $R_2$ are the reflectances of the Fabry-Perot faces. To achieve the threshold for lasing, the amount of population inversion within the system is increased until the optical gain is sufficient to compensate for the photon losses. The current required to do this is called the threshold current, and it must supply sufficient carriers to achieve the threshold condition, in the presence of spontaneous recombination, leakage currents, and non-radiative recombination such as Auger recombination.

### 1.2.2 THE TEMPERATURE SENSITIVITY OF THE THRESHOLD CURRENT IN LONG WAVELENGTH DH LASERS

In the long wavelength lasers now being considered for optical telecommunication, it has been experimentally observed that the temperature sensitivity of the threshold current J may empirically be described by

$$J = J_o \exp\left(\frac{T_\ell}{T_o}\right) \qquad 1.6$$

where $T_\ell$ is the lattice temperature and $T_o$ is an empirically determined constant whose value decreases abruptly above some $T_\ell$, giving a rapidly increased temperature sensitivity. Intervalence band absorption, leakage currents, and Auger recombination have all been suggested to explain this increase in the temperature sensitivity of the threshold current.

Adams et al (ref 1.5) were the first to suggest that intervalance band absorption may be responsible for the high temperature threshold current behavior of 1.6μm DH lasers. However, Henry et al (ref 1.6) have disputed this with both theoretical and experimental evidence.

Several attempts have been made to implicate Auger recombination in the temperature sensitivity of long wavelength lasers. These have arisen because long wavelength lasers may have a sufficiently small band gap for Auger recombination to be significant at relevant temperature and threshold carrier concentrations. Some theoretical attempts to explain the threshold temperature dependence of InGaAsP/InP DH lasers in terms of Auger recombination, are due to a) Dutta and Nelson (ref 1.7), who consider the direct CHCC process to be most significant, b) Sugimura (ref 1.8), who considers the direct CHSH processes to be most significant, and c) Haug (ref 1.9) who considers the phonon assisted CHCC process to be most significant. The large uncertainties in the calculation of the Auger recombination rate (see Chapters 2 and 6) allowing these several possible mechanisms to be suggested but limiting definite conclusions.

## 1.3 QUANTUM WELL LASERS

The refinement of MBE and MOCVD growth techniques has led to the development of a laser structure in which the thickness of the active region (as shown in Fig 1.2) is of the order of 100Å. The band edges of the heterostructure have the appearance shown in Fig 1.3(a) and it seen that the active region produces potential wells for both electrons and holes which can confine the carriers. With well widths of the order of 100Å the energy associated with the carriers motion perpendicular to the layer is quantized (there are discrete bound states of the one dimensional well) but free-particle motion remains in the two dimensions of the plane of the layer. The result is a set of sub-bands, each one corresponding to a different quantised state. The density of states contributed by each sub-band is that appropriate to two dimensional free particle motion ie a constant for all energies within the sub-band. The total density of states from all the sub-bands in a well therefore has the step like form shown in Fig 1.3(b). Because of the confining effect of the active layer and the quantization of the states, the structure is called a quantum well. In the context of semiconductor lasers it is found that the quantum well density of states (see Fig 1.3(b)) leads to a gain coefficient which is superior to that for a simple three dimensional (bulk) laser structure (such as DH).

FIGURE 1.3

This illustrates

a) the formation of sub-bands, the band bending caused by excess carriers being neglected.

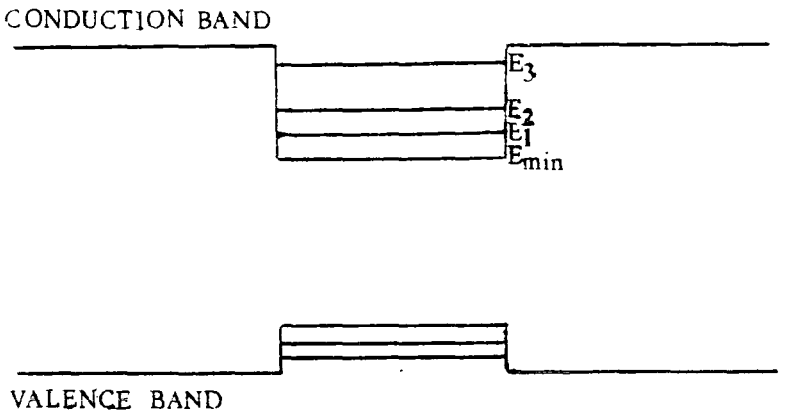


b) the density of states for unit energy

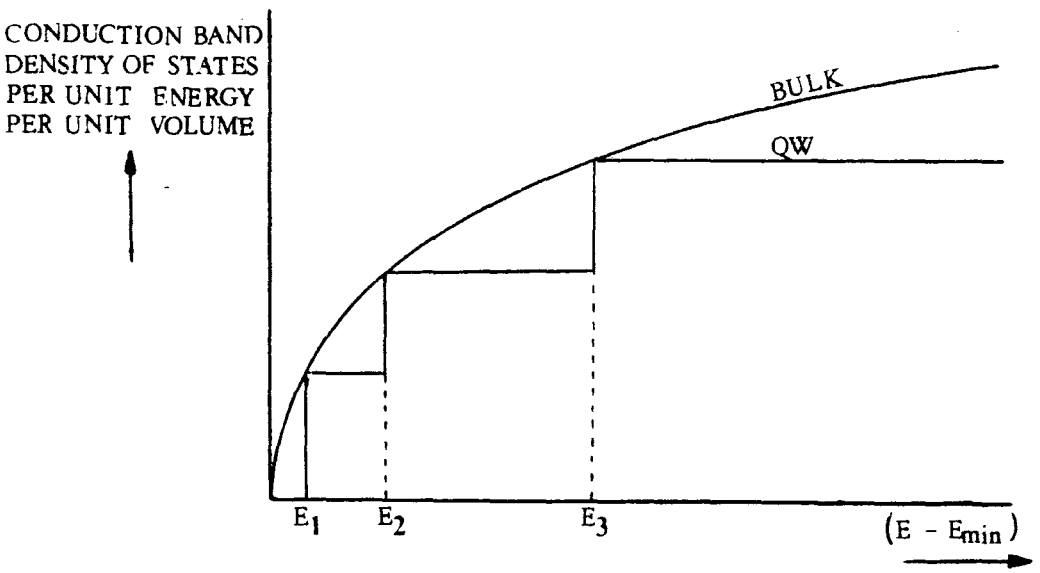

### 1.3.1 THE GAIN COEFFICIENT

The gain coefficient due to the ground electron and hole sub-bands of a perfect, undoped QW laser is

$$g(w) = \frac{1}{\bar{n}_A} \frac{1}{c\ \varepsilon_o w} \left(\frac{e}{m_o}\right)^2 \left(\frac{m_r}{\hbar^2 L}\right)(f\ (E_v) - f\ (E_v))|M_{op}|^2 \qquad 1.7$$

where L is the width of a quantum well, $\hbar w$ is the energy of the involved photon, $\bar{n}_A$ is the active region refractive index, c is the velocity of light, $\varepsilon_o$ is the permittivity constant of free space, $m_o$ is the stationary mass of an electron, $m_r$ is the reduced mass, (f (Ec)-f (Ev)) is a statistical factor, f being probability of a state being occupied by an electron, and $M_{op}$ is the optical matrix element.

This may be compared with the gain coefficient of a DH laser constructed of the same materials.

$$g(w) = \frac{1}{\bar{n}_A} \frac{1}{c\ \varepsilon_o w} \left(\frac{e}{m_o}\right)^2 \frac{1}{2\pi} \left(\frac{2m_r}{\hbar^2}\right)^{3/2} (\hbar w - Eg)^{\frac{1}{2}}\ (f\ (E_c) - f\ (E_v))|M_{op}|^2 \qquad 1.8$$

Here the $(\hbar\ w - Eg)^{\frac{1}{2}}$ mirrors the density of states of the three dimensional system. The two dimensional system with the constant density of states does not contain this factor.

The optical gain coefficient - carrier concentration relationships are found from the above by expressing the statistical factors (f (Ec) - f (Ev)) in terms of carrier concentrations. This may be done either using tables of

the Fermi-Dirac integrals such as those in Blakemore (ref 1.10) or an appropriate analytical expression such as that due to Joyce and Dixon (ref 1.11). (The Joyce-Dixon approximation being an expansion of a quasi-fermi level as a rapidly decreasing series in the ratio of the carrier concentration to the degenerate carrier concentration. An expansion which does not fail when the quasi-fermi level is close to a band extremity.) Using the Joyce-Dixon approximation, Dutta (ref 1.12) has calculated the maximum gain coefficient against carrier concentration in a 200Å well by assuming all carriers remain in the ground electron and hole sub-bands. These results are reproduced in figure 1.4, and for this particular example the same peak gain coefficient as a DH laser can be produced with a lower carrier concentration in the equivalent QW laser.

As the well width varies, the carrier concentration - gain coefficient relationship in a QW laser changes. This is due to a) the variation of the density of states with well width, and b) the dependence of the distribution of carriers between sub-bands on well width. Taking these into account and assuming perfect carrier thermalisation between the sub-bands, Sugimura (ref 1.13) has calculated the variation of maximum gain coefficient with well width for various carrier concentrations in a 1.07 μm InGaAsP/InP QW system. Figure 1.5 reproduces these results,

FIGURE 1.4

This figures shows the relationship between the maximum gain coefficient and first sub-band carrier concentration in a 1.3 μm InP/InGaAsP 200Å wide single QW laser at carrier temperatures of 300K and 400K

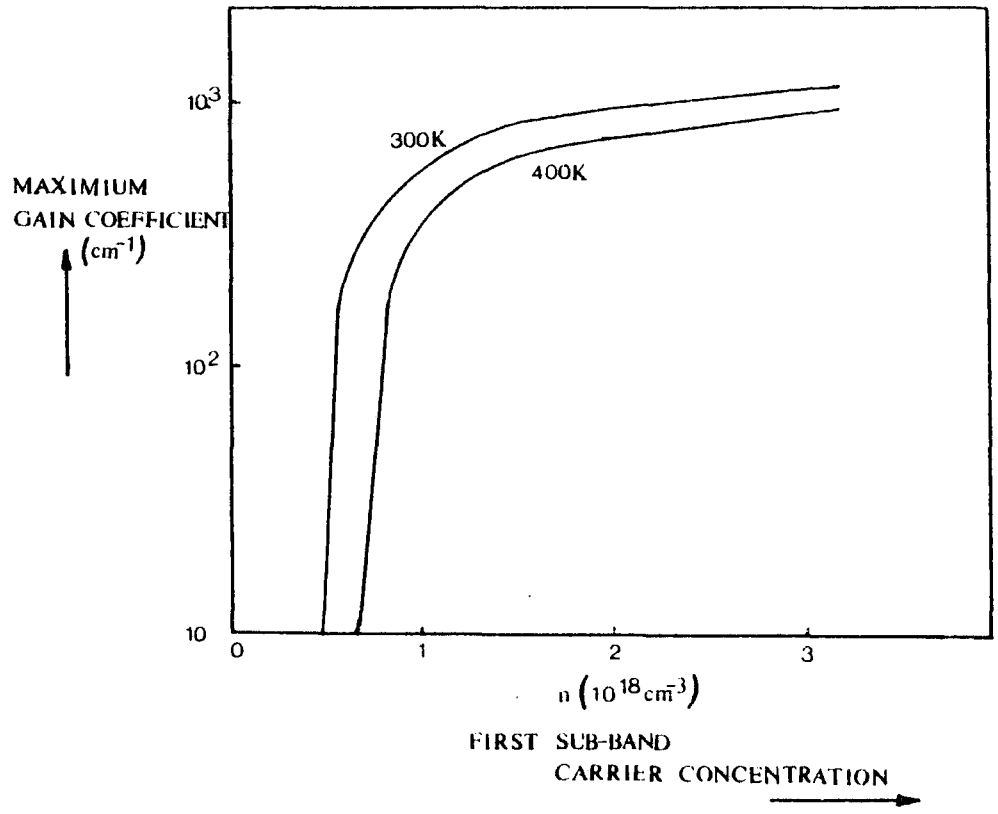

FIGURE 1.5

This figure, which is due to Sugimura (ref 1.13), illustrates the variation in the maximum gain coefficient - carrier concentration relationship with well width. It does this for a 1.07 μm InGaAsP/InP QW system

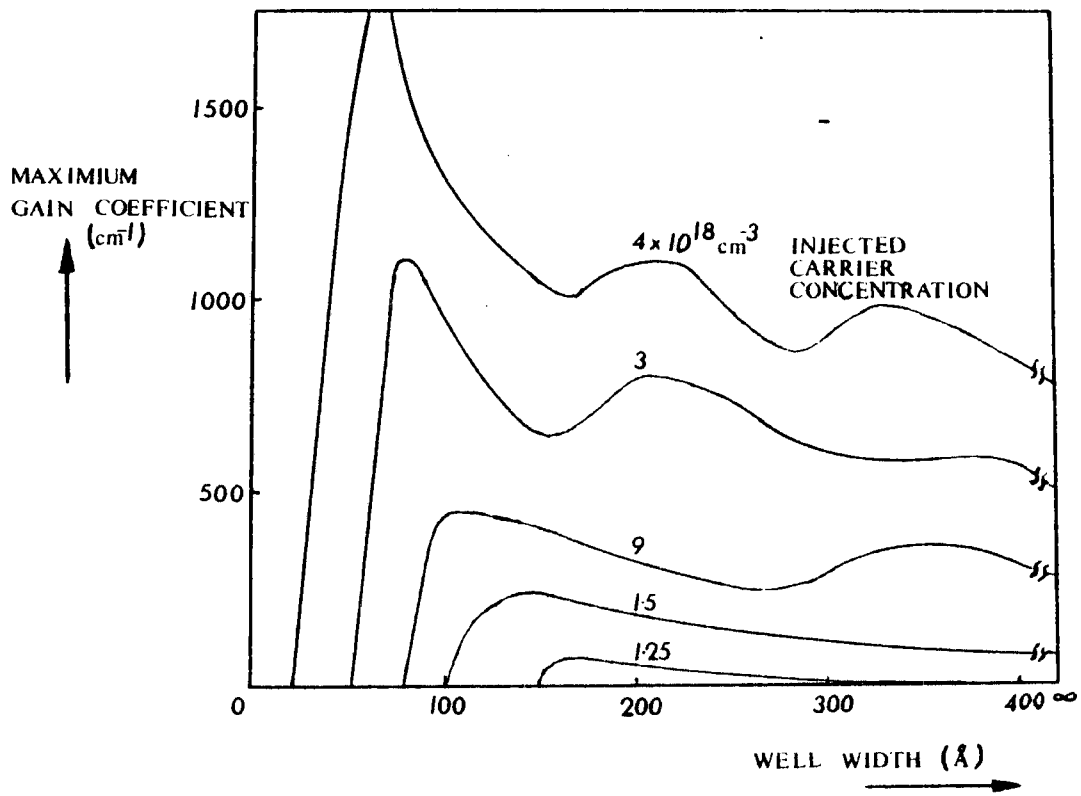

from which it may be observed that a) the gain coefficient - carrier concentration relationship has a different form for each well width, and b) the density of states in a QW laser is always such as to require less population inversion than in a DH laser to produce the same maximum gain.

### 1.3.2 THE OPTICAL CONFINEMENT FACTOR

The dependence of the optical confinement factor on well geometry and device structure is now examined. The optical confinement factor of an isolated single QW may be found using a similar treatment to that used for a DH laser. (See for example ref 1.4).

The problem is simplified to some extent because it is found for typical well dimensions that only the fundamental TE mode exists (For example for 1.3 μm InGaAsP/InP laser only the fundamental mode is present below an active region width of approximately 0.59 μm, and for a 0.9 μm GaAs/GaAlAs laser below approximately 0.38 μm). Further, the small width of the active region allows the optical confinement factor, $\Gamma$, to be approximated by

$$\Gamma = \left(\bar{n}_2^{\,2} - \bar{n}_1^{\,2}\right) \frac{Lw}{2c} \qquad 1.9$$

where $\bar{n}_2$ and $\bar{n}_1$ are respectively the refractive indices of the active and surrounding regions. The validity of this

approximation depends on the refractive indices involved. For the 1.3 μm InGaAsP/InP system Sugimura (ref 1.14) estimates that it is adequate below an active region width of about 0.2 μm, and for the 0.9 μm GaAs/GaAlAs system ref 1.4 may be used to estimate that it is adequate below about 0.1 μm. Using expression 1.9 it is seen that the small width of the QW active region causes the optical confinement of a single well QW laser to be very much smaller than that for a comparable DH laser. This acts to negate the advantage of high gain in a QW. However the optical confinement can be improved considerably by placing several wells together to form a multi-quantum well system (MQW).

Strifer et al (ref 1.15) has shown that for the GaAs/GaAlAs MQW system, a reasonable approximation to the optical confinement factor is given by considering the multi-well system as a three region waveguide with identical cladding layers and a central region whose thickness t, and average refractive index $\bar{n}_{average}$ are given by

$$t = N_A t_A + N_B t_B, \quad \bar{n}_{average} = \frac{N_A t_A \bar{n}_A - N_B t_B \bar{n}_B}{t} \qquad 1.10$$

where $N_A$ is the number of active layers of thickness $t_A$ and refractive index $\bar{n}_A$, and $N_B$ is the number of barrier layers of thickness $t_B$ and refractive index $\bar{n}_B$. Then

reducing the optical confinement factor found using these quantities by the ratio of the combined total width of the central active region to the central passive region. Sugimura (refs 1.13 and 1.14) has used this approximation for the InGaAsP/InP system.

### 1.3.3 THE THRESHOLD CONDITION

The higher gain for a given carrier concentration, but inferior optical confinement in a QW have consequence for the threshold condition. It turns out that it is possible to produce QW lasers with lower threshold current than achieved with DH lasers. Indeed Tsang (ref 1.16) has experimentally reported a threshold current density of 250A per $cm^2$, which compares with typical DH threshold current densities of around 1000A per $cm^2$. But because of the smaller active region volume, this may involve a higher threshold carrier concentration.

As indicated in the previous two sections a quantitative prediction of the threshold current is a complex business even if some simple assumption about the cavity losses is made. The validity of such calculations (see for example ref 1.12 and 1.13) must be further questioned because of the large uncertainties in the calculation of Auger recombination rate.

The best that can be reasonably done is to compare the QW and the bulk Auger recombination rates under similar approximations, for similar carrier concentrations, and make a few semi-quantitative rather than precise statements about the likely importance of Auger recombination. To make a few observations on Auger recombination it is worth anticipating the result from Chapter 5 that the QW and the bulk CHCC Auger recombination rates for the same carrier concentration are similar, except in thin wells. Let us also assume that the CHCC Auger recombination process is important and that other loss mechanisms, such as leakage currents, can be kept under control. Then it is already clear that the importance of Auger recombination will vary with well width because of the variations in the gain - carrier concentration relationship, optical confinement factor, and cavity losses. Also the Auger recombination rate will be higher in a QW if the threshold carrier concentration is higher. Finally Auger recombination will be much more important in single isolated well lasers than multi-well lasers, because of the lower optical confinement factor of isolated single wells.

### 1.3.4 THE TEMPERATURE DEPENDENCE OF THE THRESHOLD CURRENT

As in DH lasers it has been observed experimentally that the temperature dependence of the threshold current 'J' may be expressed by

$$J = J_o \exp\left(\frac{T_\ell}{T_o}\right)$$

A major advantage of QW lasers over DH lasers is lower temperature sensitivity (ie higher $T_o$) for the threshold current. To illustrate this the 0.85 μm GaAs/GaAlAs QW system is now first considered. In this system Auger recombination is unlikely to be important because of the system's large band gap. It has been suggested by Hess (ref 1.17) that the low temperature dependence in a QW can be explained by the smaller temperature dependence of the quasi-fermi level in a QW and/or the high carrier temperature. However because of the uncertainties in the estimation of carrier temperature due to the phonon distribution function and scattering rates not being well known, he was unable to decide between the explanations. The quasi-fermi level argument is essentially that the quasi-fermi level depends inversely upon the degenerate carrier concentration and since this goes as T for a QW structure and $T^{3/2}$ for a bulk material, the threshold carrier concentrations (and hence threshold current) in QW laser must change less rapidly with temperature to maintain the same quasi-fermi level separation.

For the 1.16 μm InP/InGaAlAs multi-well laser Rezek (ref 1.18) finds that the temperature sensitivity increases at high temperatures ie $T_o \simeq 150$ for $T_\ell < 300K$ and $T_o \simeq 60$ for $T_\ell > 300K$. In this case Auger recombination may be responsible for this behavior because the process is more probable in narrower band gap semiconductors. It is thus of interest to study Auger recombination in a QW system to try to understand the temperature dependence of the threshold current.

**REFERENCES FOR CHAPTER 1**


1.1 Takeshima M 1972 J. Appl. Phys 453 4114.

1.2 Haug 1972 Theoretical Solid State Physics, Volume 2.

1.3 Sze S M 1981 Physics of Semiconductor Devices.

1.4 Casey H C and Panish M B 1978 Heterostructure Lasers.

1.5 Adams A R, Asada M, Suemetsu Y, and Arai S 1980 Jpn. J. Appl. Phys 19 L621.

1.6 Henry C H, Logan R A, Merritt F R, and Luongo J P 1983 J. Quantum Electron. QE-19 947.

1.7 Dutta N K and Nelson R J 1982 J. Appl. Phys 53 74.

1.8 Sugimura A 1981 IEEE J. Quantum Electron QE-17 627.

1.9 Haug A 1983 Appl. Phy Lett 43(6) 512.

1.10 Blakemore 1962 Semiconductor Statistics.

1.11 Joyce W B, and Dixon R W 1977 Appl. Phys. Lett. 31 354.

1.12 Dutta N K 1983 J. Appl. Phys. 53 1236.

1.13 Sugimura A 1983 J. Quantum Electron. QE-19 932.

1.14 Sugimura A 1982 Appl. Phys. Lett. 42(1) 17.

1.15 Streifer W, Scifres D R, and Burnham R D 1979 Appl. Opt. 18 3547.

1.16 Tsang W T 1981 Appl. Phys. Lett 42(1) 17.

1.17 Hess K, Vojak B A, Holonyak N, Chin R, and Dapkus P D 1980 Solid-state Electronics Vol 23 page 585.

1.18 Rezek E A, Holonyak N, Fuller B K 1980 J. Appl. Phys. 51 2402.

# CHAPTER 2 - THE MODEL USED AND THE EARLY COMMON STEPS IN THE QW AUGER RECOMBINATION RATE EVALUATION

This chapter examines the major approximations and assumptions of the direct band to band non-phonon assisted CHCC calculations presented in Chapters 3 and 4.

## 2.1 THE SQUARE WELL MODEL OF A QW HETEROSTRUCTURE

Ideally the results of a large scale bandstructure calculation should be used to find the carrier wavefunctions, energy levels, and E-K (energy-wavevector) relationships which are used to calculate the Auger recombination rate. However such calculations are not well developed and in any case the results could not easily be incorporated in a quantitative theory of Auger recombination. Therefore a simple square well model is used which is treated in the effective mass approximation. This has the additional advantage of allowing physical insight into the important features of the Auger recombination calculation.

### 2.1.1 THE CALCULATION OF ENERGY LEVELS

The QW system is made up of an active layer sandwiched between two barrier layers of wider band gap semiconductor. It is assumed that the heterostructure presents simple square well potentials to the electrons and holes as shown in figure 2.1. These potentials being taken to be quite independent of the carrier wavefunction.

FIGURE 2.1

This illustrates the square well potential model which is used. It also defines two energies $E_{con}$ and $E_{vcon}$ which will be used in later analyses.

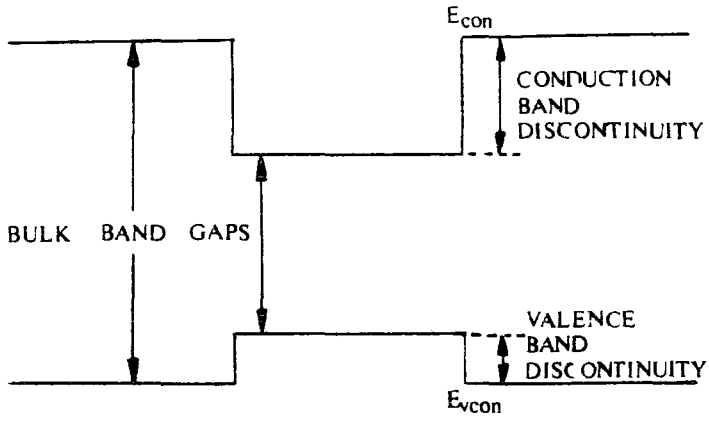

Effective mass theory is assumed to be valid and effective masses are used which are appropriate to the active layer. Also wavefunctions are taken as the multiple of a cell periodic oscillating part and an envelope function part.

In this way the problem of motion perpendicular to the layer reduces to the simple quantum mechanics problem of a particle in a finite potential well. An example of the treatment of which can be found in Schiff 'Quantum Mechanics' (ref 2.1). Here we simply present the results.

Figures 2.2 and 2.3 show the discrete states in the 1.3 μm and 1.55 μm InGaAsP/InP systems as a function of well width. Note, as the well width changes the gap between the lowest allowed conduction band energy and highest allowed heavy hole band energy is kept constant (to keep the laser wavelength the same) by varying the active layer alloy composition. Also for these calculations the conduction band discontinuity is always taken as twice the valence band discontinuity.

For each bound state of the square well a sub-band occurs by the inclusion of the kinetic energy due to motion in the plane of the well. For example a carrier in the lowest square well state of the conduction band has a total energy E where

$$E = E_1 + \frac{\hbar^2 K_{\parallel}^2}{2m_c^*} \qquad 2.1$$

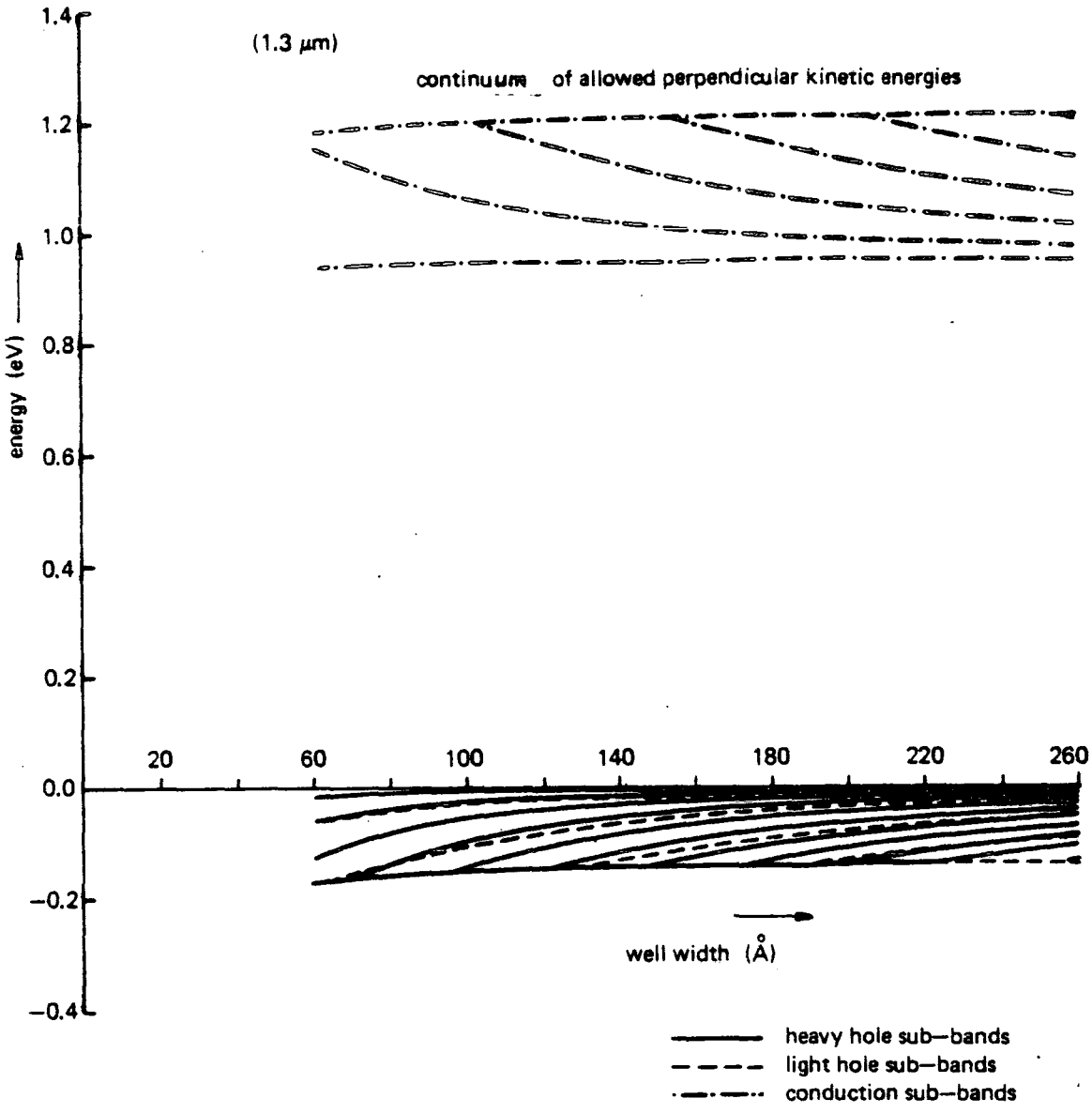


FIGURE 2.2

This figure shows how the allowed perpendicular kinetic energy levels in a InGaAsP/InP QW heterostructure vary with well width when the band gap between the first conduction and the first heavy hole sub-bands is kept constant at 0.96 eV (~ 1.3 μm). To do this the active layer composition is varied, and the ratio of the conduction and valence band discontinuities is kept constant at 2:1 ——— shows the heavy hole sub-bands, – – – – shows the light hole sub-bands, and —·—·—· shows the conduction sub-bands.

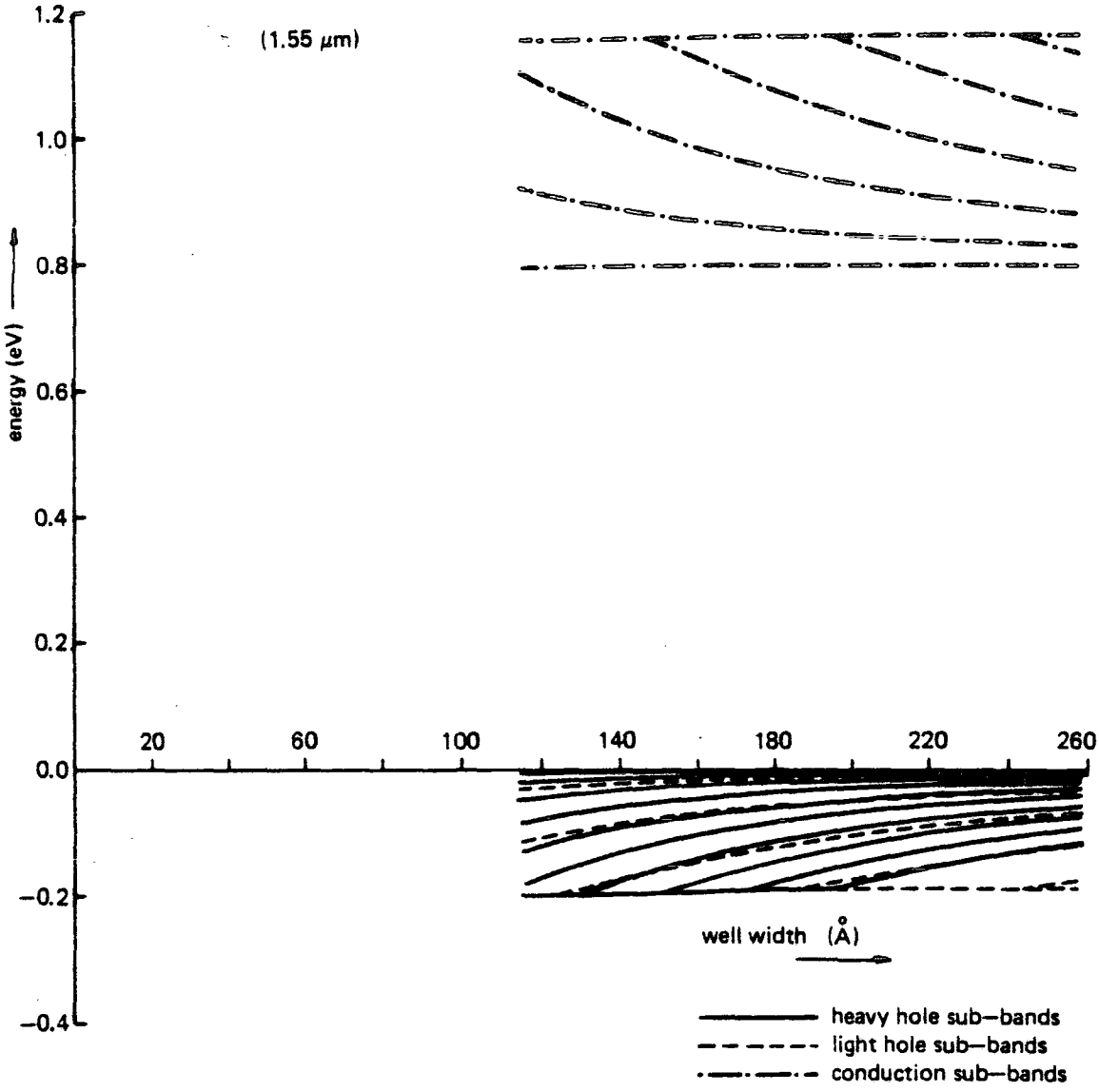


FIGURE 2.3

As figure 2.2 but maintain a band gap between the first conduction and first heavy hole sub-bands of 0.8 eV (~ 1.5 μm). It is observed that below 114Å a band gap of 0.8 eV cannot be maintained.

$E_1$ being the lowest square well state energy and the second term being the kinetic energy due to motion in the plane of the well in which $K_{\parallel}$ is the in-plane wavevector and $m_c^*$ is the conduction band effective mass which is taken to be isotropic.

For the unbound states of the square well there are a continuum of allowed energies, each state of the continuum also leading to a sub-band when the motion in the plane of the layer is included.

### 2.1.2 THE DENSITY OF STATES

Having considered the nature of the states of the quantum well, the resultant density of states per unit energy is now derived. Isotropic parabolic bands being assumed throughout this derivation.

Each sub-band corresponds to a state of the one dimensional well and motion in the two dimensions of the well layer. Hence each sub-band contributes a density of states per unit energy for a free particle in two dimensions. Including a factor of 2 for spin, this is given by

$$ds(E)_{2D} = \frac{2}{(2\pi)^2} \int_0^{\infty} \delta\left(E - \frac{\hbar^2 K_{\parallel}^2}{2m^*}\right) 2\pi K_{\parallel} dK_{\parallel} \qquad 2.2$$

where E is the energy, and m* is the sub-band effective mass.

Since $ds(E)_{2D}$ is a constant, the density of states per unit volume due to all bound states $ds(E_{DISCRETE})_{3D}$ is found from this by multiplying $ds(E)_{2D}$ by n, the number of bound states contributing a sub-band at energy E, and dividing by L, the width of the well

$$ds(E_{DISCRETE})_{3D} = \frac{nm^*}{\pi\hbar^2 L} \qquad 2.3$$

Also each unbound state of the one dimensional well contributes a sub-band. The unbound states forming a continuum with the (one dimensional) density of states per unit length of the system (well+barriers) per unit energy at energy $E_{c2'}$ given by

$$ds(E_{c2'}) = \frac{1}{\pi}\left(\frac{2m^*}{\hbar^2}\right)^{\frac{1}{2}} \frac{1}{(E_{c2'} - E_{c2'min})^{\frac{1}{2}}} \qquad 2.4$$

where $E_{c2'min}$ is the energy of the top of the well (barrier layer conduction band).

Hence the density of states per unit energy per unit volume due to all unbound states is given by integrating over all unbound states contributing a sub-band at energy E

$$ds(E)_{3D} = \frac{m^*}{2\pi\hbar^2}\,\frac{2}{2\pi}\left(\frac{2m^*}{\hbar^2}\right)^{\frac{1}{2}} \int_{E_{c2'min}}^{E} \frac{1}{(E_{c2'} - E_{c2'min})^{\frac{1}{2}}}\, dE_{c2'} \qquad 2.5$$

$$ds(E)_{3D} = \frac{1}{2\pi^2}\left(\frac{2m^*}{\hbar^2}\right)^{3/2} (E - E_{c2'min})^{\frac{1}{2}} \qquad 2.6$$

### 2.1.3 THE CHANGES A BETTER BANDSTRUCTURE WOULD MAKE TO THE CALCULATED AUGER RATE

In the absence of better QW bandstructure the Auger rate calculations which follow, can only give a semi-quantitative indication of the CHCC Auger rate. However it is possible to get some impression of the effects of better bandstructure on the Auger rates.

Changing the energies of the bound sub-bands can cause quite large changes in the Auger rate because the rates depend exponentially on these energies. Non-parabolicity in the E-K relations for the sub-bands can also have significant effects.

The effect of non-parabolicity, which have not been incorporated in this treatment, may be roughly estimated by recognizing that it is most important for the promoted Auger electron and describing the final state of this electron using a larger effective mass. Dutta (ref 2.2) has done this using a final state effective mass for the promoted electrons which is twice the effective mass of the other electron states. For a 200Å thick well with a carrier concentration of 10E+18 $cm^{-3}$ he finds that the CHCC Auger rate for electrons and holes, which remain in the first sub-bands, decreases by more than a order of magnitude for the 1.55 μm InGaAsP/InP laser, and significantly more than this for the 1.3 μm InGaAsP/InP laser.

Better estimates of the effects of non-parabolicity in a QW's are unavailable. However estimates for bulk DH InGaAsP/InP lasers due to Haug (ref 2.3) suggest that non-parabolicity may be even more important than indicated above. Haug interpolates the InGaAsP bulk bandstructure from Chelikowsky and Cohen InP and GaAs bandstructures and then finds the Auger rate using a graphical method to determine when energy conservation and wavevector conservation are simultaneously satisfied. He claims that the direct CHCC rate is more than four orders of magnitude less than that calculated with parabolic bands. The CHSH and phonon assisted CHCC rate are however effected much less because of the smaller wavevectors changes involved.

The failure to include an accurate bandstructure may therefore present a serious short fall in the quantitative accuracy of the calculations presented in this thesis. However the aim is to present trends rather than absolute values. For this purpose the analytical approach allowed by the simple model is more useful, provided there is an awareness of possible inaccuracies.

## 2.2 AN INTRODUCTION TO THE AUGER RATE CALCULATION

### 2.2.1 CHCC IN A QUANTUM WELL

In a QW heterostructure the calculation of Auger recombination rates is more complex than in a bulk semiconductor because of the more complicated electronic states of the well system.

The important types of direct, non-phonon assisted CHCC processes which can occur in a QW are illustrated in figure 2.4. They fall into two types. Those for which all carriers taking place have an insufficient perpendicular kinetic energy to escape from the well (which we call bound-bound processes), and those where the excited carrier has sufficient perpendicular kinetic energy to escape from the well (which we call bound-unbound processes). Processes in which the excited carrier starts in a unbound state are unlikely because there are very few carriers in the unbound states in the model adopted. Chapter 3 analyses the bound-bound processes and Chapter 4 analyses the bound-unbound processes.

### 2.2.2 AN INTRODUCTION TO THE CALCULATION OF THE AUGER RECOMBINATION RATE

To calculate the Auger recombination rate R the electron-electron interaction between the colliding particles is treated as the perturbation H" on the system which causes

FIGURE 2.4

This illustrates the various types of CHCC direct band to band Auger recombination processes which can take place in a QW heterostructure, introduces the numbering of sub-bands n = 1, 2, 3 etc and defines the notation of states. ie (1) and (2) are taken as the colliding electron states, (1´) as the heavy hole state and (2´) as the promoted (Auger) electron state

bound processes

bound-unbound processes

An example of a process involving intra sub-band transition

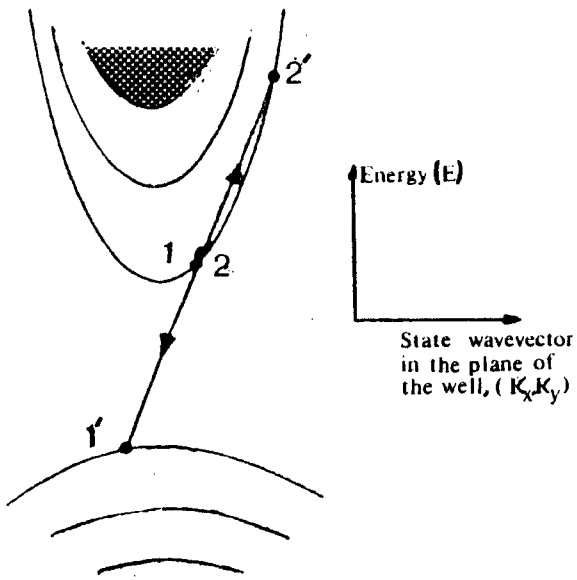


An example of a process involving inter sub-band transition

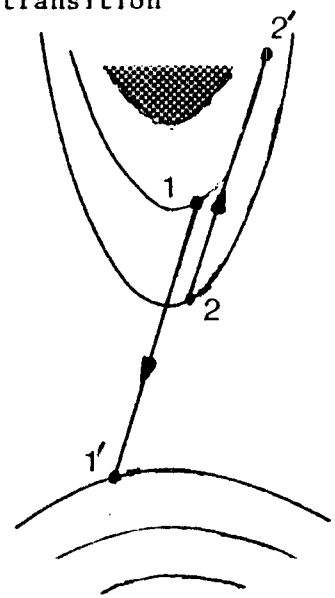


An example of a process involving a bound to unbound electron transition

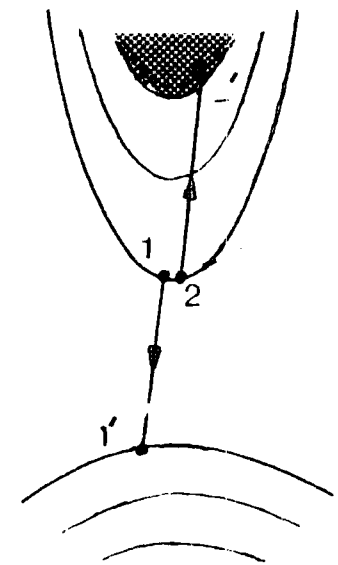

the excess number of carriers to recombine (see ref 2.4). Fermi's Golden Rule gives

$$R = \frac{2\pi}{\hbar} \Sigma P \left| \langle \Phi_{\substack{\text{INITIAL SYSTEM} \\ \text{STATE}}} | H'' | \Phi_{\substack{\text{FINAL SYSTEM} \\ \text{STATE}}} \rangle \right|^2 \delta(E) \qquad 2.7$$

where the summation is carried out over all combinations of initial and final states, P is a statistical factor included during the summation to weigh each transition according to the probability of its initial and final states being appropriately occupied, and $\langle \Phi_{\substack{\text{INITIAL SYSTEM} \\ \text{STATE}}} | H'' | \Phi_{\substack{\text{FINAL SYSTEM} \\ \text{STATE}}} \rangle$ is the matrix element of the perturbing interaction H" .

## 2.3 THE STATISTICAL FACTOR P

The statistical factor P determines the weighting (based on state occupancy) given to each possible transition in the Fermi Golden Rule summation (equation 2.7). It is given by the probability of the correct state occupancies for the forward process (electron and hole recombination) minus the probability of the correct states occupancies for the reverse process (impact ionization).

$$P_{n_1,n_2,n_{1'},n_{2'}} = f_{cn_1}(E_1)f_{cn_2}(E_2)f_{vn_{1'}}(E_{1'})\,[1-f_{cn_{2'}}(E_{2'})] \qquad 2.8$$

$$- [1-f_{vn_{1'}}(E_{1'})]\,f_{cn_{2'}}(E_{2'})[1-f_{cn_1}(E_1)][1-f_{cn_2}(E_2)]$$

where $n_1$ , $n_2$ , and $n_{2'}$ indicate the conduction (c) sub-bands, and $n_{1'}$ the valence (v) sub-band, $f_c$ $(E_c)$ determines the probability of a state with energy $E_c$ being occupied by an electron, and $f_v(E_v)$ determines the probability of a state with energy $E_v$ being occupied by a hole.

Using the approximations $1-f_v \triangleq 1$ and $1-f_c \triangleq 1$ give the simplification

$$P_{n_1,n_2,n_{1'},n_{2'}} \triangleq f_{cn_1}(E_1)f_{cn_2}(E_2)f_{vn_{1'}}(E_{1'}) - f_{cn_{2'}}(E_{2'}) \qquad 2.9$$

Now before further progress can be made it is necessary to assume a form for the distribution functions $f_c(E_c)$ and $f_v(E_v)$. The following section discuss these.

### 2.3.1 THE BOLTZMANN APPROXIMATION

During lasing the distribution functions will depend on the device current, the device structure, interband scattering, intraband scattering, the lattice temperature etc. Here we assume that the distribution function corresponding to each sub-band and unbound continuum of states can be described by a quasi-fermi level and Boltzmann statistics.

Assuming a Boltzmann distribution of carriers in an operating laser is obviously suspect. However some bulk semiconductor evidence does exist which indicates that it is not too drastic a simplification. In an operating DH laser the hole quasi-fermi level is above the top of the valence band and therefore Boltzmann statistics are adequate to describe holes. However, for conduction band electrons the quasi-fermi level is within the conduction band and Fermi-Dirac statistics are required. An approximate estimate of the importance of using Fermi-Dirac statistics in bulk material can be obtained from the comparison by Takeshima (ref 2.5) of the variation with temperature of the CHCC Auger lifetime using Fermi-Dirac and Boltzmann statistics in n-type InAs. These results can be used to make rough estimates of trends in other materials and suggest that the use of Boltzmann statistics underestimates the CHCC Auger rate in GaAs with $n = 10E+18\ cm^{-3}$ $T_c = 300k$ by a factor of 3. The situation is obviously somewhat different in a QW but is expected that Boltzmann statistics will be reasonably adequate.

Using Boltzmann statistics gives

$$f_{cn}(E) = e^{-(E - \mathcal{F}_{cn})/x_B T_c} \quad \text{for } E > E_{cn} \qquad 2.10$$

and

$$f_{vn}(E) = e^{(E - \mathcal{F}_{vn})/x_B T_c} \quad \text{for } E < E_{vn} \qquad 2.11$$

where $E_{cn}$ ($E_{vn}$) is the energy of the state at the bottom (top) of nth conduction (valence) band, and $\mathcal{F}_{cn}$ ($\mathcal{F}_{cv}$) are the conduction (valence) quasi-fermi levels.

Substituting these into 2.9 gives

$$P_{n_1,n_2,n_1',n_2'} = e^{(-E_1+\mathcal{F}_{cn_1}-E_2+\mathcal{F}_{cn_2}+E_{1'}-\mathcal{F}_{vn_{1'}})/x_B T_c} - e^{(-E_{2'}+\mathcal{F}_{cn_{2'}})/x_B T_c} \qquad 2.12$$

Conservation of energy in the transition requires $E_1' + E_2' - E_1 - E_2 = 0$ (see section 3.2) and Eq (2.12) can then be written as

$$P_{n_1,n_2,n_1',n_2'} = e^{-(E_2-E_{c2'})/x_B T_c} \, e^{-(E_{c2'}-\mathcal{F}_{cn_{2'}})/x_B T_c} \left( \frac{N_1}{N_{01}} \frac{N_2}{N_{02}} \frac{P_{1'}}{P_{01'}} \frac{N_{02'}}{N_{2'}} - 1 \right) \qquad 2.13$$

where $N_1$, $N_2$, $N_2$, and $P_1$ are the carrier concentrations in each sub-band and $N_{01'}$, $N_{02}$, $N_{02'}$ and $P_{01'}$ are the carrier concentrations under equilibrium conditions in each sub-band.

Using

$$N_n = \bar{N}_c \, e^{-(E_{cn} - \mathcal{P}_{cn})/x_B T_c} \qquad 2.14$$

(where $\bar{N}c = \frac{m_c^* \, x_B T_c}{\pi \hbar^2 L}$, the effective density of states per unit volume for the conduction band sub-bands)

Eq (2.13) becomes

$$P = e^{-(E_{2'} - E_{c2'})/x_B T_c} \frac{N_{2'}}{\bar{N}_c} \left( \frac{N_1}{N_{01}} \frac{N_2}{N_{02}} \frac{P_{1'}}{P_{01'}} \frac{N_{02'}}{N_{2'}} - 1 \right) \qquad 2.15$$

The equilibrium carrier concentrations for individual sub-bands being given by

$$N_{on} = \bar{N}_c \, e^{-(E_{cn} - \mathcal{P})/x_B T_c} \qquad 2.16$$

and

$$P_{on'} = \bar{N}_{vn'} \, e^{+(E_{vn'} - \mathcal{P})/x_B T_c} \qquad 2.17$$

where $\mathcal{P}$ is the fermi level under equilibrium conditions, and $Nvn' = \frac{m_H^* \, x_B T_c}{\pi \hbar^2 L}$ is the effective density of states per unit volume for holes in sub-band n'. Thus Eq (2.15) can now be rewritten as

$$P = \frac{e^{-(E_{2'} - E_{c2'})/x_B T_c} N_{2'}}{\bar{N}_c} \left( \frac{e^{(E_{c1} - E_{v1'})/x_B T_c} N_1 N_2 P_{1'} \, e^{-(E_{c2'} - E_{c2})/x_B T_c}}{\bar{N}_c \, \bar{N}_{v1'} \, N_{2'}} - 1 \right) \qquad 2.18$$

and to proceed assumptions are now made about $N_1$, $N_2$, $N_{2'}$, and $P_{1'}$.

### 2.3.2 THE NUMBER OF CARRIERS IN EACH SUB-BAND

In the most general form the formalism to be developed allows the number of carriers in each sub-band to be chosen to correspond to the best estimates of the carrier distribution in a working device. This is achieved by the choice of a separate quasi-fermi level for each sub-band which has the implication that intra-sub-band scattering is strong enough to maintain thermal equilibrium within a particular sub-band.

However, in the calculations presented explicitly here we choose to assume that electrons are thermalised between all the conduction sub-bands, and holes are thermalised between all the hole sub-bands. That is, for example considering the conduction sub-bands, we take all the conduction band quasi-fermi levels to be equal

$$\mathcal{P}_{cn_{2'}} = \mathcal{P}_{cn_1} = \mathcal{P}_{cn_{2'}} = \mathcal{P}_c \qquad 2.19$$

Then the total number of conduction band electrons $\delta N$ is

$$\delta N = \left( \sum_{\substack{\text{sub-}\\\text{bands}\\ n}} \int_{E_{cn}}^{\infty} \frac{1}{2\pi} \frac{1}{L} \left(\frac{2m_c^*}{\hbar^2}\right) e^{-(E-\mathcal{P}_c)/x_B T_c} \, dE \right) \qquad 2.20$$

$$+ \int_{E_{con}}^{\infty} \frac{1}{2\pi^2} \left(\frac{2m_c}{\hbar^2}\right)^{3/2} E^{\frac{1}{2}} e^{-(E-\mathcal{P}_c)/x_B T_c} \, dE$$

$$\delta N = \left( \sum_n \bar{N}_c \, e^{-(E_{cn}-\mathcal{P}_c)/x_B T_c} \right) + \frac{1}{4} \left( \frac{2m_c^* x_B T_c}{\pi \hbar^2} \right)^{3/2} e^{(E_{con}-\mathcal{P}_c)/x_B T_c} \qquad 2.21$$

where $E_{con}$ is the energy at the top of the well (see figure 2.1).

Hence

$$e^{\mu_c/x_B T_c} = \frac{\delta N}{\sum_n \bar{N}_c\, e^{-E_{cn}/x_B T_c} + \frac{1}{4}\left(\frac{2m^*_c}{\pi\hbar^2}\, x_B T_c\right)^{3/2} e^{-(E_{con})/x_B T_c}} \qquad 2.22$$

and the number of electrons in a particular sub-band $n'$ is given by

$$N_{n'} = \bar{N}_c\, e^{-E_{cn'}/x_B T_c}\, \frac{\delta N}{\left(\sum_n \bar{N}_c\, e^{-E_{cn}/x_B T_c}\right) + \frac{1}{4}\left(\frac{2m^*_c}{\pi\hbar^2}\, x_B T_c\right)^{3/2} e^{-E_{con}/x_B T_c}} \qquad 2.23$$

Similarly for holes

$$P_{n'x'} = \bar{N}_{vx'}\, e^{+E_{vn'}/x_B T_c}\, \frac{\delta N}{\sum_{nx} \bar{N}_v\, e^{+E_{vn}/x_B T_c} + \frac{1}{4}\left(\frac{2x_B T_c}{\pi\hbar^2}\right)^{3/2}} \cdot \frac{1}{e^{+E_{vcon}/x_B T_c}\left((m^*_{HH})^{3/2} + (m^*_{LH})^{3/2} + (m^*_S)^{3/2} e^{-(E_{vcon}-\Delta_s)/x_B T_c}\right)} \qquad 2.24$$

where x' denotes either a heavy hole or light hole sub-band, x ranges over both heavy hole and light hole sub-bands, $m^*_{HH}$, $m^*_{LH}$, and $m^*_S$ are respectively the heavy hole, light hole, and spin split-off bulk effective masses and $\Delta_s$ is the bulk $\Gamma$ energy separation between spin split off and heavy hole bands.

Figures 2.5 and 2.6 show how a concentration of 10E+18 $cm^{-3}$ electrons and holes are distributed between the sub-bands of 1.3 $\mu$m (figure 2.2) and 1.55 $\mu$m (figure 2.3) InGaAsP/InP QW lasers. For clarity only the population of conduction band and heavy hole band sub-bands being shown.

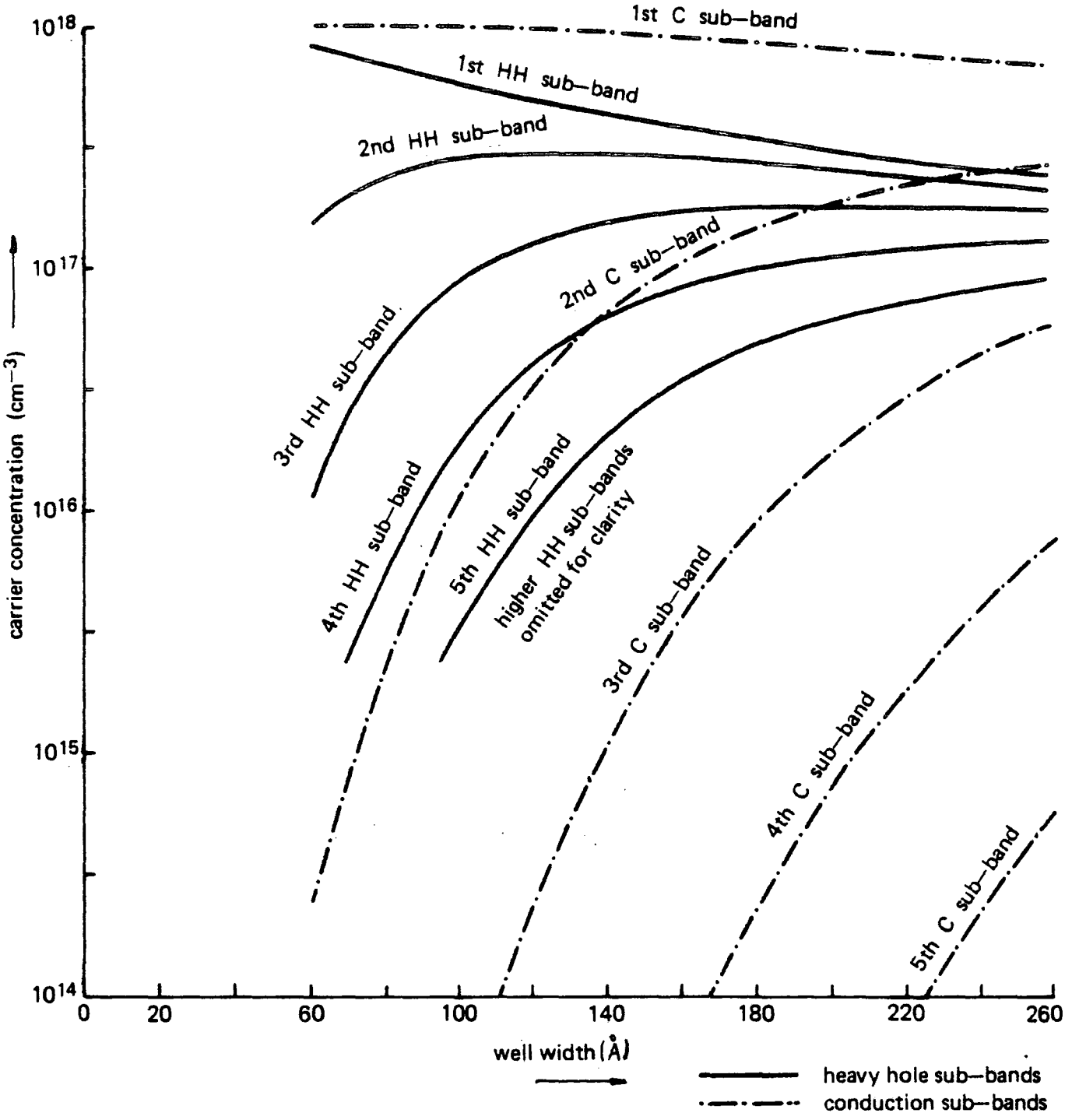


FIGURE 2.5

This figure shows respectively the electron and hole populations in the conduction (C) sub-bands and heavy hole (HH) sub-bands when $10^{18}$ electron $cm^{-3}$ and $10^{18}$ $cm^{-3}$ holes are injected into the active region of a 1.3 μm InGaAsP/InP system. Boltzmann statistics and carrier thermalisation are assumed.

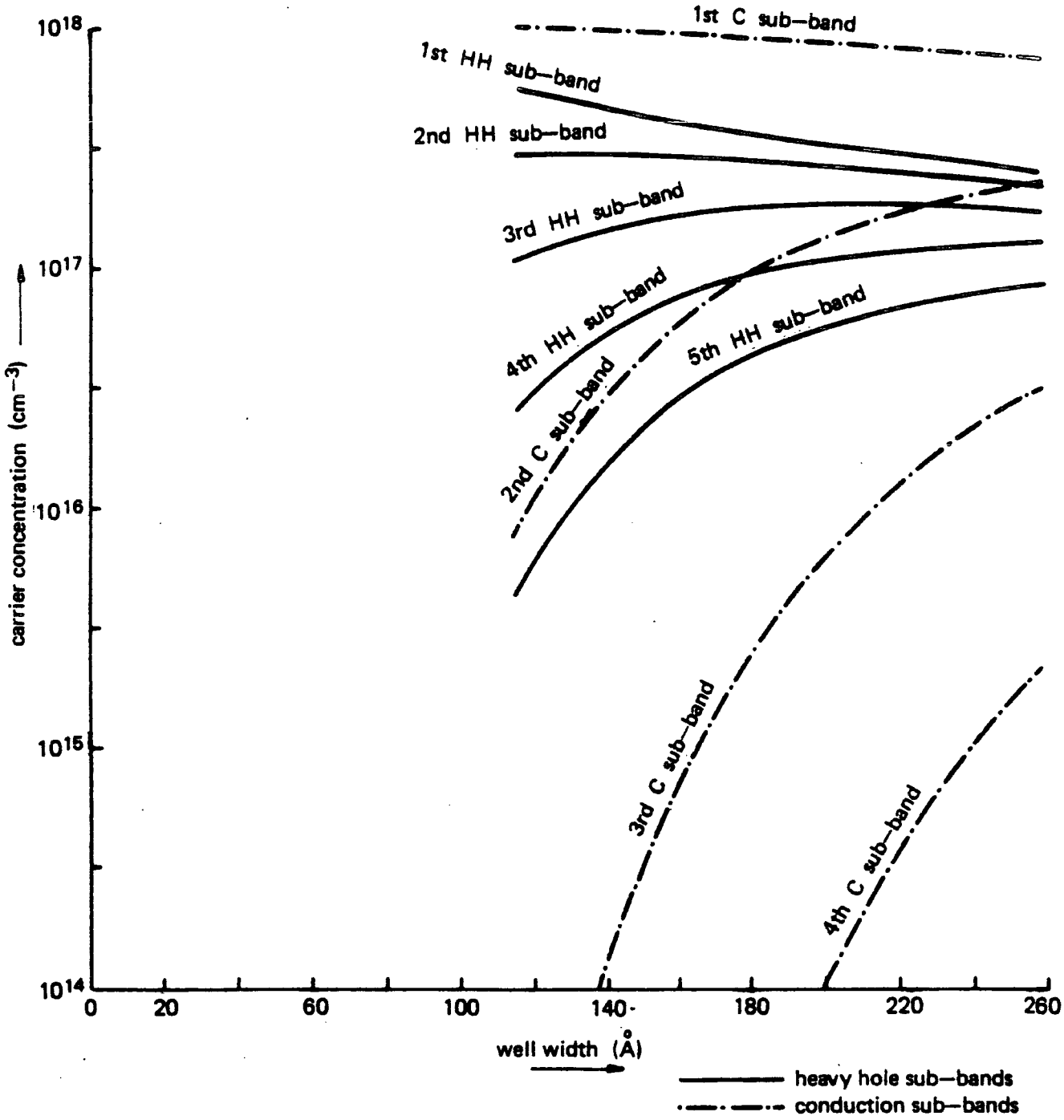


FIGURE 2.6

As figure 2.5 but for the 1.55 μm InGaAsP/InP system.

These populations are used in the evaluations of the Auger rate.

For the bound-unbound calculations (Chapter 4) it is helpful to recognise that

$$N_{2'} = N_1 \, e^{-(E_{c2'} - E_{c1})/x_B T_c} \qquad 2.25$$

and for both bound-bound and bound-unbound calculations that

$$\frac{N_2}{N_{02}} \cdot \frac{N_{02'}}{N_{2'}} = 1 \qquad 2.26$$

## 2.4 THE NATURE OF THE ELECTRON-ELECTRON INTERACTION

### 2.4.1 THE FORM OF THE MATRIX ELEMENT

Using a Hartree-Fock Hamiltion and a Slater determinant for the wavefunctions the matrix element of the electron-electron interaction which appears in the Golden Rule expression for the Auger rate (Eq 2.7) is

$$M = \left\langle \frac{\psi_1(r_1s_1)\psi_2(r_2s_2) - \psi_1(r_2s_2)\psi_2(r_1s_1)}{\sqrt{2}} \middle| H''(r_1,r_2) \right. \qquad 2.27$$

$$\left. \frac{|\psi_{1'}(r_1s_1)\psi_{2'}(r_2s_2) - \psi_{1'}(r_2s_2)\psi_{2'}(r_1s_1)}{\sqrt{2}} \right\rangle$$

where H'' is the electron-electron interaction which is discussed in Sec 2.4.2, $\psi_1$ and $\psi_2$ represent the initial states, $\psi_{1'}$ and $\psi_{2'}$ represent the final states, and r and s are the position and spin coordinates respectively.

Now defining

$$M_{12} \equiv \langle \psi_1(r_1s_1)\psi_2(r_2s_2)|H''(r_1,r_2)|\psi_{1'}(r_1s_1)\psi_{2'}(r_2s_2) \rangle$$

$$= \langle \psi_1(r_2s_2)\psi_2(r_1s_1)|H''(r_1,r_2)|\psi_{1'}(r_2s_2)\psi_{2'}(r_1s_1) \rangle \qquad 2.29$$

$$M_{21} \equiv \langle \psi_1(r_1s_1)\psi_2(r_2s_2)|H''(r_1,r_2)|\psi_{1'}(r_2s_2)\psi_{2'}(r_1s_1) \rangle$$

$$= \langle \psi_1(r_2s_2)\psi_2(r_1s_1)|H''(r_1,r_2)|\psi_{1'}(r_1s_1)\psi_{2'}(r_2s_2) \rangle \qquad 2.30$$

and using spin orthogonality one obtains

$$|M|^2 = |M_{12} - M_{21}|^2 + |M_{12}|^2 + |M_{21}|^2 \qquad 2.31$$

$$|M_{12}|^2 + |M_{21}|^2 \geqslant |M_{12} - M_{21}|^2 \qquad 2.32$$

$$|\underline{M}|^2 = \bar{\beta}(|M_{12}|^2 + |M_{21}|^2) \qquad 2.33$$

where $\bar{\beta}$ is a function of the initial and final states whose value is between 1 and 2. Now summing over the initial and final states we obtain a number for an effective $\bar{\beta}$. An indication of the size which can be obtained by considering which transitions are most probable. Appendix 1 concludes that $K_{\parallel_1} \approx K_{\parallel_2}$ transitions are important. Using this and the assumption of electron thermalisation (see equation 2.19) the most appropriate value for an effective $\bar{\beta}$ is seen to be one. This may be interpreted physically by reference to equations 2.29 and 2.30 as showing that collisions between electrons of unlike spin are more probable than the analogous collisions for electrons of like spin.

Omitting $\bar{\beta}$ we have

$$|\underline{M}|^2 = (2 + 2\delta_{n_1,n_2})|M|^2 \qquad 2.34$$

where $M = \langle \psi_1(r_1)\psi_2(r_2)|H''(r_1,r_2)|\psi_{1'}(r_1)\psi_{2'}(r_2) \rangle$ 2.35

In equation 2.34 one factor of 2 arises from 2.33, and the other because the initial impacting electron can have two values ie spin up or spin down. The $\delta_{n_1}, n_2$ prevents overcounting (see Table 3.1) when the summation is later made over sub-bands.

### 2.4.2 SCREENING

The form of the perturbing interaction is now considered. In general the electron-electron interaction has the form of a screened coulomb interaction which in q, w space can be written as

$$H'' = \frac{\text{constant}}{\varepsilon(q,w)\ q^2} \qquad 2.36$$

where $\varepsilon$ (q,w) is the dielectric constant of the active region. $\varepsilon$ (q,w) can now be considered to consist of two contributions. The first $\varepsilon_{INT}$ being the intrinsic dielectric constant of the semiconductor and the second ( $\varepsilon g$ (q,w)-1) being the susceptibility of the conduction band electrons and valence band holes. The change in $\varepsilon_{INT}$ due to the states occupied by carriers is neglected because the carriers occupy only a small part of the Brillouin zone. Hence

$$\varepsilon(q,w) = \varepsilon_{INT} + (\varepsilon g(q,w) - 1) \qquad 2.37$$

where most of the wavevector and frequency dependence is in $\varepsilon g$ (q,w). Rewriting equation 2.37

$$\varepsilon(q,w) = \varepsilon_{INT}\ \varepsilon_{gs}(q,w) \qquad 2.38$$

where $\varepsilon_{gs}(q,w) = 1 + \frac{x_g(q,w)}{\varepsilon_{INT}}$ and $x_g = \varepsilon_g(q,w) - 1.$ 2.39

A useful and accurate analytical expression for $\varepsilon_{gs}(q,w)$ is now given by the plasmon pole approximation which assumes that most of the screening is due to the collective motion of electrons (ref 2.6). It gives for an isotropic, parabolic conduction band

$$(\varepsilon_{gs}(q,w))^{-1} = 1 + \frac{w_p^{\,2}}{w^2 - w_1^{\,2}(q)} \qquad 2.40$$

where

$$w_1^{\,2}(q) = w_p^{\,2} + \frac{4}{3} w_{cq}\, w_F + w_{cq}^{\,2}$$

$$= w_p^{\,2}\,(1 + q^2/K_F^{\,2}) + w_{cq}^{\,2} \qquad 2.41$$

$\hbar w_{cq}$ being the conduction band dispersion relation, $\hbar w_F$ being the Fermi energy, $K_F$ being the Thomas Fermi wavevector and $w_p$ being the plasmon angular frequency at q=0. Considering both electrons and holes to be present the parameters are modified in the following way:

$$w_p^{\,2} = w_p^{\,2}(\text{electrons}) + w_p^{\,2}(\text{holes}) \qquad 2.42$$

$$K_F^{\,2} = K_F^{\,2}(\text{electrons}) + K_F^{\,2}(\text{holes}) \qquad 2.43$$

and

$$w_{cq}^{\,2} = \frac{\hbar\, q^2}{2} \; \frac{3}{(m^*_c + m^*_{HH} + m^*_{LH})} \qquad 2.44$$

where $m^*_c$ is the conduction band effective mass, $m^*_{HH}$ is the heavy hole effective mass, and $m^*_{LH}$ is the light hole effective mass.

Now for electrons we have

$$w_p(\text{electrons}) = \left(\frac{Ne^2}{\varepsilon_{INT}\, m^*_c}\right)^{\frac{1}{2}} \qquad 2.45$$

and

$$K_F^{\,2} = \frac{1}{\pi^2}\,\frac{m^*_c}{\hbar^2}\,\frac{e^2}{\varepsilon_{INT}}\,(3\pi^2 N)^{\frac{1}{3}} \qquad 2.46$$

where N is the conduction band electron concentration. Similarly for holes we have

$$w_p(\text{holes}) = \left[\left(\frac{P_{HH}}{m^*_{HH}} + \frac{P_{LH}}{m^*_{LH}}\right)\frac{e^2}{\varepsilon_{INT}\,\varepsilon_o}\right]^{\frac{1}{2}} \qquad 2.47$$

and

$$K_F^{\,2} = \frac{1}{2\pi^2}\,\frac{2(m^*_{HH} + m_{LH})}{\hbar}\,\frac{e^2}{\varepsilon_{INT}}\,(3\pi^2(P_{HH} + P_{LH}))^{\frac{1}{3}} \qquad 2.48$$

where $P_{LH}$ and $P_{HH}$ are the concentrations light holes and heavy holes respectively.

Hence 2.40 and 2.41 can now be applied to the screening the Auger electron-electron interaction. In $\varepsilon(q,w)$, w is determined by the energy exchanged between the colliding electrons ($\hbar w$) which is somewhat larger than the band gap. Similarly q is given by the wavevector transfer. So considering 10E+18 carriers $cm^{-3}$ it is found that $w > w_1(q)$ and $w > w_p$ for the typical semiconductor lasers used for optical fibres. It thus follows

$$\varepsilon(q,\infty) \simeq \varepsilon_{INT} \qquad 2.49$$

That is the frequency associated with the interaction is too high for the free carriers to respond as plasmons and cause screening.

This (2.49) contrasts with the customary treatment of screening in Auger theory. Conventionally in narrow bandgap materials the static limit (w = 0) has been taken, giving the Thomas-Fermi expression when q is small,

$$\varepsilon(q,0) = \varepsilon_{INT}\left(\frac{K^2}{q^2} + 1\right) \qquad 2.50$$

This is an accurate approximation in the limit of very narrow band gaps but unfortunately some authors (see for example ref 2. 2) have carried it over to the larger band gap semiconductors. Burt (2.7) was the first to point out explicitly that this was a questionable procedure. For the wider band gap semiconductors it being more accurate to assume there is no free carrier screening. In this thesis therefore expression 2.49 is carried from the bulk to QW's without any further comment, further in applying 2.49 no account of the q dependence of '$\varepsilon_{INT}$' the intrinsic dielectric constant is made.

### 2.4.3 THE WAVEFUNCTIONS OF THE QUANTUM WELL AND THE AUGER MATRIX ELEMENT

#### 2.4.3.1 THE PARITY OF THE WAVEFUNCTION

The wavefunctions of the square well have either even or odd parity about the well centre. This allows us to make some conclusions about the matrix elements without requiring the explicit forms of the wavefunctions. The fourier transform of the electron-electron interaction is

$$\frac{e^2}{\varepsilon_{INT}|\underline{r}_1-\underline{r}_2|} = \frac{1}{\varepsilon_{INT}} \frac{e^2}{(2\pi)^3} \int \frac{4\pi}{q^2} e^{i\underline{q}.(\underline{r}_1-\underline{r}_2)} d^3\underline{q} \qquad 2.52$$

where it is assumed that the barrier regions have the same dielectric constant as the well region. Substituting this into the matrix element expressions gives

$$M_{12} = \int \psi_1(\underline{p}_{\parallel 1},z_1)\psi_2(\underline{p}_{\parallel 2},z_2) \frac{e^2}{\varepsilon_{INT}} \frac{1}{(2\pi)^3} \frac{4\pi}{q^2} e^{i\underline{q}_{\parallel}.(\underline{p}_{\parallel 1}-\underline{p}_{\parallel 2})} e^{iq_z(z_1-z_2)}$$
$$\psi_{1'}(\underline{p}_{\parallel 1},z_1)\psi_{2'}(\underline{p}_{\parallel 2},z_2)\, d^2\underline{q}_{\parallel}dq_z d^2\underline{p}_{1\parallel}d^2\underline{p}_{2\parallel}dz_1dz_2 \qquad 2.53$$

and

$$M_{21} = \int \psi_1(\underline{p}_{\parallel 1},z_1)\psi_2(\underline{p}_{\parallel 2},z_2) \frac{e^2}{\varepsilon_{INT}} \frac{1}{(2\pi)^3} \frac{4\pi}{q^2} e^{i\underline{q}_{\parallel}.(\underline{p}_{\parallel 1}-\underline{p}_{\parallel 2})} e^{iq_z(z_1-z_2)}$$
$$\psi_{1'}(\underline{p}_{\parallel 2},z_2)\psi_{2'}(\underline{p}_{\parallel 1},z_1)\, d^2\underline{q}_{\parallel}dq_z d^2\underline{p}_{\parallel 1}d^2\underline{p}_{\parallel 2}dz_1dz_2 \qquad 2.54$$

where $\underline{q}_{\parallel}$, $\underline{p}_{\parallel 1}$, and $\underline{p}_{\parallel 2}$ are respectively the components of $\underline{q}$, $\underline{r}_1$, and $\underline{r}_2$ in the plane of the well, and $q_z$, $z_1$, and $z_2$ are respectively the components of $\underline{q}$, $\underline{r}_1$, and $\underline{r}_2$ perpendicular to the plane of the well.

First considering the direct term $M_{12}$ and supposing that $\psi_1(z_1)$ and $\psi_{1'}(z_1)$ have the same parity then we may write

$$\int_{-\frac{L}{2}}^{+\frac{L}{2}} \psi_1^*(z_1)\psi_{1'}(z_1)\, e^{-iq_z z_1}\, dz_1 = \int_{-\frac{L}{2}}^{+\frac{L}{2}} \psi_1(z_1)\psi_{1'}(z_1) \cos q_z z_1 dz_1 \qquad 2.55$$

which is an even function of $q_z$. Now since $\frac{1}{q_{\parallel}^2+q_z^2}$ is also an even function of $q_z$ we require the integral

$$\int_{-\frac{L}{2}}^{+\frac{L}{2}} \psi_2^*(z_2)\psi_{2'}(z_2)\, e^{-iq_z z_2}\, dz_2$$

to be an even function of $q_z$ if 2.53 is not to vanish. Hence if $\psi_2(z_2)$ and $\psi_{2'}(z_2)$ have different parity the integral

$$\int_{-\frac{L}{2}}^{+\frac{L}{2}} \psi_2^*(z_2)\psi_{2'}(z_2)\, e^{-iq_z z_2}\, dz_2$$

will be odd in $q_z$ and the matrix element $M_{12}$ will be zero. That is if $\psi_1(z_1)$ and $\psi_{1'}(z_1)$ have the same parity $\psi_2(z_2)$ and $\psi_{2'}(z_2)$ are also required to have the same parity if the matrix element is to be non-zero.

If $\psi_1(z_1)$ and $\psi_{1'}(z_1)$ have different parities then the integral

$$\int_{-\frac{L}{2}}^{+\frac{L}{2}} \psi_1^*(z_1)\psi_{1'}(z_1)\, e^{+iq_z z_1}\, dz_1$$

is odd in $q_z$ and $\psi_2(z_2)$ and $\psi_{2'}(z_2)$ must have different parities for the matrix element to be non-zero.

Table 2.1 summarizes the above argument for various combinations of wavefunctions and considers both the direct and exchange matrix elements.

For transitions between bound states the results can be summarised by requiring $\Delta n = 0,2,4$, etc where n numbers the sub-bands (see figure 2.2), and $\Delta$ indicates difference.

For transitions to unbound states, parity lowers the final density of states available to the promoted Auger electron by a factor of two.

**TABLE 2.1** $E_z$ = even function of z $E_q$ = even function of qz

$O_z$ = odd function of z $O_q$ = odd function of qz

**INT = INTEGRAL**

| THE DIRECT TERM | | | | | | | | THE EXCHANGE TERM | | | | | | | |
|---|---|---|---|---|---|---|---|---|---|---|---|---|---|---|---|
| $\psi_1'$ | $\psi_1$ | $\psi_2$ | $\psi_2'$ | 1st INT | 2nd INT | 3rd INT | RESULT | $\psi_1$ | $\psi_2'$ | $\psi_2$ | $\psi_1'$ | 1st INT | 2nd INT | 3rd INT | RESULT |
| $E_z$ | $E_z$ | $E_z$ | $E_z$ | $E_q$ | $E_q$ | $E_q$ | | $E_z$ | $E_z$ | $E_z$ | $E_z$ | $E_q$ | $E_q$ | $E_q$ | |
| $E_z$ | $E_z$ | $E_z$ | $O_z$ | $E_q$ | $E_q$ | $O_q$ | zero | $E_z$ | $O_z$ | $E_z$ | $E_z$ | $E_q$ | $O_q$ | $E_q$ | zero |
| $E_z$ | $E_z$ | $O_z$ | $E_z$ | $E_q$ | $E_q$ | $O_q$ | zero | $E_z$ | $E_z$ | $O_z$ | $E_z$ | $E_q$ | $E_q$ | $O_q$ | zero |
| $E_z$ | $O_z$ | $E_z$ | $E_z$ | $E_q$ | $O_q$ | $E_q$ | zero | $O_z$ | $E_z$ | $E_z$ | $E_z$ | $E_q$ | $O_q$ | $E_q$ | zero |
| $O_z$ | $E_z$ | $E_z$ | $E_z$ | $E_q$ | $O_q$ | $E_q$ | zero | $E_z$ | $E_z$ | $E_z$ | $O_z$ | $E_q$ | $E_q$ | $O_q$ | zero |
| $O_z$ | $E_z$ | $E_z$ | $O_z$ | $E_q$ | $O_q$ | $O_q$ | | $E_z$ | $O_z$ | $E_z$ | $O_z$ | $E_q$ | $O_q$ | $O_q$ | |
| $O_z$ | $E_z$ | $O_z$ | $E_z$ | $E_q$ | $O_q$ | $O_q$ | | $E_z$ | $E_z$ | $O_z$ | $O_z$ | $E_q$ | $E_q$ | $E_q$ | |
| $O_z$ | $O_z$ | $E_z$ | $E_z$ | $E_q$ | $E_q$ | $E_q$ | | $O_z$ | $E_z$ | $E_z$ | $O_z$ | $E_q$ | $O_q$ | $O_q$ | |
| $O_z$ | $E_z$ | $O_z$ | $O_z$ | $E_q$ | $O_q$ | $E_q$ | zero | $E_z$ | $O_z$ | $O_z$ | $O_z$ | $E_q$ | $O_q$ | $E_q$ | zero |
| $O_z$ | $O_z$ | $O_z$ | $E_z$ | $E_q$ | $E_q$ | $O_q$ | zero | $O_z$ | $E_z$ | $O_z$ | $O_z$ | $E_q$ | $O_q$ | $E_q$ | zero |
| $O_z$ | $O_z$ | $O_z$ | $O_z$ | $E_q$ | $E_q$ | $E_q$ | | $O_z$ | $O_z$ | $O_z$ | $O_z$ | $E_q$ | $E_q$ | $E_q$ | |
| $E_z$ | $O_z$ | $E_z$ | $O_z$ | $E_q$ | $O_q$ | $O_q$ | | $O_z$ | $O_z$ | $E_z$ | $E_z$ | $E_q$ | $E_q$ | $E_q$ | |
| $E_z$ | $E_z$ | $O_z$ | $O_z$ | $E_q$ | $E_q$ | $E_q$ | | $E_z$ | $O_z$ | $O_z$ | $E_z$ | $E_q$ | $O_q$ | $O_q$ | |
| $E_z$ | $O_z$ | $O_z$ | $E_z$ | $E_q$ | $O_q$ | $O_q$ | | $O_z$ | $E_z$ | $O_z$ | $E_z$ | $E_q$ | $O_q$ | $O_q$ | |
| $E_z$ | $O_z$ | $O_z$ | $O_z$ | $E_q$ | $O_q$ | $E_q$ | zero | $O_z$ | $O_z$ | $O_z$ | $E_z$ | $E_q$ | $E_q$ | $O_q$ | zero |
| $O_z$ | $O_z$ | $E_z$ | $O_z$ | $E_q$ | $E_q$ | $O_q$ | zero | $O_z$ | $O_z$ | $E_z$ | $O_z$ | $E_q$ | $E_q$ | $O_q$ | zero |

### 2.4.3.2 THE FORM, NORMALISATION, AND ORTHOGONALITY OF THE WAVEFUNCTION

**BOUND STATES**

For bound states the evanescent parts of the wavefunctions are ignored. They being assumed to be small. We have

$$\psi_m(\underline{r}) = A^{-\frac{1}{2}} \left(B^{(+)} u_m^{(+)}(r)\, e^{iK_{zm}z} + B^{(-)} u_m^{(-)}(r)\, e^{-iK_{zm}z}\right) e^{i\underline{K}_{\parallel}\cdot\underline{p}} \qquad 2.56$$

inside the well $(0<z<L)$

and $\psi_m(\underline{r})=0$ outside the well

where $u_m(\underline{r})$ is the periodic part of the Bloch function (normalised to the unit cell). The (+) and (-) signs indicate the dependence of the Bloch functions on the z direction of momentum. $\underline{k}_{\parallel}$ is the two dimensional wavevector in the plane of the well and $\underline{p}$ is the corresponding two dimensional position vector. $k_{zm}$ is the wavevector perpendicular to the plane of the well, and as a simplification is given the value appropriate to an infinite square well, $\frac{n\pi}{L}$ (n being a positive integer). B is the normalisation constant associated with the z dependent part of the wavefunction

$$B^{(\pm)} = \mp i\, V_{\substack{\text{UNIT}\\ \text{CELL}}}^{\frac{1}{2}} \left(\frac{1}{2L}\right)^{\frac{1}{2}} \qquad 2.57$$

and A is the area of the QW layer.

**UNBOUND STATES**

The wavefunctions of carriers with sufficient perpendicular kinetic energy to be not bound by the well are found by matching the envelope parts of the wavefunctions inside and outside the well at the boundaries of the well. Assuming sinusoidial envelope wavefunctions inside and outside the well region (see figure 2.7), the usual boundary conditions give for the case of even parity states.

$$B' \cos\left(\frac{K_{z2'}L}{2}\right) = A' \cos\left(\frac{\bar{K}_z L}{2} + \delta\right) \qquad 2.58$$

and

$$K_{z2'} B' \sin\left(\frac{K_{z2'}L}{2}\right) = \bar{K}_z A' \sin\left(\frac{\bar{K}_z L}{2} + \delta\right) \qquad 2.59$$

where A' and B' are the normalisation constants of the wavefunctions outside and inside the well, $\delta$ is a phase constant, and $\bar{K}_z$ and $K_{z2'}$ are the respective z components of wavevector.

Squaring and adding Eqs 2.58 and 2.59 gives

$$B'^2 = A'^2 \cos^2\left(\frac{\bar{K}_2 L}{2} + \delta\right) + \frac{\bar{K}_z^{\,2}}{K_{z2'}^{\,2}} A' \sin^2\left(\frac{\bar{K}_z L}{2} + \delta\right) \qquad 2.60$$

$$B'^2 = A'^2 \left(1 + \left(\frac{\bar{K}_z^{\,2}}{K_{z2'}^{\,2}} - 1\right) \sin^2\left(\frac{\bar{K}_z L}{2} + \delta\right)\right) \qquad 2.61$$

FIGURE 2.7

This figure shows the envelope parts of the unbound wavefunctions, the large assumption that the corresponding cell periodic parts are the same both inside and outside the well, being made.

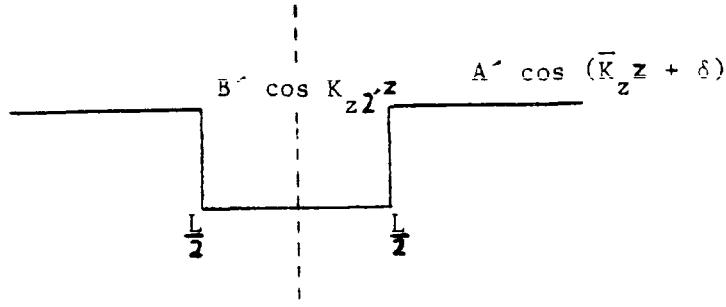

Now, since $\frac{\bar{K}_z^{\,2}}{K_{z2'}^{\,2}} < 1$, the second term is always negative and the maximum value of A' is given by

$$A'^2 = B'^2 \text{ when } \sin^2\left(\frac{\bar{K}_z L}{2} + \delta\right) = 0 \qquad 2.62$$

also the minimum value of A' is given by

$$A'^2 = B'^2 \frac{\bar{K}_z^{\,2}}{K_{z2'}^{\,2}} \text{ when } \sin^2\left(\frac{\bar{K}_z L}{2} + \delta\right) = 1 \qquad 2.63$$

An expression for $\delta$ can now be derived from the matching conditions. From them

$$B' \cos\left(\frac{K_{z2'}L}{2}\right) = A'\left(\cos\frac{\bar{K}_z L}{2}\cos\delta - \sin\frac{\bar{K}_z L}{2}\sin\delta\right) \qquad 2.64$$

and

$$K_{z2'}\, B' \sin\left(\frac{K_{z2'}L}{2}\right) = \bar{K}_z A'\left(\sin\frac{\bar{K}_z L}{2}\cos\delta + \cos\frac{\bar{K}_z L}{2}\sin\delta\right) \qquad 2.65$$

hence

$$K_{z2'} \tan\left(\frac{K_{z2'}L}{2}\right) = \bar{K}_z \left(\frac{\sin\bar{K}_z L/2 + \cos\bar{K}_z L/2 \tan\delta}{\cos\bar{K}_z L/2 - \sin\bar{K}_z L/2 \tan\delta}\right) \qquad 2.66$$

Therefore

$$\delta = \arctan\left(\frac{-\sin\bar{K}_z L/2 + \frac{K_{z2'}}{\bar{n}_z}\tan\left(\frac{K_{z2'}L}{2}\right)\cos\bar{K}_z L/2}{\cos\bar{K}_z L/2 + \frac{K_{z2'}}{\bar{n}_z}\tan\left(\frac{K_{z2'}L}{2}\right)\sin\bar{K}_z L/2}\right) \qquad 2.67$$

Finally we need to derive an expression for B'. To do this the envelope part of the wavefunction is normalised over the crystal z dimension $2\ell$.

$$B'^2 \int_0^{\frac{L}{2}} \cos^2 K_{z2'}z \, dz + A'^2 \int_{\frac{L}{2}}^{\ell} \cos^2 (\bar{K}_z{}^2 + \delta) \, dz = \tfrac{1}{2} \qquad 2.68$$

Choosing $\ell$ large enough so that only the second term needs to be considered

$$\frac{A'^2}{2} \int_{\frac{L}{2}}^{\ell} (1 + \cos (2\bar{K}_z z + 2\delta)) \, dz = \tfrac{1}{2}$$

$$\frac{A'^2}{2} \left[ z + \frac{\sin (2\bar{K}_z z + 2\delta)}{2\bar{K}_z} \right]_{\frac{L}{2}}^{\ell} = \tfrac{1}{2} \qquad 2.69$$

and retaining only the dominant terms for large gives

$$A' = \sqrt{\frac{1}{\ell}} \qquad 2.70$$

From which B′ can be found using equations 2.61, 2.67 and 2.70.

For the case of odd parity wavefunctions normalisation follows in a similar fashion.

**ORTHOGONALITY**

The neglect of the evanescent parts of bound state wavefunctions means that the approximate bound wavefunctions are not exactly orthogonal to the unbound wavefunctions except for special cases, such as between the nth bound state and a unbound state with perpendicular wavevector $K_{z2'} = \frac{m\pi}{L}$ where $n \neq m$. This non-orthogonality turns out not to be significant for the Auger calculations but is considered in more detail at the appropriate time.

### 2.4.4 INITIAL STEPS IN THE EVALUATION OF THE MATRIX ELEMENTS

The direct matrix element term is given by Eqs 2.29 and 2.56 as

$$M_{12} = \frac{1}{A^2} \int_{\substack{p=-\infty \\ z=0}}^{\substack{p=+\infty \\ z=L}} e^{i(\underline{K}''_1 - \underline{K}''_{1'}) \cdot \underline{p}_1} \left( B_1^{(+)} u_1^{(+)}(\underline{r}_1)\, e^{iK_{z1'} z_1} + B_{1'}^{(-)} u_{1'}^{(-)}(\underline{r}_1)\, e^{-iK_{z1'} z_1} \right)^*$$

$$\left( B_1^{(+)} u_1^{(+)}(\underline{r}_1)\, e^{iK_{z1} z_1} + B_1^{(-)} u_1^{(-)}(\underline{r}_1)\, e^{-iK_{z1} z_1} \right) \frac{e^2}{\varepsilon_{INT} |\underline{r}_1 - \underline{r}_2|}\, e^{i(\underline{K}''_2 - \underline{K}_{2'}) \cdot \underline{p}_2}$$

$$\left( B_{2'}^{(+)} u_{2'}^{(+)}(\underline{r}_2)\, e^{iK_{z2'} z_2} + B_{2'}^{(-)} u_{2'}^{(-)}(\underline{r}_2)\, e^{-iK_{z2'} z_2} \right)^*$$

$$\left( B_2^{(+)} u_2^{(+)}(\underline{r}_2)\, e^{iK_{z2} z_2} + B_2^{(-)} u_2^{(-)}(\underline{r}_2)\, e^{-K_{z2} z_2} \right) d^3\underline{r}_1\, d^3\underline{r}_2 \qquad 2.71$$

where $B^{(\pm)}$ is given by $B^{(\pm)} = \mp i \; V^{\frac{1}{2}}_{\substack{\text{UNIT}\\ \text{CELL}}} \left(\frac{1}{2L}\right)^{\frac{1}{2}}$ for bound states and by

$$B^{(\pm)} = \frac{B'}{2} V^{\frac{1}{2}}_{\substack{\text{UNIT}\\ \text{CELL}}} \; e^{\mp i \frac{\pi}{2} L} \qquad \text{even parity} \tag{2.72}$$

or

$$B^{(\pm)} = \pm i \frac{B'}{2} V^{\frac{1}{2}}_{\substack{\text{UNIT}\\ \text{CELL}}} \; e^{\pm i \frac{\pi}{2} L} \qquad \text{odd parity}$$

for unbound states.

Taking the Fourier transform of the electron-electron interaction (see 2.52) gives

$$M_{12} = \frac{4\pi e^2}{\varepsilon_{INT}} \frac{1}{(2\pi)^3} \frac{1}{A^2} \int \frac{1}{q^2} I_{1'1} \, I_{2'2} \; d^3\underline{q} \tag{2.73}$$

with

$$\begin{aligned} I_{1'1} = \int & e^{i(\underline{K}''_1 - \underline{K}''_{1'} + \underline{q}'')\cdot \underline{\rho}_1} \; e^{iq_z z_1} \left( B^{(+)}_{1'} u^{(+)}_{1'}(\underline{r}_1) \; e^{iK_{z1'} z_1} \right. \\ & \left. + B^{(-)}_{1'} u^{(-)}_{1'}(\underline{r}_1) \; e^{-iK_{z1'} z_1} \right)^* \left( B^{(+)}_1 u^{(+)}_1(\underline{r}_1) \; e^{iK_{z1} z_1} \right. \\ & \left. + B^{(-)}_1 u^{(-)}_1(\underline{r}_1) \; e^{-iK_{z1} z_1} \right) d^3\underline{r}_1 \end{aligned} \tag{2.74}$$

and

$$\begin{aligned} I_{2'2} = \int & e^{i(\underline{K}''_2 - \underline{K}''_{2'} - \underline{q}'')\cdot \underline{\rho}_2} \; e^{-iq_z z_2} \left( B^{(+)}_{2'} u^{(+)}_{2'}(\underline{r}_2) \; e^{iK_{z2'} z_2} \right. \\ & \left. + B^{(-)}_{2'} u^{(-)}_{2'}(\underline{r}_2) \; e^{iK_{z2'} z_2} \right)^* \left( B^{(+)}_2 u^{(+)}_2(\underline{r}_2) \; e^{iK_{z2} z_2} \right. \\ & \left. + B^{(-)}_2 u^{(-)}_2(\underline{r}_2) \; e^{-iK_{z2} z_2} \right) d^3\underline{r}_2 \end{aligned} \tag{2.75}$$

Upon expanding $I_{1'1}$ the first term is

$$B_{1'}^{(+)*} B_1^{(+)} \int u_{1'}^{(+)*}(\underline{r}_1)\, e^{i(\underline{K}_{\parallel 1} - K_{\parallel 1'} + \underline{q}_\parallel)\cdot \underline{p}_1}\, e^{i(K_{z1} - K_{z1'} + q_z) z_1}\, d^3\underline{r}_1 \qquad 2.76$$

Now expanding the Bloch periodic parts in a sum over reciprocal lattice vectors:

$$u(r) = \frac{1}{V_{CELL}^{\frac{1}{2}}} \sum_{\substack{G \\ \text{reciprocal lattice} \\ \text{vectors}}} C_{\underline{G}}\, e^{i\, \underline{G}.\underline{r}} \qquad 2.77$$

Then writing $d^3\underline{r}_1 \equiv d^2\underline{p}_1\, dz_1$, gives the first term as

$$\frac{B_1^{(+)*}\, B_1^{(+)}}{V_{\substack{UNIT \\ CELL}}} \int \sum_{\underline{G}_{1'}} \sum_{\underline{G}_1} C_{\underline{G}_{1'}}^{(+1')*}\, C_{\underline{G}_1}^{(+1)}\, e^{i(\underline{K}_1 - \underline{K}_{1'} + \underline{q}_\parallel + \underline{G}_{\parallel 1} - \underline{G}_{\parallel 1'})\cdot \underline{p}_1}\, e^{i(K_{z1} - K_{z1'} + q_z + G_{z1} - G_{z1'}) z_1}\, d^2\underline{p}_1\, dz_1 \qquad 2.78$$

Next carrying out the integral over $\underline{p}_1$ gives

$$(2\pi)^2 \frac{B_{1'}^{(+)*}\, B_1^{(+)}}{V_{\substack{UNIT \\ CELL}}} \int_0^L \sum_{\underline{G}_{1'}} \sum_{\underline{G}_1} C_{\underline{G}_{1'}}^{(+1')*}\, C_{\underline{G}_1}^{(+1)}\, \delta(\underline{K}_{\parallel 1} - \underline{K}_{\parallel 1'} + \underline{q}_\parallel + \underline{G}_{\parallel 1} - \underline{G}_{\parallel 1'})\, e^{i(K_{z1} - K_{z1'} + q_z + G_{z1} - G_{z1'})}\, dz_1 \qquad 2.79$$

Treating the other terms in $I_{11'}$ in the same way

$$I_{1'1} = \frac{(2\pi)^2}{} \int_0^L \sum_{\underline{G}_1} \sum_{\underline{G}_{1'}} \delta(\underline{K}_{\parallel 1} - \underline{K}_{\parallel 1'} + \underline{q}_{\parallel} + \underline{G}_{\parallel 1} - \underline{G}_{1'})$$

$$\left\{ \frac{B_1^{(+)*} B_1^{(+)}}{V_{\substack{\text{UNIT}\\\text{CELL}}}} C_{\underline{G}1'}^{(+1')*} C_{\underline{G}1}^{(+1)} e^{i(K_{z1} - K_{z1'} + q_z + G_{z1} - G_{z1'})} \right.$$

$$+ \frac{B_1^{(-)*} B_1^{(-)}}{V_{\substack{\text{UNIT}\\\text{CELL}}}} C_{\underline{G}1'}^{(-1')*} C_{\underline{G}1}^{(-1)} e^{i(K_{z1'} - K_{z1} + q_z + G_{z1} - G_{z1'})}$$

$$+ \frac{B_{1'}^{(+)*} B_1^{(-)}}{V_{\substack{\text{UNIT}\\\text{CELL}}}} C_{\underline{G}1'}^{(+1')*} C_{\underline{G}1}^{(-1)} e^{i(-K_{z1} - K_{z1'} + q_z + G_{z1} - G_{z1'})} \qquad 2.80$$

$$\left. + \frac{B_{1'}^{(-)*} B_1^{(+)}}{V_{\substack{\text{UNIT}\\\text{CELL}}}} C_{\underline{G}1'}^{(-1')*} C_{\underline{G}1}^{(+1)} e^{i(K_{z1'} + K_{z1} + q_z + G_{z1} - G_{z1'})} \right\} dz_1$$

or

$$I_{1'1} = \frac{(2\pi)^2}{} \int_0^L \sum_{\underline{G}_1} \sum_{\underline{G}_{1'}} \delta(\underline{K}_{\parallel 1} - \underline{K}_{\parallel 1'} + \underline{q}_{\parallel} + \underline{G}_{\parallel 1} - \underline{G}_{\parallel 1'}) \left\{ 1', 1, \underline{G}_{1'}, \underline{G}_1 \right\} dz_1 \qquad 2.81$$

where $\left\{ \quad \right\}$ has been introduced to simplify the expressions. Treating $I_{22'}$ in a similar way and substituting into $M_{12}$ gives

$$M_{12} = \frac{4\pi e^2}{\varepsilon_{INT}} \frac{2\pi}{A^2} \int \sum_{\underline{G}1} \sum_{\underline{G}1'} \sum_{\underline{G}2} \sum_{\underline{G}2'} \frac{\delta(\underline{K}_{\parallel 1} - \underline{K}_{\parallel 1'} + \underline{q}_{\parallel} + G_{\parallel 1} - \underline{G}_{\parallel 1'})}{q^2} \left\{ 1', 1, \underline{G}_{1'}, \underline{G}_1 \right\}$$

$$\delta(\underline{K}_{\parallel 2'} - \underline{K}_{\parallel 2} - \underline{q}_{\parallel} + \underline{G}_{\parallel 2} - \underline{G}_{\parallel 2'}) \left\{ 2', 2, \underline{G}_{2'}, \underline{G}_2 \right\} d\, z_1\, dz_2\, d^2\underline{q}_{\parallel} dq_z$$

$$M_{12} = \frac{4\pi e^2}{\varepsilon_{INT}} \frac{2\pi}{A} \int_{-\infty}^{+\infty}_{q_z} \int_{0}^{L}_{z_1} \int_{0}^{L}_{z_2} \sum_{\underline{G}_1} \sum_{\underline{G}_{1'}} \sum_{\underline{G}_2} \sum_{\underline{G}_{2'}}$$

$$\frac{\delta(\underline{K}''_1-\underline{K}''_{1'}+\underline{K}''_2-\underline{K}''_{2'}+\underline{G}''_1-\underline{G}''_{1'}+\underline{G}''_2-\underline{G}''_{2'})}{|\underline{K}''_1-\underline{K}''_{1'}+\underline{G}''_1-\underline{G}''_{1'}|^2 + q_z^2} \left\{1',1,\underline{G}_{1'},\underline{G}_1\right\}\left\{2',2,\underline{G}_{2'},\underline{G}_2\right\} dq_z\, dz_1\, dz_2 \qquad 2.82$$

Now since wavevectors of the states involved in the Auger transitions are small compared to the reciprocal lattice vectors , the delta function argument will only contribute if we choose

$$\underline{G}''_1-\underline{G}''_{1'} = \underline{G}''_2-\underline{G}''_{2'} \qquad 2.83$$

Also because of the denominator in Eq (2.82) the terms with

$$\underline{G}''_1-\underline{G}''_{1'} = 0 \qquad 2.84$$

in the summation are dominant and to a good approximation all other terms can be neglected.*

Similarly the terms which contribute most when the integrals over $z_1$ and $z_2$ are carried out are those for which $G_{z1} = G_{z1'}$ and $G_{z2} = G_{z2'}$. So using

$$\sum_{\underline{G}_1} C^{(+1')*}_{\underline{G}_1} C^{(+1)}_{\underline{G}_1} = \int_{\substack{\text{UNIT}\\\text{CELL}}} u^{(+)}_{1'}(\underline{r})u^{(+)}_1(\underline{r})\, d^3\underline{r} \qquad 2.85$$

$$= M^{++}_{1'1} \text{ say} \qquad 2.86$$



*see reference 2.9

and similar definitions for $M^{++}_{2'2}$, $M^{--}_{1'1}$, $M^{--}_{2'2}$, $M^{+-}_{1'1}$, $M^{+-}_{2'2}$, $M^{-+}_{1'1}$, and $M^{-+}_{2'2}$ we obtain

$$M_{12} = \frac{4\pi e^2}{\varepsilon_{INT}} \frac{2\pi}{A^2} \delta(\underline{K}_{\parallel 1} - \underline{K}_{\parallel 1} + \underline{K}_{\parallel 2'} - \underline{K}_{\parallel 2}) \int_{-\infty}^{\infty} \frac{1}{|\underline{K}_{\parallel 1'} - \underline{K}_{\parallel 1}|^2 + q_z^2} \left\{1, 1'\right\}\left\{2', 2\right\} dq_z \qquad 2.87$$

where

$$\left\{1', 1\right\} = \left\{ \frac{B^{(+)*}_{1'} B^{(+)}_{1}}{V_{\substack{UNIT\\CELL}}} M^{++}_{1'1} H(K_{z1} - K_{z1'} + q_z) + \frac{B^{(-)*}_{1'} B^{(-)}_{1}}{V_{\substack{UNIT\\CELL}}} M^{--}_{1'1} H(K_{z1'} - K_{z1} + q_z) \right.$$

$$\left. + \frac{B^{(+)*}_{1'} B^{(-)}_{1}}{V_{\substack{UNIT\\CELL}}} M^{+-}_{1'1} H(-K_{z1} - K_{z1'} + q_z) + \frac{B^{(-)*}_{1'} B^{(+)}_{1}}{V_{\substack{UNIT\\CELL}}} M^{-+}_{1'1} H(K_{z1'} + K_{z1} + q_z) \right\} \qquad 2.88$$

$$\left\{2', 2\right\} = \left\{ \frac{B^{(+)*}_{2'} B^{(+)}_{2}}{V_{\substack{UNIT\\CELL}}} M^{++}_{2'2} H(K_{z2} - K_{z2'} - q_z) + \frac{B^{(-)*}_{2'} B^{(-)}_{2}}{V_{\substack{UNIT\\CELL}}} M^{--}_{2'2} H(K_{z2'} - K_{z2} - q_z) \right.$$

$$\left. + \frac{B^{(+)*}_{2'} B^{(-)}_{2}}{V_{\substack{UNIT\\CELL}}} M^{+-}_{2'2} H(-K_{z2} - K_{z2'} - q_z) + \frac{B^{(-)*}_{2'} B^{(+)}_{2}}{V_{\substack{UNIT\\CELL}}} M^{-+}_{2'2} H(K_{z2'} + K_{z2} - q_z) \right\} \qquad 2.89$$

and

$$H(x) = \int_0^L e^{ixz} dz = \frac{2 \sin \frac{xL}{2} e^{i \frac{xL}{2}}}{x} \qquad 2.90$$

From which (2.87) the delta function $\delta(\underline{K}_{\parallel 1}' - \underline{K}_{\parallel 1} + \underline{K}_{\parallel 2}' - \underline{K}_{\parallel 2})$ requires that in-plane momentum is conserved. For wavevectors perpendicular to the plane of the well however the dependence of the matrix element on these wavevectors is more complex depending on the behaviour of function H and on the overlap integrals between the periodic parts of the Bloch functions involved.

**REFERENCES FOR CHAPTER 2**


2.1 Schiff L I Quantum Mechanics 3rd. edition

2.2 Dutta N K 1983 J. Appl. Phys 53(3) 1236.

2.3 Sugimura A 1981 IEEE J. Quantum Electron. QE-17 627

2.4 Landsberg P T 1965 Lectures in Theoretical Physics, Boulder Vol. 8A Ed. Brittin W E.

2.5 Takeshima M 972 J. Appl. Phys 43 4114.

2.6 Abram R A, Childs G, and Saunderson P 1984 J. Phys. C Vol 17 6105.

2.7 Burt M G 1981 J. Phys C: Solid State Phys. 14 3269.

2.8 Haug A 1983 Appl. Phys. Lett 432(6) 512.

2.9 Brand S and Abram R A 1984 J. Phys. C: Solid State Phys., 17 L571-L574.

## CHAPTER 3 - AUGER TRANSITIONS BETWEEN BOUND STATES

This Chapter extends the analysis of Chapter 2 and specifically develops the theory for Auger recombination transitions between bound states. First the matrix element is examined and then the summation in Fermi's golden rule is performed and an analytical expression for the Auger recombination rate between bound states obtained.

### 3.1 MATRIX ELEMENT IN THE COMMON OVERLAP APPROXIMATION

The matrix element expressions 2.87, 2.88 and 2.89 may be evaluated numerically. However, a simple analytical expression in K (where $K = |\underline{K}_{\parallel'} - \underline{K}_{\parallel}|$ ) is required if an algebraic expression for the Auger rate between bound states is to be obtained. Therefore we make the approximation in the matrix element of neglecting* the perpendicular wavevector dependence of the periodic parts of the Bloch functions. This approximation being hence forth be referred to as the common overlap approximation.

Taking in 2.86-2.89

$$M^{+-}_{2'2} = M^{-+}_{2'2} = M^{++}_{2'2} = M^{--}_{2'2} \simeq 1 \qquad 3.1$$

$$M^{+-}_{1'1} = M^{-+}_{1'1} = M^{++}_{1'1} = M^{--}_{1'1} \equiv M_{BF} \text{ when } \frac{KL}{(n_1+n_1')\pi} \gg 1 \qquad 3.2$$



*see section 3.1.4

from an effective mass sum rule expression such as Beattie and Smith's (ref 3.1). Equation 2.57 gives $B^{(\pm)} = \mp i\, V^{\frac{1}{2}}_{\substack{UNIT\\CELL}} \left(\frac{1}{2L}\right)^{\frac{1}{2}}$ and it follows that

$$M_{12} = \frac{4\pi e^2}{\varepsilon_{INT}} M_{BF} \left(\frac{2\pi}{A^2}\right) \delta(K_{\parallel 1'} - K_{\parallel 1} + K_{\parallel 2'} - K_{\parallel 2})\, I_b' \qquad 3.3$$

where

$$I_b' = \left(\frac{2}{L}\right)^2 \int \frac{1}{K^2 + q_z^2} \sin\frac{n_1\pi}{L} z_1 \sin\frac{n_{1'}\pi}{L} z_1\, e^{iq_z z_1} \sin\frac{n_2\pi}{L} z_2 \sin\frac{n_{2'}\pi}{L} z_2\, e^{-iq_z z_2}\, dz_1 dz_2 dq_z \qquad 3.4$$

$I_b'$ being essentially the integral of the envelope parts of the wavefunctions and the coulombic interaction.

### 3.1.1 AN EXACT ANALYTIC EXPRESSION FOR THE MATRIX ELEMENT WITHIN THE COMMON OVERLAP APPROXIMATION

The integration in 3.4 w.r.t. $q_z$ can now easily be performed using Jordans Lemma. One obtains

$$I_b' = \left(\frac{2}{L}\right)^2 \int_0^L \frac{\pi}{K} e^{-Kz_1} \sin \frac{n_1\pi}{L} z_1 \sin \frac{n_{1'}\pi}{L} z_1 \int_0^{z_1} e^{+Kz_2} \sin \frac{n_2\pi}{L} z_2 \sin \frac{n_{2'}\pi}{L} z_2 \, dz_2 dz_1$$

$$+ \left(\frac{2}{L}\right)^2 \int_0^L \frac{\pi}{K} e^{+Kz_1} \sin \frac{n_1\pi}{L} z_1 \sin \frac{n_{1'}\pi}{L} z_1 \int_{z_1}^{L} e^{-Kz_2} \sin \frac{n_2\pi}{L} z_2 \sin \frac{n_{2'}\pi}{L} z_2 \, dz_2 dz_1 \qquad 3.5$$

Writing

$$\sin n_2\frac{\pi}{L} z_2 \sin n_{2'}\frac{\pi}{L} z_2 = \frac{\cos (n_2-n_{2'})\frac{\pi}{L} z_2 - \cos (n_2+n_{2'})\frac{\pi}{L} z_2}{2} \qquad 3.6$$

and using Gradshteyn and Ryzhik (ref 3.2) (hereafter referred to as G+R) page 196 eq 2.663.3

$$\int_0^{z_1} \frac{\pi}{K} e^{+Kz_2} \sin \frac{n_2\pi}{L} z_2 \sin \frac{n_{2'}\pi}{L} z_2 \, dz_2$$

$$= \frac{\pi}{2K}\left[\frac{e^{+Kz_1}}{K^2 + (\frac{\pi}{L}(n_2-n_{2'}))^2} \left\{K \cos (n_2-n_{2'})\frac{\pi}{L} z_1 + \frac{\pi}{L}(n_2-n_{2'}) \sin (n_2-n_{2'})\frac{\pi}{L} z_1\right\}\right]$$

$$- \frac{\pi}{2K}\left[\frac{e^{+Kz_1}}{K^2 + (\frac{\pi}{L}(n_2+n_{2'}))^2} \left\{K \cos (n_2+n_{2'})\frac{\pi}{L} z_1 + \frac{\pi}{L}(n_2+n_{2'}) \sin (n_2+n_{2'})\frac{\pi}{L} z_1\right\}\right]$$

$$+ \frac{\pi}{2K}\left[\frac{-K}{K^2 + (\frac{\pi}{L}(n_2-n_{2'}))^2}\right] + \frac{\pi}{2K}\left[\frac{K}{K^2 + (\frac{\pi}{L}(n_2+n_{2'}))^2}\right] \qquad 3.7$$

similarly

$$\int_{z_1}^{L} \frac{\pi}{K} e^{-Kz_2} \sin \frac{n_2\pi}{L} z_2 \sin \frac{n_{2'}\pi}{L} z_2 \, dz_2$$

$$= \frac{\pi}{2K}\left[\frac{e^{-KL}}{K^2+(\frac{\pi}{L}(n_2-n_{2'}))^2}\left\{-K\cos(n_2-n_{2'})\pi\right\}\right] - \frac{\pi}{2K}\left[\frac{e^{-KL}}{K^2+(\frac{\pi}{L}(n_2+n_{2'}))^2}\left\{-K\cos(n_2+n_{2'})\right\}\right]$$

$$- \frac{\pi}{2K}\left[\frac{e^{-Kz_1}}{K^2+(\frac{\pi}{L}(n_2-n_{2'}))^2}\left\{-K\cos(n_2-n_{2'})\frac{\pi}{L}z_1 + \frac{\pi}{L}(n_2-n_{2'})\sin\frac{\pi}{L}(n_2-n_{2'})z_1\right\}\right]$$

$$+ \frac{\pi}{2K}\left[\frac{e^{-Kz_1}}{K^2+(\frac{\pi}{L}(n_2+n_{2'}))^2}\left\{-K\cos(n_2+n_{2'})\frac{\pi}{L}z_1 + \frac{\pi}{L}(n_2+n_{2'})\sin\frac{\pi}{L}(n_2+n_{2'})z_1\right\}\right]$$

3.8

Now writing $A = (n_2 - n_{2'})\frac{\pi}{L}$ , $B = (n_2 + n_{2'})\frac{\pi}{L}$ , and

$$\sin \frac{n_1\pi}{L} z_1 \sin \frac{n_{1'}\pi}{L} z_1 = \frac{\cos(n_1-n_{1'})\frac{\pi}{L}z_1 - \cos(n_1+n_{1'})\frac{\pi}{L}z_1}{2} \qquad 3.9$$

gives

$$I_b' = \left(\frac{2}{L}\right)^2 \frac{\pi}{4K} \int_0^L \mp \cos(n_1 \pm n_{1'})\frac{\pi}{L}z_1 \left(\frac{2K\cos Az_1}{A^2+K^2} - \frac{2K\cos Bz_1}{B^2+K^2}\right)$$

$$\mp \cos(n_1 \pm n_{1'})\frac{\pi}{L}z_1 \left(\frac{-K}{A^2+K^2} + \frac{K}{B^2+K^2}\right) e^{-Kz_1}$$

$$\mp \cos(n_1 \pm n_{1'})\frac{\pi}{L}z_1 \left(\frac{-K\cos AL}{A^2+K^2} + \frac{K\cos BL}{B^2+K^2}\right) e^{K(z_1-L)} \, dz_1 \qquad 3.10$$

where first all the top and then all bottom signs are taken. Finally from

$$\int_0^{\pi} \cos nx \cos mx dx = \delta n, m \frac{\pi}{2} \qquad n = m \neq 0 \qquad 3.11$$

and

$$\int_0^{\pi} \cos nx \cos mx \, dx = \pi \qquad n = m = 0 \qquad 3.12$$

we get an exact expression within the common overlap approximation (neglect of perpendicular wavevectors in the periodic parts of the Bloch functions)

$$I_b' = \left(\frac{2}{L}\right)^2 \left( \frac{\mp \frac{\pi L}{4} \delta|n_1 \pm n_{1'}|, |n_2 - n_{2'}| \; (1 + \delta n_1 \pm n_{1'}, 0)}{A^2 + K^2} \right.$$

$$\frac{\pm \frac{\pi L}{4} \delta|n_1 \pm n_{1'}|, |n_2 + n_{2'}|}{B^2 + K^2}$$

$$\mp \frac{\pi K/4}{((n_1 \pm n_{1'})\frac{\pi}{L})^2 + K^2} \left\{ \frac{+e^{-KL} (-1)^{n_1 \pm n_{1'}} - 1}{A^2 + K^2} + \frac{-e^{-KL} (-1)^{n_1 \pm n_{1'}} + 1}{B^2 + K^2} \right\}$$

$$\left. \pm \frac{\pi K/4 \; (-1)^{n_2 - n_{2'}}}{((n_1 \pm n_{1'})\frac{\pi}{L})^2 + K^2} \left\{ \frac{-e^{-KL} (-1)^{n_1 \pm n_{1'}} + 1}{A^2 + K^2} + \frac{+e^{-KL} (-1)^{n_1 \pm n_{1'}} - 1}{B^2 + K^2} \right\} \right)$$

3.13

### 3.1.3 ASYMPTOTIC EXPRESSIONS

Expression 3.13 is still too complex to allow the calculation to proceed analytically. Therefore further approximations need to be considered.

In this section both large KL and small KL approximations to 3.13 are considered. The small KL expressions obtained are obviously suspect because of the condition in Eq (3.3) ie the requirement for the common overlap approximation to be valid. However they are still included because like the large KL approximations they provide important checks on the analysis in Chapter 4. The large KL and small KL approximations are then both checked, because of their importance, in a number of ways. These checks being relegated to Appendix 2 because, although they are referred to later during similar checks in Chapter 4, they may be omitted on a first reading.

**THE APPROXIMATIONS TO $I_b'$**

a) FOR LARGE KL

When KL >> $(n_1+n_{1'})\frac{\pi}{L}$ , KL >> $(n_2+n_{2'})\frac{\pi}{L}$ then 3.13 becomes

$$I_b' = \frac{\pi}{K^2L}\Big[\delta|n_1-n_{1'}|,|n_2-n_{2'}|(1+\delta n_1-n_{1'},0)-\delta|n_1+n_{1'}|,|n_2-n_{2'}|-\delta|n_1-n_{1'}|,$$
$$|n_2+n_{2'}| + \delta|n_1+n_{1'}|,|n_2+n_{2'}|\Big] \qquad 3.14$$

which gives a simple expression for $I_b'$ . The numerical results from which are tabulated in Table 3.1 for processes involving the first three heavy hole sub-bands and the first three conduction sub-bands.

**STATE SUB-BANDS**

| N1 | N1' | N2 | N2' | $I_b'/\left(\frac{\pi}{K^2L}\right)$ |
|---|---|---|---|---|
| 1 | 1 | 1 | 1 | 3 |
| 1 | 1 | 1 | 2 | 0 |
| 1 | 1 | 1 | 3 | -1 |
| 1 | 1 | 2 | 1 | 0 |
| 1 | 1 | 2 | 2 | 2 |
| 1 | 1 | 2 | 3 | 0 |
| 1 | 1 | 3 | 1 | -1 |
| 1 | 1 | 3 | 2 | 0 |
| 1 | 1 | 3 | 3 | 2 |
| 1 | 2 | 1 | 1 | 0 |
| 1 | 2 | 1 | 2 | 2 |
| 1 | 2 | 1 | 3 | 0 |
| 1 | 2 | 2 | 1 | 2 |
| 1 | 2 | 2 | 2 | 0 |
| 1 | 2 | 2 | 3 | 1 |
| 1 | 2 | 3 | 1 | 0 |
| 1 | 2 | 3 | 2 | 1 |
| 1 | 2 | 3 | 3 | 0 |
| 1 | 3 | 1 | 1 | -1 |
| 1 | 3 | 1 | 2 | 0 |
| 1 | 3 | 1 | 3 | 2 |
| 1 | 3 | 1 | 1 | 0 |
| 1 | 3 | 2 | 2 | 1 |
| 1 | 3 | 2 | 3 | 0 |
| 1 | 3 | 3 | 1 | 2 |
| 1 | 3 | 3 | 2 | 0 |
| 1 | 3 | 3 | 3 | 0 |
| 2 | 1 | 1 | 1 | 0 |
| 2 | 1 | 1 | 2 | 2 |
| 2 | 1 | 1 | 3 | 0 |
| 2 | 1 | 2 | 1 | 2 |
| 2 | 1 | 2 | 2 | 0 |
| 2 | 1 | 2 | 3 | 1 |
| 2 | 1 | 3 | 1 | 0 |
| 2 | 1 | 3 | 2 | 1 |
| 2 | 1 | 3 | 1 | 0 |
| 2 | 1 | 3 | 2 | 1 |
| 2 | 1 | 3 | 3 | 0 |
| 2 | 2 | 1 | 1 | 2 |
| 2 | 2 | 1 | 2 | 0 |
| 2 | 2 | 1 | 3 | 1 |
| 2 | 2 | 2 | 1 | 0 |
| 2 | 2 | 2 | 2 | 3 |
| 2 | 2 | 2 | 3 | 0 |
| 2 | 2 | 3 | 1 | 1 |
| 2 | 2 | 3 | 2 | 0 |
| 2 | 2 | 3 | 3 | 2 |
| 2 | 3 | 1 | 1 | 0 |
| 2 | 3 | 1 | 2 | 1 |
| 2 | 3 | 1 | 3 | 0 |

| | | | | |
|---|---|---|---|---|
| 2 | 3 | 2 | 1 | 1 |
| 2 | 3 | 2 | 2 | 0 |
| 2 | 3 | 2 | 3 | 2 |
| 2 | 3 | 3 | 1 | 0 |
| 2 | 3 | 3 | 2 | 2 |
| 2 | 3 | 3 | 3 | 0 |
| 3 | 1 | 1 | 1 | -1 |
| 3 | 1 | 1 | 2 | 0 |
| 3 | 1 | 1 | 3 | 2 |
| 3 | 1 | 2 | 1 | 0 |
| 3 | 1 | 2 | 2 | 1 |
| 3 | 1 | 2 | 3 | 0 |
| 3 | 1 | 3 | 1 | 2 |
| 3 | 1 | 3 | 2 | 0 |
| 3 | 1 | 3 | 3 | 0 |
| 3 | 2 | 1 | 1 | 0 |
| 3 | 2 | 1 | 2 | 1 |
| 3 | 2 | 1 | 3 | 0 |
| 3 | 2 | 2 | 1 | 1 |
| 3 | 2 | 2 | 2 | 0 |
| 3 | 2 | 2 | 3 | 2 |
| 3 | 2 | 3 | 1 | 0 |
| 3 | 2 | 3 | 2 | 2 |
| 3 | 2 | 3 | 3 | 0 |
| 3 | 3 | 1 | 1 | 2 |
| 3 | 3 | 1 | 2 | 0 |
| 3 | 3 | 1 | 3 | 0 |
| 3 | 3 | 2 | 1 | 0 |
| 3 | 3 | 2 | 2 | 2 |
| 3 | 3 | 2 | 3 | 0 |
| 3 | 3 | 3 | 1 | 0 |
| 3 | 3 | 3 | 2 | 0 |
| 3 | 3 | 3 | 3 | 3 |

b) FOR SMALL KL

Here Eq (3.13) can be rewritten as

$$I_b' = \left(\frac{2}{L}\right)^2 \left( \frac{1}{A^2+K^2} \left\{ \mp \frac{\pi L}{4} \delta|n_1 \pm n_{1'}|, |n_2 - n_{2'}| \; (1+\delta n_1 \pm n_{1'}, 0) \right.\right.$$

$$\mp \frac{\frac{\pi K}{4}}{((n_1 \pm n_{1'})\frac{\pi}{L})^2 + K^2} \; (+e^{-KL}(-1)^{n_1 \pm n_{1'}} - 1) \; (1+(-1)^{n_2 - n_{2'}} \Big\}$$

$$+ \frac{1}{B^2+K^2} \left\{ \pm \frac{\pi L}{4} \delta|n_1 \pm n_{1'}|, |n_2 + n_{2'}| \right.$$

$$\left.\left. \mp \frac{\frac{\pi K}{4}}{((n_1 \pm n_{1'})\frac{\pi}{L})^2 + K^2} \; (-e^{-KL}(-1)^{n_1 \pm n_{1'}} + 1) \; (1 + (-1)^{n_2 - n_{2'}}) \right\} \right) \qquad 3.15$$

From which when $KL << 1$, $A^2 = (n_2 - n_{2'})^2 \frac{\pi^2}{L^2}$ and $B^2 = (n_2 + n_{2'})^2 \frac{\pi^2}{L^2}$ are much larger than $K^2$ except when $n_2 - n_{2'} = 0$ in which case the terms involving $(A^2 + K^2)^{-1}$ dominate and

$$I_{b_{n_2=n_{2'}}}' \simeq \frac{4}{L^2K^2} \left\{ + \frac{2\pi L}{4} \delta n_1 - n_{1'}, 0 \mp \frac{\frac{\pi K}{4}}{((n_1 \pm n_{1'})\frac{\pi}{L}^2 + K^2} \; (e^{-KL}(-1)^{n_1 \pm n_{1'}} - 1 \right\} \qquad 3.16$$

Given additionally that $n_1 - n_{1'} = 0$ then

$$I_{b_{n_2=n_{2'}, n_1=n_{1'}}}' \simeq \frac{4}{L^2K^2} \left\{ \frac{\pi L}{2} + \frac{\pi}{2K} \; (-KL + \frac{K^2L^2}{2} \; \ldots\ldots) \right\} \qquad 3.17$$

$$\simeq \frac{\pi}{K} \qquad 3.18$$

This (3.18), like 3.14, has a sufficiently simple form to allow the calculation to continue analytically. But before doing so however 3.14 and 3.16 are checked (see Appendix 2), and compared to both the full expression (2.87-2.89), and the common overlap approximation expression 3.13.

### 3.1.4 COMPARISON OF THE COMMON OVERLAP APPROXIMATION WITH THE FULL MATRIX ELEMENT EXPRESSION

Figures 3.1, 3.2, and 3.3 compare the above approximations to the integral in 2.87 with the full expression. Fig 3.1 makes the comparisons for the important first sub-band process. Fig 3.2 makes the comparisons for an example of a processes where $n_1 - n_{1'}$ is odd, namely the process where the colliding electrons are in the first conduction sub-band, the promoted (Auger) electron is in the second conduction sub-band, and the hole is in the second heavy hole sub-band. And Fig 3.3 makes the comparisons for an example of a process where $n_1 - n_{1'}$ is even and non-zero, namely the process where the colliding electrons are in the first conduction sub-band, the promoted (Auger) electron is in the third sub-band, and the hole is in the first heavy hole sub-band.

Anticipating the uncertainty in the factor multiplying the wavevector dependence of the overlap integrals between the periodic parts of the conduction and heavy-hole band wavefunctions (see Chapter 6), figures 3.1, 3.2, and 3.3 plot the integral divided by this multiplying factor. The size of which, when estimated conventionally (see for example ref 3.1) varies slightly with well width.

FIGURE 3.1

This figure compares the integral approximations of section 3.1 with the full integral expression in equation 2.87 with 2.88, 2.89 and 2.90, for the first sub-band process (see insert) in a 1.3 μm InGaAsP/InP QW system where the band gap between the first sub-bands is kept constant at 0.96 eV, and K is taken (anticipating 3.46) as

$$\sqrt{(E_{c1} - E_{v1'} + E_{c2} - E_{c2'}) \frac{2m^*_c}{\hbar^2} \frac{(\mu+1)}{(2\mu+1)}}$$

where $\mu = \frac{m^*_c}{m^*_v}$

——— indicates the full solution

—·— indicates the exact solution within the common overlap approximation (ie expression 3.13)

- - - - - indicates the large KL approximation to 3.13 (ie $\frac{3\pi}{KL}$ from expression 3.14)

..... indicates the small KL approximation to 3.13 (ie $\pi$ from 3.18)

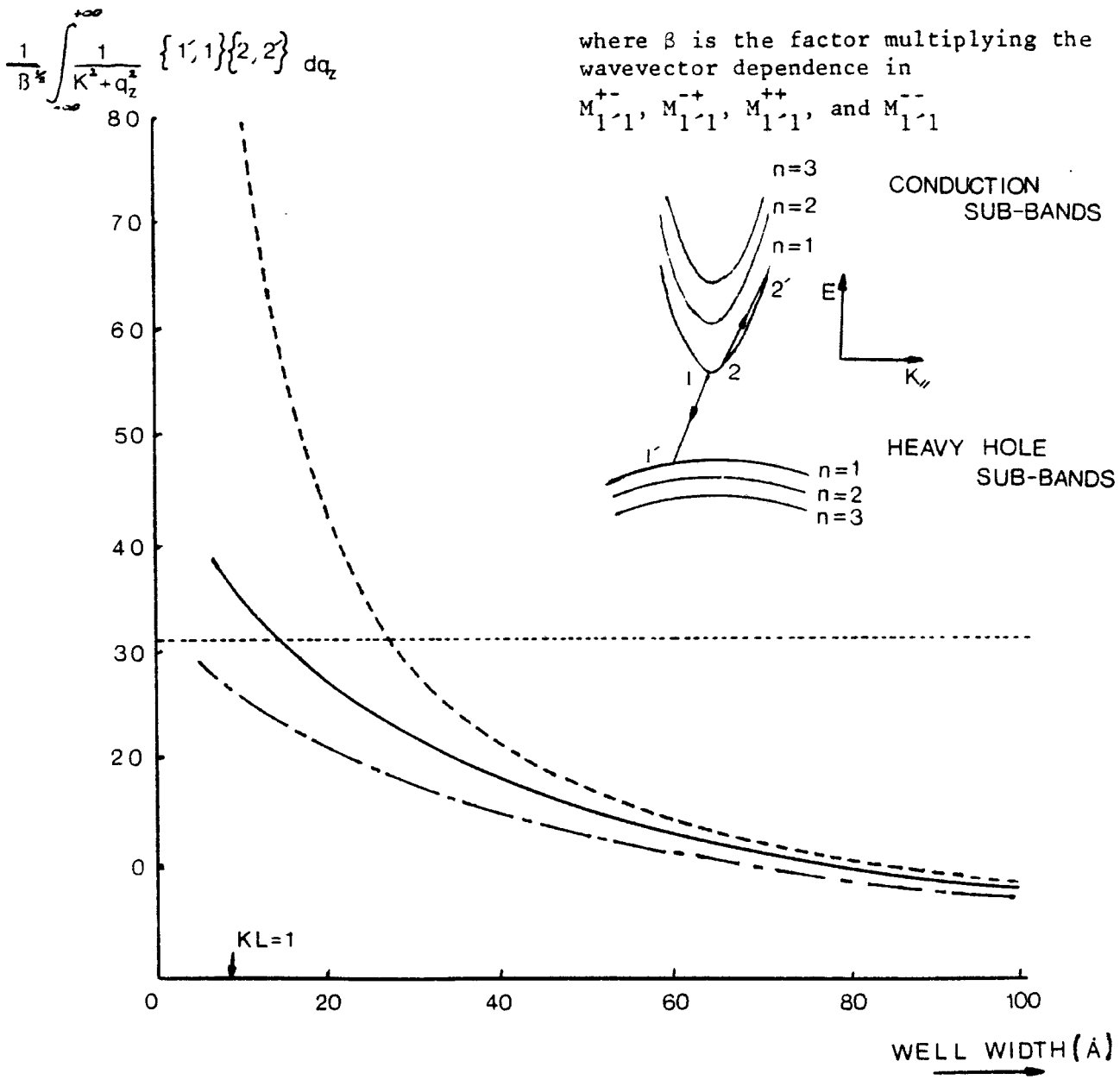

FIGURE 3.2

As figure 3.1 but for the processes where the colliding electrons are in the first sub-band, the promoted (Auger) electron is in the second sub-band, and the heavy hole is in the second heavy hole sub-band. (see insert)

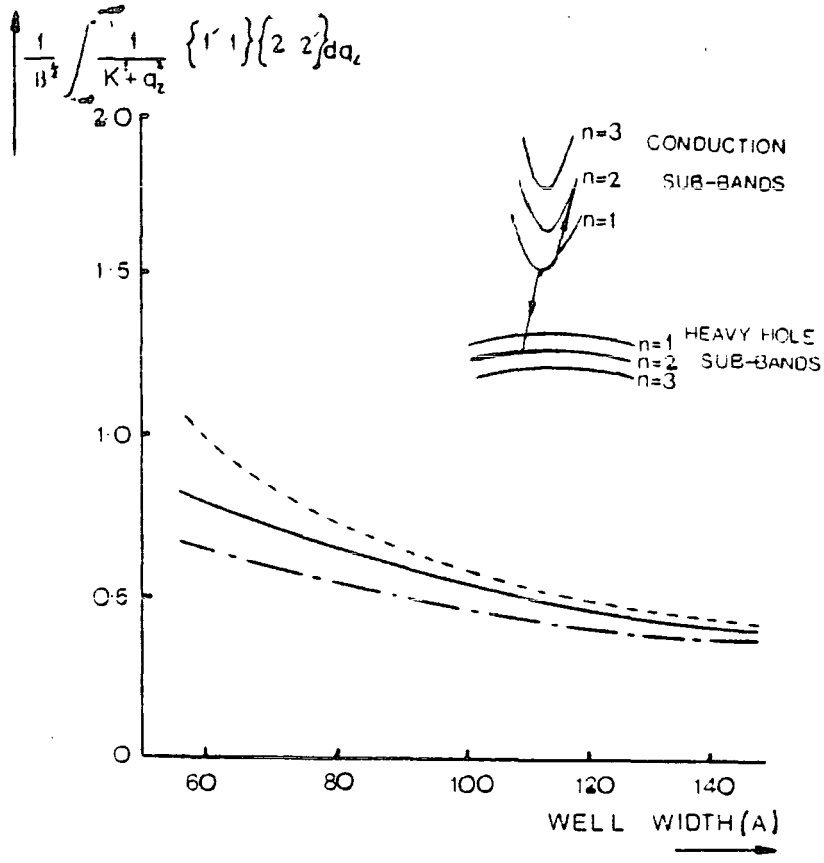


FIGURE 3.3

As figure 3.1 but for the processes where the colliding electrons are in the first sub-band, the promoted (Auger) electron is in the third sub-band, and the heavy hole in the first heavy hole sub-band (see insert)

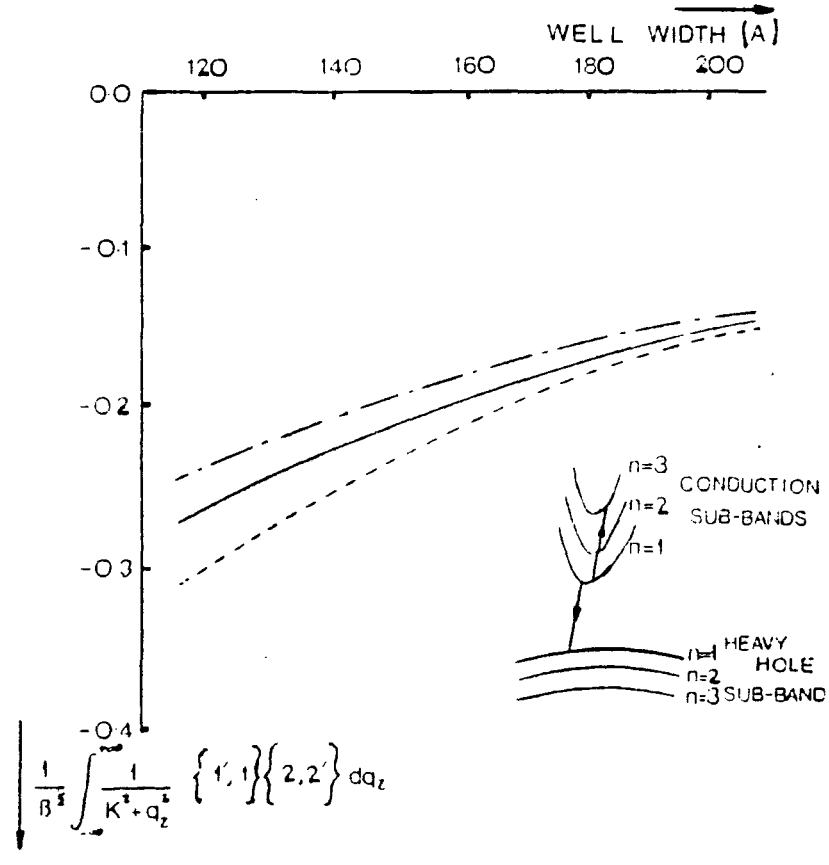

The plots are for the 1.3 μm InP/InGaAsP system in which the InGaAsP composition is varied so as to keep the band gap between the first conduction and first heavy hole sub-band constant at 0.96 eV. From these plots, and the importance on statistical grounds of the first sub-band process (see Section 2.3.2 and Chapter 5), it is seen that the large KL, common overlap approximation (ie expressions 3.14) gives reasonable results for well widths of 60Å and above. Therefore expression 3.14 is used for the remainder of the calculation.

## 3.2 THE SUMMATION OVER ALL BOUND STATES

The Auger recombination rate was given in Chapter 2 (eq 2.7 ) as

$$R = \frac{2\pi}{\hbar} \Sigma P |\langle \psi_{\substack{\text{INITIAL SYSTEM}\\ \text{STATE}}} | H'' | \psi_{\substack{\text{FINAL SYSTEM}\\ \text{STATE}}} \rangle|^2 \delta(E) \qquad 3.19$$

Using the statistical factor P given by eq 2.15 and the matrix element from 2.34 where M is given by 3.3

$$R_b = \frac{1}{A.L} \frac{2\pi}{\hbar} \sum_{\substack{n_1 n_{1'} \\ n_2 n_{2'}}} \sum_{\substack{\underline{K}''_1 \underline{K}''_{1'} \\ \underline{K}''_2 \underline{K}''_{2'}}} e^{-(E_{2'}-E_{c2'})/x_B T_c} \frac{N_{2'}}{\bar{N}_c} \left( \frac{N_1}{N_{01}} \frac{N_2}{N_{02}} \frac{P_{1'}}{P_{01'}} \frac{N_{02'}}{N_{2'}} - 1 \right) \qquad 3.20$$

$$(2+2\delta n_1 n_2) \left(\frac{4\pi e^2}{\varepsilon_{INT}}\right)^2 M_{BF}^2 I_b'^2 \left(\frac{2\pi}{A}\right)^2 \delta(\underline{K}''_{1'} - \underline{K}''_1 + \underline{K}''_{2'} - \underline{K}''_2)\ \delta(\underline{K}''_{1'} - \underline{K}''_1 + \underline{K}''_{2'} - \underline{K}''_2)\ \delta(E)$$

where '$R_b$' is the total bound sub-band to bound sub-band CHCC Auger recombination rate per unit volume. $n_{1'}, n_{2'}, n_2$, and $n_1$ are summed over all appropriate bound sub-bands. $\underline{K}''_1$, $\underline{K}''_2$, and $\underline{K}''_{2'}$ are summed, for each bound conduction sub-band, over all wavevectors in the plane of the well, and $\underline{K}''_{1'}$ is summed, for each bound heavy-hole sub-band, over all wavevectors in the plane of the well.

Converting the summations over $\underline{K}''_1$, $\underline{K}''_{1'}$, $\underline{K}''_2$, and $\underline{K}''_{2'}$ to integrals, and changing $\delta(\underline{K}''_{1'} - \underline{K}''_1 + \underline{K}''_{2'} - \underline{K}''_2)$ $\delta(\underline{K}''_{1'} - \underline{K}''_1 + \underline{K}''_{2'} - \underline{K}''_2)$ to $\frac{A}{(2\pi)^2} \delta(\underline{K}''_{1'} - \underline{K}''_1 + \underline{K}''_{2'} - \underline{K}''_2)$ in the normal way gives

$$R_b = \frac{1}{L} \frac{2\pi}{\hbar} \sum_{\substack{n_1 n_{1'} \\ n_2 n_{2'}}} 4 . \left(\frac{4\pi e^2}{\varepsilon_{INT}}\right)^2 \frac{1}{(2\pi)^8} \frac{N_{2'}}{\bar{N}_c} \left( \frac{N_1}{N_{01}} \frac{N_2}{N_{02}} \frac{P_{1'}}{P_{01'}} \frac{N_{02}}{N_{02'}} - 1 \right) Q \qquad 3.21$$

where

$$Q = \int M_{BF}^2(\underline{K}_{1'}-\underline{K}_1) I_b'^2(\underline{K}_{1'}-\underline{K}_1)\, e^{-(E_{2'}-E_{c2'})/x_B T_c}$$

$$\delta(\underline{K}''_{1'}-\underline{K}''_1+\underline{K}''_{2'}-\underline{K}''_2)\delta(E) d^2\underline{K}''_1 d^2\underline{K}''_{1'} d^2\underline{K}''_2 d^2\underline{K}''_{2'} \qquad 3.22$$

These integrals are now evaluated.

In eq (3.22) carrying out the integral over $\underline{K}''_{2'}$ first gives

$$Q = \int M_{BF}^2(\underline{K}) I_b'^2(K) e^{-(E_{2'}-E_{c2'})/x_B T_c}\ \delta(E)\ d^2\underline{K}\ d^2\underline{K}''_{1'}\ d^2\underline{K}''_2 \qquad 3.23$$

where $\underline{K} = \underline{K}''_1 - \underline{K}''_{1'}$ 3.24

Now expressing $\underline{K}$ in polars coordinates $(K, \theta)$, and $\underline{K}_{1'}$ and $\underline{K}_2$ in cartesian coordinates ($x_{1'}, y_{1'}$ respectively) with $y_1$ and $y_2$ being taken to lie along $\underline{K}$ we can write

$$E_i = E_{ci} + \alpha K''^2_i \quad \text{for } i = 1,2, \text{ and } 2' \text{ where } \alpha = \frac{\hbar^2}{2m_c} \qquad 3.25$$

and

$$E_{1'} = E_{v1'} - \mu\alpha K''^2_{1'} \quad \text{where } \mu = m_c/m_v \qquad 3.26$$

Therefore

$$E_{2'} = E_{c2'} + \alpha(\underline{K}''_1+\underline{K}''_2-\underline{K}''_{1'})^2 = E_{c2'} + \alpha(\underline{K}+\underline{K}''_2)^2$$

$$E_{2'} - E_{c2'} = \alpha(x_2^2+(K+Y_2)^2) \qquad 3.27$$

Also

$$-E = E_1 - E_2 - E_{1'} - E_{2'}$$

$$= E_{c1} - E_{c2} - E_{v1} - E_{c2'} + \alpha(\mu K''^2_1 - K''^2_{2'} + K_1{}^2 + K_2{}^2)$$

$$= \Delta E + \alpha(\mu K''^2_{1'} - (\underline{K}''_1 + \underline{K}''_2 - \underline{K}''_{1'})^2 + K_1{}^2 + K_2{}^2) \qquad 3.28$$

where

$$\Delta E = E_{c1} + E_{c2} - E_{v1'} - E_{c2'} \qquad 3.29$$

Now

$$(\underline{K}''_1 + \underline{K}''_2 - \underline{K}''_{1'})^2 = K''^2_1 + K''^2_2 + K''^2_{1'} + 2(\underline{K}''_1 . \underline{K}''_2) - 2(\underline{K}''_1 . \underline{K}''_1) - 2(\underline{K}''_2 . \underline{K}''_{1'}) \qquad 3.30$$

therefore

$$-E = \Delta E + \alpha\ (\mu-1)K''^2_{1'} - 2(\underline{K}''_1 . \underline{K}''_2) + 2(\underline{K}''_1 . \underline{K}''_{1'}) + 2(\underline{K}''_2 . \underline{K}''_{1'})$$

$$= \Delta E + \alpha\ (\mu+1)K''^2_{1'} + 2(\underline{K}.(\underline{K}''_{1'} - \underline{K}''_2)) \quad \text{since } \underline{K} = \underline{K}''_1 - \underline{K}''_{1'}$$

$$= \Delta E + \alpha\ (\mu+1)(x^2_{1'} + y^2_{1'}) + 2\ \alpha\ K(y_{1'} - y_2) \qquad 3.31$$

and hence

$$Q = \int M^2_{BF}(\underline{K}) I^2_b(K) e^{-\alpha(x^2_2 + (K+Y_2)^2)/x_B T_c}\ \delta(\alpha(\mu+1)(x^2_{1'} + y^2_{1'}) + 2\alpha K(y_{1'} - y_2) + \Delta E)$$

$$K d\theta dK dx_{1'} dy_{1'} dx_2 dy_2 \qquad 3.32$$

The integration over $\theta$ is trivial if $M_{BF}$ is taken to be independent of $\theta$, and gives

$$Q = 2\pi \int M^2_{BF}(K) I^2_b(K) e^{-\alpha(x_2 + (K+y_2)^2)/x_B T_c}\ \delta(\alpha(\mu+1)(x^2_{1'} + y^2_{1'}) + 2\alpha K(y_{1'} - y_2) + \Delta E)\ K dK dx_{1'} dy_{1'} dx_2 dy_2 \qquad 3.33$$

The important contributions to the $x_2$ integral come from a small region well away from the boundary of the Brillouin Zone and therefore its limits can be extended to infinity. Do so the integration over $x_2$ becomes Guassian giving

$$\int_{-\infty}^{+\infty} e^{-\alpha x_2/x_B T_c}\, dx_2 = 2\int_{0}^{\infty} e^{-\alpha x_2/x_B T_c}\, dx_2 = \sqrt{\frac{\pi\, x_B T_c}{\alpha}} \qquad 3.34$$

Now the integral over $x_{1'}$ is considered. Using

$$\int_{-\infty}^{\infty} \delta(f(x))dx = \sum_i \frac{\delta(x-x_i)}{\left|\frac{df}{dx}\right|_i} \quad \text{with the i's as the roots of } f(x) \qquad 3.35$$

gives

$$\int_{-\infty}^{\infty} \delta(\alpha(\mu+1)x_{1'}^2 - D)dx_1 = \frac{1}{\sqrt{D}\,\sqrt{\alpha(\mu+1)}} \qquad 3.36$$

where

$$x_{1'i} = \pm\sqrt{\frac{D}{\alpha(\mu+1)}} \qquad 3.37$$

$$-D = \alpha(\mu+1)y_{1'}^2 + 2\alpha K(y_{1'}-y_2) + \Delta E \qquad 3.38$$

and $D > 0$ otherwise $= 0$ since $x_{1'}$ is real.

Next considering the $y_{1'}$ integral, the condition on D limits the range of integration over $y_{1'}$. D being positive only when $y_{1'}$ lies between

$$\frac{-2\alpha K \pm \sqrt{4\alpha^2K^2 - 4\alpha(\mu+1)\ (\Delta E - 2\alpha K y_2)}}{2\alpha(\mu+1)} \qquad 3.39$$

Now using G+R page 81 eq 2.261

$$\int_i \frac{1}{i\sqrt{D}}\ dy_{1'} = \frac{\ell n(-1)}{i\ \sqrt{\alpha(\mu+1)}} \qquad 3.40$$

and taking the principal value

$$\int_i \frac{1}{\sqrt{D}}\ dy_{1'} = \frac{\pi}{\sqrt{\alpha(\mu+1)}} \qquad 3.41$$

Combining the above

$$Q = \frac{2\pi^{5/2}\ (x_BT_c)^{\frac{1}{2}}}{\alpha^{3/2}\ (\mu+1)} \int M_{BF}^2(K) L_{b'}^2(K)\ e^{-\alpha(K+y_2)^2/x_BT_c}\ KdKdy_2 \qquad 3.42$$

The range of the $y_2$ integration is specified by the requirement that the limits on $y_{1'}$ must be real. That is

$$y_2 \geqslant y_{2min} = \frac{\Delta E}{2\alpha K} - \frac{K}{2(\mu+1)} \qquad 3.43$$

Using the substitution $u = \sqrt{\frac{\alpha}{x_B T_c}}\ (K+y_2)$ converts the $y_2$ integral to the form

$$\sqrt{\frac{x_B T_c}{\alpha}} \int_{u_{min}=K+y_{2min}}^{\infty} \exp -u^2\, du = \sqrt{\frac{x_B T_c}{\alpha}} \sqrt{\frac{\pi}{2}}\ \mathrm{erfc}\sqrt{\frac{\alpha}{x_B T_c}}\ (K+y_{2min}) \qquad 3.44$$

leaving

$$Q = \frac{\pi^3\ x_B T_c}{\alpha^2\ (\mu+1)} \int M_{BF}^2(K) I_b^2\ (K)\ \mathrm{erfc}\sqrt{\frac{\alpha}{x_B T_c}} \left(\frac{\Delta E}{2\alpha K} + \frac{(2\mu+1)K}{2(\mu+1)}\right) K\ dK \qquad 3.45$$

Now for typical semiconductor parameters the complementary error function is highly peaked at

$$K = K_o = \sqrt{\frac{\Delta E}{\alpha}\ \frac{(\mu+1)}{(2\mu+1)}} \qquad \text{for } \Delta E >> 0 \qquad 3.46$$

In comparison $M_{BF}^2\ (K).I_b^2(K)$ is slowly varying and may be taken outside the integral with it value at $K = K_o$ . The remaining integral over K being then be carried out using G+R page 651 eg 6.297.1

$$Q = \frac{\pi^3}{\alpha^3}\ (x_B T_c)^2\ \frac{(\mu+1)}{(2\mu+1)^2}\ M_{BF}^2(K_o) I_b^2\ (K_o)\ \exp\left(-\frac{(2\mu+1)}{(\mu+1)}\ \frac{\Delta E}{x_B T_c}\right) \qquad 3.47$$

Substituting this into 3.21 gives a analytical expression for $R_b$

$$R_b = \sum_{\substack{n_1 n_1' \\ n_2 n_2'}} \frac{(2+2\delta n_1 n_2) e^4\ m_c^*(x_B T_c)^2}{L\ \pi^2\ \varepsilon_{INT}^2\ \hbar^7}\ \frac{\mu+1}{(2\mu+1)^2}\ \frac{N_{2'}}{\bar{N}_L}\left(\frac{N_1}{N_{01}}\ \frac{N_2}{N_{02}}\ \frac{P_1}{P_{01}}\ \frac{N_{02}}{N_2} - 1\right) \qquad 3.48$$

$$M_{BF}^2(K_o)\ I_b^2(K_o) \exp\left(\frac{-(2\mu+1)}{(\mu+1)}\ \frac{\Delta E}{x_B T_c}\right)$$

and this may be checked by alternative derivations.

**REFERENCES FOR CHAPTER 3**

3.1 Beattie A R and Smith G 1967 Phys. Status Solidi. 19 557

3.2 Gradshteyn I S and Ryzhik I M 1980 Table of Integrals, Series and Products (London: Academic)

## CHAPTER 4 - AUGER TRANSITIONS IN WHICH THE PROMOTED (AUGER ELECTRON IS UNBOUND

This Chapter extends the analysis in Chapter 2 specifically for the CHCC Auger recombination processes where the colliding electrons and hole are bound to the well, but the promoted (Auger) electron is unbound.

### 4.1 THE MATRIX ELEMENT FOR THE BOUND TO UNBOUND TRANSITION

To make feasible the numerical calculations of the summation in Fermi's golden rule an analytical expression is required for the matrix element of the process where all states, except the promoted (Auger) electron state, are bound. To obtain such an analytical expression it is necessary, as in Chapter 3, to neglect the perpendicular wavevector dependence in the periodic parts of the Bloch wavefunctions.

Neglecting the perpendicular wavevector dependence of the periodic parts of the Bloch functions gives from 2.87, 2.88, and 2.89 with 2.90.

$$M_{12} = \left(\frac{4\pi e^2}{\varepsilon_{INT}}\right) M_{BF} \left(\frac{2\pi}{A^2}\right) \delta(\underline{K}''_{1'} - \underline{K}''_1 + \underline{K}''_{2'} - \underline{K}''_2)\ I'_{ub} \qquad 4.1$$

$$I'_{ub} = \left(\frac{2}{L}\right)^{3/2} \int \frac{1}{K^2+q_2^2} \sin\frac{n_1\pi}{L} \sin\frac{n_{1'}\pi}{L}\, e^{iq_z z_1} \sin\frac{n_2\pi}{L} z_2$$

$$(a' \sin K_{z_2} z + a \cos K_{z_2} z)\, e^{iq_z z_2}\, dz_1 dz_2 dq_z \qquad 4.2$$

where origin is taken at one edge of the well and hence

$$a' = B' \sin \frac{K_{z2'}L}{2} \quad \text{and} \quad a = B' \cos \frac{K_{z2'}L}{2} \qquad 4.3$$

when the promoted electron's envelope function has even parity with respect to the centre of the well, or

$$a' = B' \cos \frac{K_{z2'}L}{2} \quad \text{and} \quad a = -B' \sin \frac{K_{z2'}L}{2} \qquad 4.4$$

when the promoted electron's envelope function has odd parity with respect to the centre of the well.

$I'_{ub}$ is now evaluated, there being two possible approaches to evaluating it. Either the $q_z$ integral can be done first, or alternatively the $z_1$ and $z_2$ integrals can be done first. Doing the $z_1$ and $z_2$ integrals first leaves a tedious integration over $q_z$ with a large number of terms. But this rather defeats the object of having an analytical approach, and therefore the $q_z$ integral is done first.

The $q_z$ integral is done by observing that $I'_{ub}$ has poles at $q_z = \pm iK$, with residues $= \pm\frac{1}{2iK}$. Choosing suitable contours when $z_1 > z_2$ and $z_1 < z_2$ then gives

$$I'_{ub} = \left(\frac{2}{L}\right)^{3/2} \left[\int_0^L \frac{\pi}{K} e^{-Kz_1} \sin \frac{n_1\pi}{L} z_1 \sin \frac{n_{1'}\pi}{L} z_1 \int_0^{z_1} e^{+Kz_2} \sin \frac{n_2\pi}{L} z_2 \left\{a \cos K_{z2}z + a \sin K_{z2}z\right\} dz_2 dz_1\right.$$

$$+ \int_0^L \frac{\pi}{K} e^{+Kz_1} \sin \frac{n_1\pi}{L} z_1 \sin \frac{n_{1'}\pi}{L} z_1 \int_{z_1}^L e^{-Kz_2} \sin \frac{n_2\pi}{L} z_2 \left\{a \cos K_{z2}z + a' \sin K_{z2}z\right\} dz_2 dz_1$$



4.5

Next the $z_2$ integrals are done using G+R page 196 eq's 2.664.1 and 2.663.3. Assembling the results of these $z_2$ integrals, leaves $\left(\text{if } A=\left(\frac{n_2\pi}{L} - K_{z2'}\right),\ B=\left(\frac{n_2\pi}{L} + K_{z2'}\right)\right)$

$$I'_{ub} = \left(\frac{2}{L}\right)^{3/2} \int_0^L \frac{\pi}{K} e^{-Kz_1} \sin\frac{n_1\pi}{L} z_1 \sin\frac{n_{1'}\pi}{L} z_1 \left[\frac{a}{2}\left(\frac{B}{K^2+B^2} + \frac{A}{K^2+A^2}\right) - \frac{a'}{2}\left(\frac{K}{K^2+A^2} - \frac{K}{K^2+B^2}\right)\right] dz_1$$

$$+ \left(\frac{2}{L}\right)^{3/2} \int_0^L \frac{\pi}{K} e^{+Kz_1} e^{-KL} \sin\frac{n_1\pi}{L} z_1 \sin\frac{n_{1'}\pi}{L} z_1 \left[\frac{a}{2}\left(\frac{-K\sin BL - B\cos BL}{K^2+B^2} + \frac{-K\sin AL - A\cos AL}{K^2+A^2}\right) + \frac{a'}{2}\left(\frac{-K\cos AL + A\sin AL}{K^2+A^2} - \frac{-K\cos BL + B\sin BL}{K^2+B^2}\right)\right] dz_1$$

$$+ \left(\frac{2}{L}\right)^{3/2} \int_0^L \frac{\pi}{K} \sin\frac{n_1\pi}{L} z_1 \sin\frac{n_{1'}\pi}{L} z_1 \left[\frac{a}{2}\left(\frac{2K\sin Bz_1}{K^2+B^2} + \frac{2K\sin Az_1}{K^2+A^2}\right) + \frac{a'}{2}\left(\frac{2K\cos Az_1}{K^2+A^2} - \frac{2K\cos Bz_1}{K^2+B^2}\right)\right] dz_1 \qquad 4.6$$

The first two $z_1$ integrals are then evaluated in a similar manner. Taking the first one for example, we have using

$$\sin\frac{n_1\pi}{L} z_1 \sin\frac{n_{1'}\pi}{L} z_1 = \frac{1}{2}\cos(n_1-n_{1'})\frac{\pi}{L} z_1 - \frac{1}{2}\cos(n_1+n_{1'})\frac{\pi}{L} z_1 \qquad 4.7$$

and G+R page 196 eq 2.633.3

$$I'_{ub}\begin{pmatrix}\text{FIRST}\\ \text{INTEGRAL}\end{pmatrix} = \frac{\pi}{2}\left(\frac{1-e^{-KL}\cos(n_1-n_{1'})\pi}{K^2 + ((n_1-n_{1'})\frac{\pi}{L})^2} - \frac{1-e^{-KL}\cos(n_1+n_{1'})\pi}{K^2 + ((n_1+n_{1'})\frac{\pi}{L})^2}\right)$$

$$\left[\frac{a}{2}\left(\frac{B}{K^2+B^2} + \frac{A}{K^2+A^2}\right) - \frac{a'}{2}\left(\frac{K}{K^2+A^2} - \frac{K}{K^2+B^2}\right)\right] \qquad 4.8$$

The third $z_1$ integral is evaluated using G+R page 140 eq's 2.533.2 and 2.533.4. It gives

$$
\begin{aligned}
I'_{ub}\begin{pmatrix}\text{THIRD}\\ \text{INTEGRAL}\end{pmatrix} = \left(\frac{2}{L}\right)^{3/2} \Bigg\{ & -\frac{\pi a}{(K^2+B^2)}\frac{1}{4}\Bigg[\frac{\cos((n_1-n_{1'})\pi+BL)-1}{(n_1-n_{1'})\frac{\pi}{L}+B} + \frac{\cos((n_{1'}-n_1)\pi+BL)-1}{(n_{1'}-n)\frac{\pi}{L}+B} \\
& + \frac{\cos((n_1-n_{1'})\pi-BL)-1}{(n_1+n_{1'})\frac{\pi}{L}-B} - \frac{\cos((n_1+n_{1'})\pi+BL)-1}{(n_1+n_{1'})\frac{\pi}{L}+B}\Bigg] \\
& - \frac{\pi a}{(K^2+A^2)}\frac{1}{4}\Bigg[\frac{\cos((n_1-n_{1'})\pi+AL)-1}{(n_1-n_{1'})\frac{\pi}{L}+A} + \frac{\cos((n_{1'}-n_1)\pi+AL)-1}{(n_{1'}-n)\frac{\pi}{L}+A} \\
& + \frac{\cos((n_1+n_{1'})\pi-AL)-1}{(n_1+n_{1'})\frac{\pi}{L}-A} - \frac{\cos((n_1+n_{1'})\pi+AL)-1}{(n_1+n_{1'})\frac{\pi}{L}+A}\Bigg] \\
& + \frac{\pi a'}{(K^2+A^2)}\frac{1}{4}\Bigg[\frac{\sin(AL+(n_1-n_{1'})\pi)}{(n_1-n_{1'})\frac{\pi}{L}+A} + \frac{\sin(AL-(n_1-n_{1'})\pi)}{(n_{1'}-n_1)\frac{\pi}{L}+A} \\
& - \frac{\sin(AL+(n_1+n_{1'})\pi)}{(n_1+n_{1'})\frac{\pi}{L}+A} - \frac{\sin(-AL+(n_1+n_{1'})\pi)}{(n_1+n_{1'})\frac{\pi}{L}-A}\Bigg] \\
& - \frac{\pi a'}{(K^2+B^2)}\frac{1}{4}\Bigg[\frac{\sin(BL+(n_1-n_{1'})\pi)}{(n_1-n_{1'})\frac{\pi}{L}+B} + \frac{\sin(BL-(n_1-n_{1'})\pi}{(n_{1'}-n\ )\frac{\pi}{L}+B} \\
& - \frac{\sin(BL+(n_1+n_{1'})\pi)}{(n_1+n_{1'})\frac{\pi}{L}+B} - \frac{\sin(-BL+(n_1+n_{1'})\pi)}{(n_1+n_{1'})\frac{\pi}{L}-B}\Bigg]\Bigg\}
\end{aligned}
\qquad 4.9
$$

Now assembling, for future reference, $I'_{ub}$ for the $\eta_1 = \eta_{1'} = 1$ case

$$I'_{ub\,\eta_1=\eta_{1'}=\eta_2=1} = \left(\frac{2}{L}\right)^{3/2} a \left(\frac{\pi}{K}\left\{\frac{1}{A^2+K^2}\left[\frac{(KL/2)\sin(AL/2)}{\Gamma(2+\frac{AL}{2\pi})\ \Gamma(2-\frac{AL}{2\pi})} + \frac{(1-e^{-KL})(\frac{A}{K}-\sin AL-\frac{A}{K}\cos AL)}{\frac{K^2L^2}{\pi^2}+4}\right.\right.\right.$$

$$\left.\left.\left. + \frac{1}{B^2+K^2}\left[\frac{(KL/2)\sin(BL/2)}{\Gamma(2+\frac{BL}{2\pi})\ \Gamma(2-\frac{BL}{2\pi})} + \frac{(1-e^{-KL})(\frac{B}{K}-\sin BL - \frac{B}{K}\cos AL)}{\frac{K^2L^2}{\pi^2}+4}\right]\right\}\right)$$

$$\left(\frac{2}{L}\right)^{3/2} a' \frac{\pi}{K}\left\{\frac{1}{A^2+K^2}\left[\frac{(KL/2)\cos(AL/2)}{\Gamma(2+\frac{AL}{2\pi})\ \Gamma(2-\frac{AL}{2\pi})} + \frac{(1-e^{-KL})(\frac{A}{K}\sin AL - \cos AL - 1)}{\frac{K^2L^2}{\pi^2}+4}\right]\right.$$

$$\left.\left. - \frac{1}{B^2+K^2}\left[\frac{(KL/2)\cos(BL/2)}{\Gamma(2+\frac{BL}{2\pi})\ \Gamma(2-\frac{BL}{2\pi})} + \frac{(1-e^{-KL})(\frac{B}{K}\sin BL - \cos BL - 1}{\frac{K^2L^2}{\pi^2}+4}\right]\right\}\right) \qquad 4.10$$

which is a suitable expression with which to proceed with the summation.

For other cases and a number of checks upon the above the reader is refered to Appendix 3. Note, Appendix 3 is again referred to during the interpretation of the results in Chapter 5 because the last of its checks indicates the behaviour of $I'_{ub}$ at large and small K.

## 4.2 THE SUMMATION OVER STATES

### 4.2.1 AUGER RATE EXPRESSION AND THE INITIAL INTEGRATIONS IN K SPACE

As mentioned in Chapter 2 the Auger recombination rate is found from a summation over all appropriate states. For the processes considered here we are concerned with the promoted (Auger) electron in unbound states which are described by a continuum of allowed perpendicular wavevectors. The Auger recombination rate per unit volume therefore becomes,

$$R_{ub} = \frac{1}{A.L}\frac{2\pi}{\hbar}\sum_{\substack{n_1 n_{1'} \\ n_2}}\sum_{K_{z2'}}\sum_{\substack{\underline{K}''_1 \underline{K}''_{1'} \\ \underline{K}''_2 \underline{K}''_{2'}}} e^{-(E_{2'}-E_{c2'})/x_B T_c}\, e^{-(E_{c2'}-E_{c1})/x_B T_c}$$

$$\frac{N_1}{\bar{N}_c}\left(\frac{N_1}{N_{01}}\frac{N_2}{N_{02}} - 1\right)(2+2\delta n_1,n_2)\left(\frac{4\pi e^2}{\varepsilon_{INT}}\right)^2 M^2_{BF}(\underline{K})I^2_{ub}(K,K_{z2'}) \qquad 4.11$$

$$\left(\frac{2\pi}{A}\right)^2 \delta(\underline{K}''_{1'}-\underline{K}''_1+\underline{K}''_{2'}-\underline{K}''_2)\,\delta(\underline{K}''_{1'}-\underline{K}''_1+\underline{K}''_{2'}-\underline{K}''_2)\,\delta E$$

where $K_{z2'}$ has a continuum of values, and we have substituted into the summation (2.7) suitable expressions for the statistical factor P (2.15 with 2.25 and 2.26) and matrix element M (see 2.34 and 4.1).

Converting the summations over $\underline{K}''_1$, $\underline{K}''_{1'}$, $\underline{K}''_2$, $\underline{K}''_{2'}$, and $K_{z2'}$ to integrations in $\underline{K}''_1$, $\underline{K}''_{1'}$, $\underline{K}''_2$, $\underline{K}''_{2'}$, and $E_{c2'}$ respectively and changing $\delta(\underline{K}''_{1'}-\underline{K}''_1+\underline{K}''_{2'}-\underline{K}''_2)\;\delta(\underline{K}''_{1'}-\underline{K}''_1+\underline{K}''_{2'}-\underline{K}''_2)$ to $\frac{A}{(2\pi)^2}\delta(\underline{K}''_{1'}-\underline{K}''_1+\underline{K}''_{2'}-\underline{K}''_2)$ in the normal way gives

$$R_{ub} = \frac{1}{A.L}\frac{2\pi}{\hbar}\,4.\left(\frac{4\pi e^2}{\varepsilon_{INT}}\right)^2 \frac{N_1}{\bar{N}_c}\left(\frac{N_1}{N_{01}}\frac{N_2}{N_{02}} - 1\right)\left(\frac{A}{(2\pi)^2}\right)^4 Q \qquad 4.12$$

where

$$Q = \int M_{BF}^{2}(\underline{K}) I_{ub}^{\prime 2}(K, K_{2z'})\, e^{-(E_{2'}-E_{c2'})/x_B T_c}\, e^{-(E_{c2}-E_{c1})/x_B T_c}$$

$$\delta(\underline{K}_{\parallel 1}-\underline{K}_{\parallel 1}+\underline{K}_{\parallel 2'}-\underline{K}_{\parallel 2})\,\delta(E)\, ds_{CON}(E_{c2'})\; d^2\underline{K}_{\parallel 1} d^2\underline{K}_{\parallel 1'} d^2\underline{K}_{\parallel 2} d^2\underline{K}_{\parallel 2'} dE_{c2'} \qquad 4.32$$

and where $ds_{CON}(E_{c2'})$ is the density of suitable continuum states per unit energy above the well edge. $ds_{CON}(E_{c2'})$ being given by

$$ds_{CON} = \frac{\ell}{2\pi}\left(\frac{2m}{\hbar^2}\right)^{\frac{1}{2}} \frac{1}{(E_{c2'}-E_{c2'min})} \qquad 4.13$$

ie the one dimensional density of states per unit length (see Section 2.1.2) multiplied by the system length '$2\ell$', and divided by 4. The division by four occurs because of the symmetry requirements placed on the promoted (Auger) state by Section 2.4.3.1 (only half the states have the right symmetry to give a non-zero matrix element), and because allowance for two spin states has already been included in the matrix element expression (see Section 2.4.1).

The first few integrations in the expression for $R_{ub}$ follow in much the same way as those in the bound state CHCC case, $e^{-(E_{2'}-E_{c2})/x_B T_c}$ playing the same role as $e^{-(E_{2'}-E_{c1})/x_B T_c}$ did.

The first difference of note comes from the condition that the y-component of $\underline{K}_{1'}$ must be real. Again (cf Eq (3.43))

$$Y_2 \geqslant \frac{\Delta E}{2\alpha K} - \frac{K}{2(\mu+1)} \qquad 4.14$$

but now $\Delta E$ (defined again by $\Delta E = E_{c1} + E_{c2} - E_{v1'} - E_{c2'}$) may be negative. To interpret this physically the values of K and $y_2$ which allow $y_{1'}$ to be real must be considered. These are shown in Figure 4.1 which also interpret particular cases using E-K diagrams. Mathematically the significance is that account must now be taken of the possible negative values of the argument of the complementary error function in

$$Q = \frac{\pi^3}{\alpha^2} \frac{(x_B T_c)}{(\mu+1)} \int M_{BF}^2(K) I_{ub}^2(K, K_{\parallel 2'}(E_{c2'}))\, e^{-(E_{c2'} - E_{c1})/x_B T_c}$$

$$\operatorname{erfc}\left\{\sqrt{\frac{\alpha}{x_B T_c}} \left(\frac{\Delta E}{2\alpha K} + \frac{(2\mu+1)}{(\mu+1)} \frac{K}{2}\right)\right\} ds_{CON}(E_{c2'}) K dK dE_{c2'} \qquad 4.15$$

FIGURE 4.1

This figure illustrates

(1) the allowed combinations of the parallel wavevector exchange K and the state 2 wavevector parallel to K (ie $Y_2$) for $\Delta E$ positive, $\Delta E$ zero, and $\Delta E$ negative.

and (2) interprets some of these allowed combinations, which are peculiar to the unbound process, on momentum-versus-energy diagrams

(1)

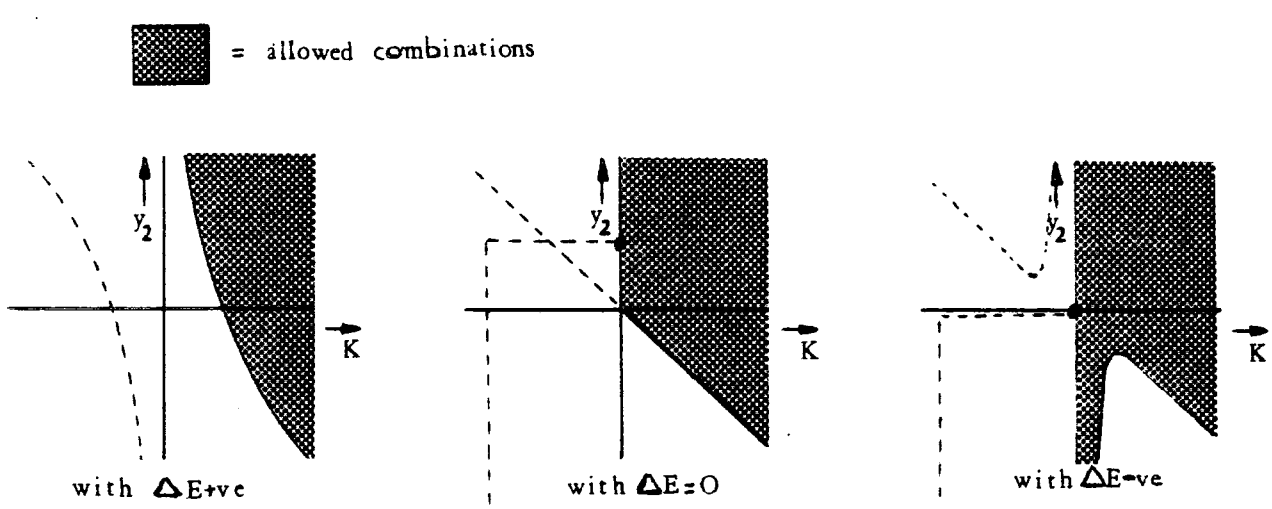


(2) Processes like

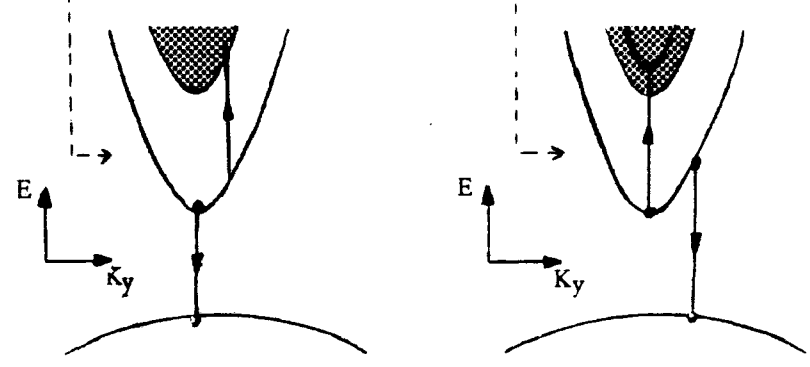


are now allowed

### 4.2.2 THE REMAINING INTEGRATIONS

Various alternative approaches to the integrals over K and $E_{c2'}$ exist. These are now considered, and it is concluded that while the most satisfactory approach is completely numerical, various analytical approaches provide useful checks and insights.

Attempting to do the $E_{c2'}$ first (see Appendix 4) immediately produces a difficult integral which can only be done analytically when both $M_{BF}(K)I'_{ub}(K, K_{\parallel 2'}(E_{c2'}))$ and $ds_{CON}(E_{c2'})$ are assumed to be independent of $E_{c2'}$. This is obviously an unsatisfactory basis on which to proceed, and therefore the K integration is done first.

The approach adopted when the K integral is done first, depends on $\Delta E$ through the complementary error function. The influence of $\Delta E$ on the behavior with K of the complementary error function is shown in figure 4.2. When $\Delta E$ is positive the complementary error function is highly peaked, and therefore the matrix element $M_{BF}(K)I'_{ub}(K, K_{\parallel 2'}, (E_{c2'}))$ may, as in the bound-bound calculation, be taken as slowly varying and removed from the integrand with $K=K_o = \sqrt{\frac{\Delta E}{\alpha}\frac{(\mu+1)}{(2\mu+1)}}$. When $\Delta E$ is zero or negative the complementary error function is not highly peaked in K and therefore the matrix element is not so easily removed form the K integrand. The simplest approach however is to assume that again the matrix element can be

FIGURE 4.2

The dependence of the complementary error function $\mathrm{erfc}\left\{\sqrt{\frac{\alpha}{x_B T_c}}\left(\frac{\Delta E}{2\alpha K} + \frac{(2\mu+1)}{(\mu+1)}\frac{K}{2}\right)\right\}$ on ΔE and K. Diagrams (i) and (ii) are for the 200Å 1.3 μm InGaAsP/InP system

(i) Plots erfc { } against ΔE and K and marks important K values

(ii) Plots $\log_{10}$ (erfc { }) against ΔE and K to ΔE + ve behaviour.

(a) (b) and (c) are schematic cross sections from (i) and are included for easy reference.

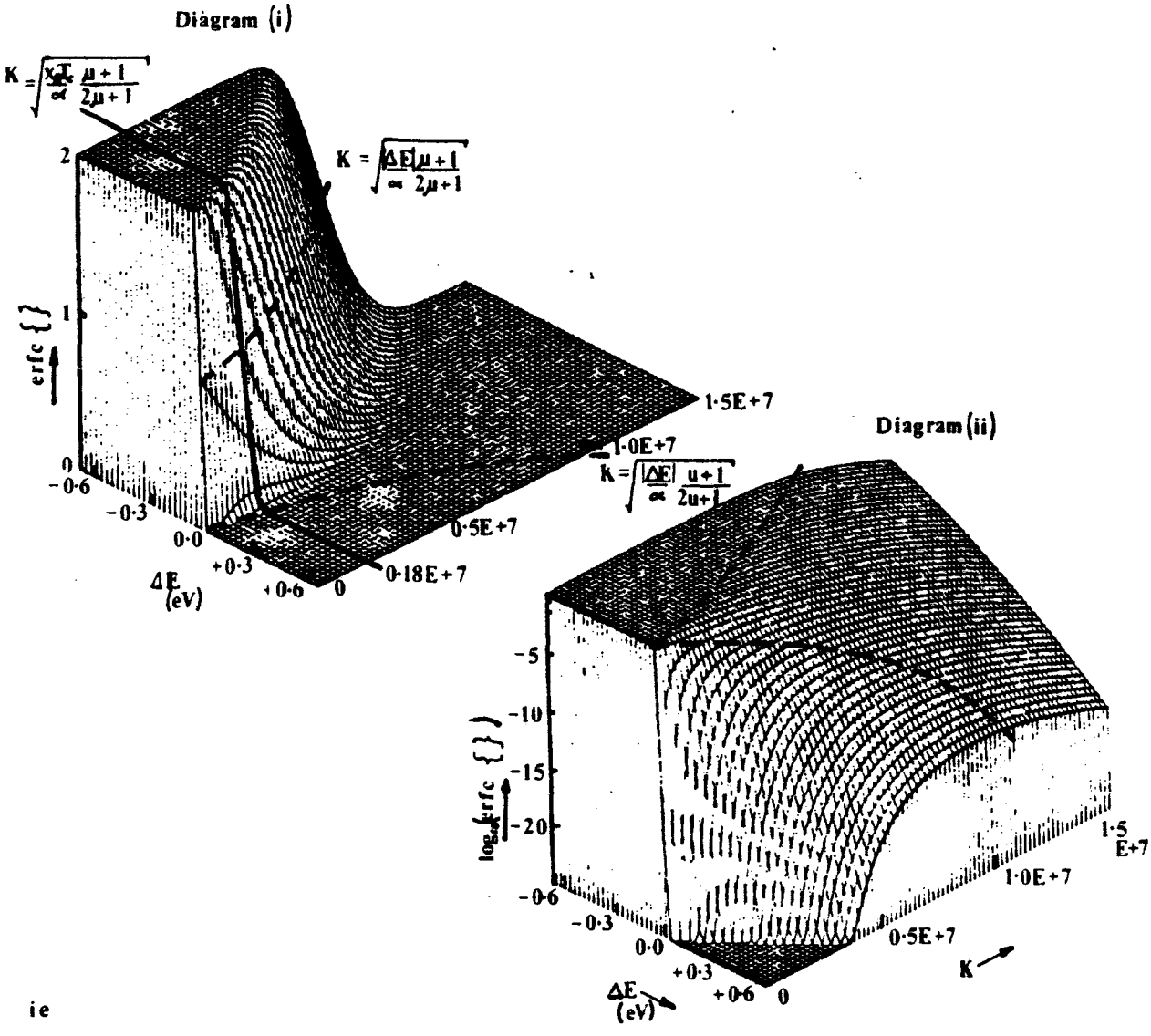


ie

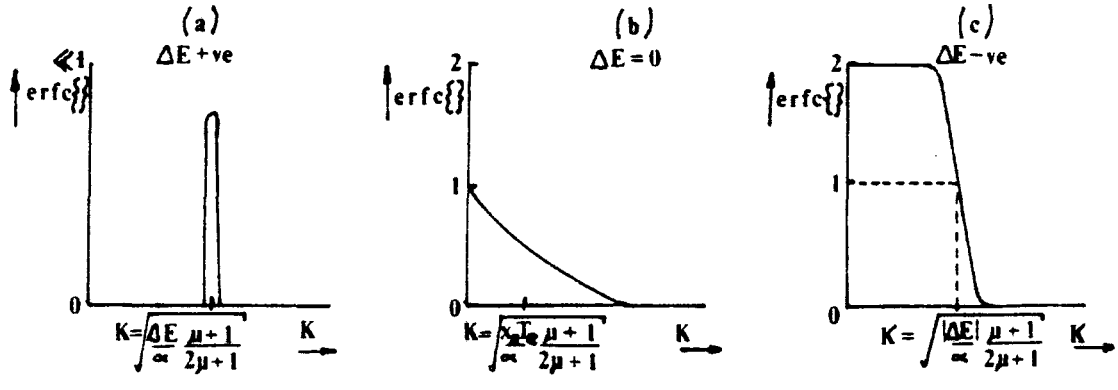

evaluated at some representative wavevector say $K = K_o$, and removed from the K integrand. Alternative approaches for the case of $\Delta E \leqslant 0$, such as expanding the matrix element $M_{BF}(K) I'_{ub}(K, K_{\parallel 2'}(E_{c2'}))$ as a power series in K and then proceeding analytically, produce results so complex that they provide no more insight than the numerical approach.

Having done the K integrals analytically using the simple approximation described above, the remaining $E_{c2'}$ integral must then be carried out numerically if the $E_{c2'}$ dependence of $M_{BF}(K_o) I'_{ub}(K_o K_{\parallel 2'}(E_{c2'}))$, both through $K_{\parallel 2'}$ and $K_o$, is to be taken into account. To proceed with the remaining $E_{c2'}$ integral analytically, the matrix element must be removed from the integrand. This is done by observing that the non-matrix element part of the integrand peaks at $\Delta E = 0$ because here energy and in-plane momentum conservation allow transitions between states which are near the band edges, and therefore more likely to be populated with electrons or holes as required. Unfortunately at $\Delta E = 0$ there is no clearly defined best choice as a result of the complementary error function dependence in K space shown in figure 4.2(b). Therefore the resultant analytical expression is inadequate for reliable results. However, it is useful for checking the numerical calculation of both K and $E_{c2'}$ integrals, and for deciding on the most appropriate numerical approach to the calculation. Thus for the remainder of this chapter the analytical approach is discussed while in Chapter 5 the complete numerical results will be presented.

### 4.2.3 THE K INTEGRAL WITH ΔE POSITIVE

For ΔE positive the K integral may be carried out in the same way as it was for the bound-bound transition considered in Chapter 3. That is $M_{BF}(K) I_{ub}(K, K_{u2'})$ is assumed to be slowly varying in K space compared to the highly peaked complementary error function, and the integral in Eq (4.15) is evaluated by using a formula in G+R (page 651 eq 6.297.1) or by the method of steepest descents, giving

$$Q = \frac{\pi^3}{\alpha^3} (x_B T_c)^2 \frac{(\mu+1)}{(2\mu+1)^2} \int_{E_{c2'min}}^{\Delta E=0} M_{BF}^2(K_o) I_{ub}^2(K_o, K_{u2'}(E_{c2'})) \, e^{-(E_{c2'}-E_{c1})/x_B T_c} \, e^{-\frac{(2\mu+1)}{(\mu+1)} \frac{\Delta E}{x_B T_c}} \, ds_{CON}(E_{c2'}) \, dE_{c2'} \qquad 4.16$$

where $K_o$ is the value at which $\mathrm{erfc}\left\{\sqrt{\frac{\alpha}{x_B T_c}}\left(\frac{-\Delta E}{2\alpha K} + \frac{(2\mu+1)}{(\mu+1)}\frac{K}{2}\right)\right\} K$ peaks.

The condition for the peak in K space in the erfc function of Eq (4.15) is

$$\frac{d}{dK}\left(\mathrm{erfc}\left\{\sqrt{\frac{2}{x_B T_c}}\left(\frac{\Delta E}{2\alpha K} + \frac{(2\mu+1)}{(\mu+1)}\frac{K}{2}\right)\right\} K\right) = 0 \qquad 4.17$$

which gives

$$\mathrm{erfc}\sqrt{\frac{\alpha}{x_B T_c}}\left(\frac{\Delta E}{2\alpha K} + \frac{(2\mu+1)}{(\mu+1)}\frac{K}{2}\right) = K\frac{2}{\sqrt{\pi}} e^{-\frac{\alpha}{x_B T_c}\left(\frac{\Delta E}{2\alpha K} + \frac{(2\mu+1)}{(\mu+1)}\frac{K}{2}\right)^2} \left(\sqrt{\frac{\alpha}{x_B T_c}}\left(\frac{-\Delta E}{2\alpha K^2} + \frac{2\mu+1}{2(\mu+1)}\right)\right) \qquad 4.18$$

where the formula of Abramowitz and Stegun (thereafter referred to as A+S) page 298 eq 7.1.19 (ref 4.1)

$$\frac{d^{m+1}}{dX^{m+1}} \operatorname{erf}(X) = (-1)^m \frac{2}{\sqrt{\pi}} H_m(X)\, e^{-X^2} \qquad (m=0,1,2...)$$

and the Hermite polynomial $H_o(X) = 1$ have been used.

Now $K = K_o = \sqrt{\frac{\Delta E}{\alpha} \frac{(\mu+1)}{(2\mu+1)}}$ satisfies the above to a good approximation provided $\sqrt{\frac{\Delta E}{x_B T_c} \frac{(2\mu+1)}{(\mu+1)}}$ is large so that $\operatorname{erfc}\sqrt{\frac{\Delta E}{x_B T_c} \frac{(2\mu+1)}{(\mu+1)}} \to 0$

### 4.2.4 THE K INTEGRAL WITH ΔE ZERO OR NEGATIVE

When $\Delta E \leqslant 0$ the integrand is no longer highly peaked in K space, however the approach described in Section (4.2.2) is adopted. The matrix element is removed from the integrand and a suitable choice of $K = K_o$ in the matrix element is anticipated. The following result is then used to evaluate the integral for Q in Eq (4.15)

$$\int_0^\infty \left[1 - \mathrm{erf}\,(gX - \frac{b}{X})\right] e^{-(g^2-u)X^2}\, dX$$

$$= \frac{1}{4g^2} + \frac{b}{g} \quad \text{when } g^2 = u \qquad 4.19$$

(This result does not appear in G+R and is therefore derived, in Appendix 4). Using 4.19 and taking $g = \sqrt{\frac{\alpha}{x_B T_c}}\,\frac{(2\mu+1)}{2(\mu+1)}$ , $b = -\sqrt{\frac{\alpha}{x_B T_c}}\,\frac{\Delta E}{2\alpha}$ the expression for Q in Eq (4.15) becomes

$$Q = \frac{\pi^3}{\alpha^3}(x_B T_c)\,\frac{2(\mu+1)}{(2\mu+1)^2}\int_{\Delta E=0}^{\infty} M_{BF}^2(K_o) I_{ub}^2(K_o, K_{n_2'}(E_{c2'}))\, e^{-(E_{c2'}-E_{c1})/x_B T_c}$$

$$\left\{-\frac{\Delta E x_B T_c}{(\mu+1)}(2\mu+1) + 1\right\} ds_{CON}(E_{c2'})\, dE_{c2'} \qquad 4.20$$

It now becomes necessary to estimate $K_o$. Figure 4.2(c) shows the dependence of the complementary error function on K when $\Delta E < 0$. Now by taking the gradient of the argument of the complementary at $K = \sqrt{\frac{|\Delta E|}{\alpha}\,\frac{\mu+1}{2\mu+1}}$ (ie when erfc(0)=1) and using this in an approximate way to find the rate of change of the argument of the complementary error function it is seen that the complementary error is a good approximation to a step function providing $\Delta E >> x_B T_c$ .

A convenient choice of $K_o$ is therefore

$$K_o = \sqrt{\frac{|\Delta E|}{\alpha} \frac{(\mu+1)}{(2\mu+1)}} \qquad 4.21$$

When $\Delta E = 0$ the choice of a suitable value of $K_o$ becomes even more difficult. By comparison with numerical calculation it has been found that the obvious choice, $K_o = 0$, leads to a spurious emphasis in the integration of this single point in K space. In fact a much better choice is to take for $0 \geqslant \Delta E \geqslant - x_B T_c$ .

$$K = K_o = \sqrt{\frac{x_B T_c}{\alpha} \frac{(\mu+1)}{(2\mu+1)}} \qquad 4.22$$

Here the thermal energy $x_B T_c$ replaces $\Delta E$ in recognition of the fact that there tends to be a blurring on energy dependences by thermal effects. This it will be seen in Section 4.2.5 produces surprisingly good results.

### 4.2.5 DOING THE INTEGRATION OVER UNBOUND SUB-BANDS (THE $E_{c2'}$ INTEGRAL) NUMERICALLY

To allow K in the matrix element to be chosen in accordance with the estimates of $K_o$ in the previous section (ie $K = K_o = \sqrt{\frac{x_B T_c}{\alpha}\frac{(\mu+1)}{(2\mu+1)}}$ when $0 \geqslant \Delta E \geqslant -x_B T_c$, and $K = K_o = \sqrt{\frac{|\Delta E|}{\alpha}\frac{(\mu+1)}{(2\mu+1)}}$ otherwise), and also to take into account the $E_{c2'}$ dependence of $K_{\parallel 2'}$, the remaining $E_{c2'}$ integral is done numerically. Figures 4.3 and 4.4 show, for the 1.3 μm and 1.55 μm InGaAsP/InP systems respectively, the results of such numerical calculations for the processes where all carriers but the promoted (Auger) electron are in the first bound sub-bands. Also shown, for comparison, are the full numerical results, where both the K and $E_{c2'}$ integrals are done numerically.

From figures 4.3 and 4.4 it is seen that the agreement between the approximate and full results is good. Also good is agreement between the full results and similar approximate results where K is taken as $K_o = \sqrt{\frac{|\Delta E| + x_B T_c}{\alpha}\frac{\mu+1}{(2\mu+1)}}$. Thus since both approximate calculations remove from the integration a significant region of K space around K = 0 through the choice of $K_o$, this region can not contribute substantially to the integral. But it is precisely this region of K space that is most sensitive to the lack of orthogonality of the bound and unbound wavefunctions, and therefore the lack of orthogonality must only have a minor effect on the results. Hence it is established that the lack of orthogonality is not a serious shortcoming in applying the theory.

FIGURE 4.3

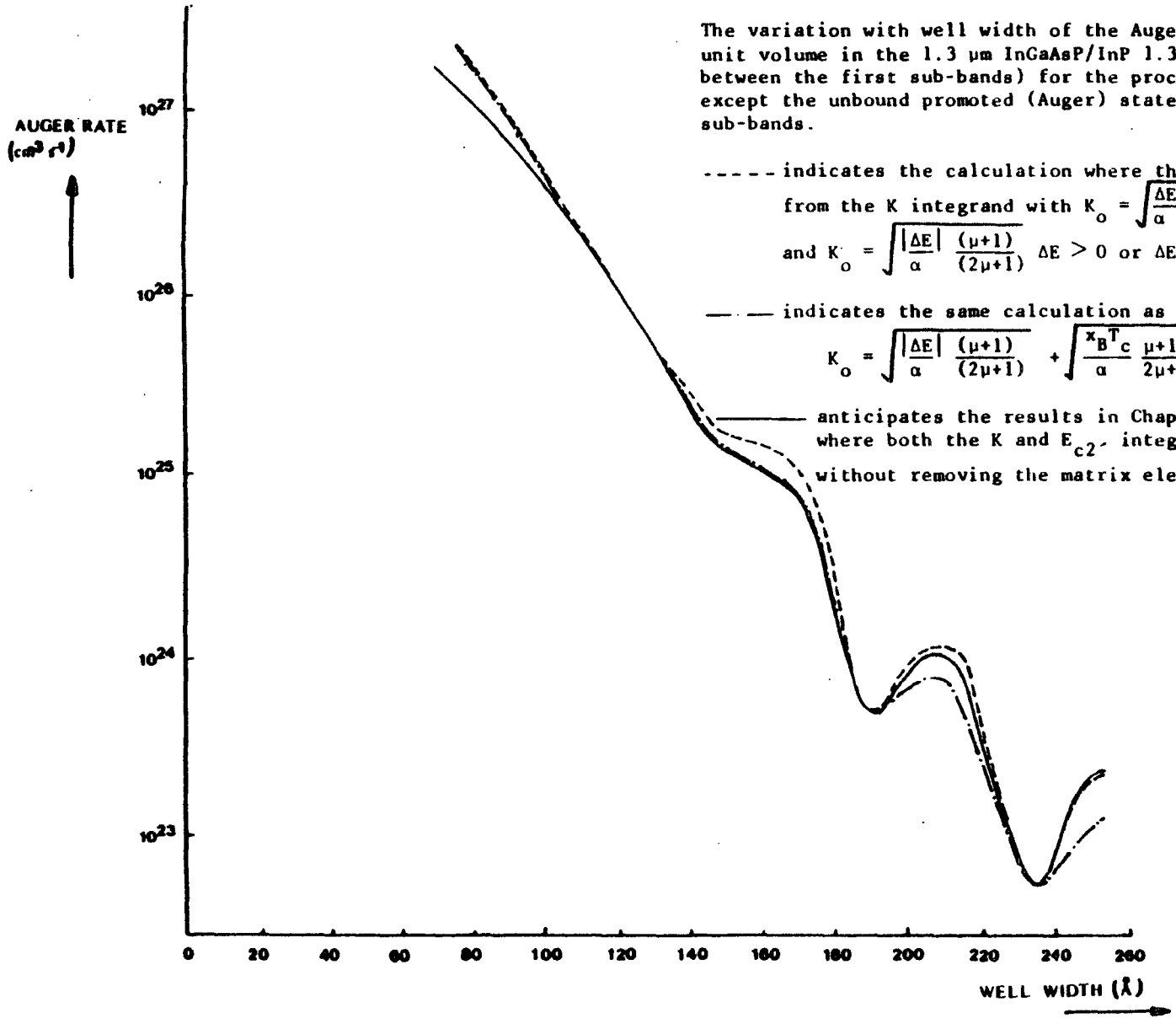


The variation with well width of the Auger recombination rate per unit volume in the 1.3 μm InGaAsP/InP 1.3 μm system (constant band gap between the first sub-bands) for the process where all involved states except the unbound promoted (Auger) state are bound and in the first sub-bands.

- - - - - indicates the calculation where the matrix element is removed from the K integrand with $K_o = \sqrt{\frac{\Delta E}{\alpha}\frac{(\mu+1)}{(2\mu+1)}}$ when $0 > \Delta E > -x_B T_c$ and $K_o = \sqrt{\frac{|\Delta E|}{\alpha}\frac{(\mu+1)}{(2\mu+1)}}$ $\Delta E > 0$ or $\Delta E < -x_B T_c$

— · — indicates the same calculation as above but with

$$K_o = \sqrt{\frac{|\Delta E|}{\alpha}\frac{(\mu+1)}{(2\mu+1)}} + \sqrt{\frac{x_B T_c}{\alpha}\frac{\mu+1}{2\mu+1}}$$

——— anticipates the results in Chapter 5, of the calculation where both the K and $E_{c2}$- integrals are done numerically without removing the matrix element from the integrands

FIGURE 4.4

As figure 4.3 but for the 1.55 μm InGaAsP/InP system (constant band gap between the first sub-bands)

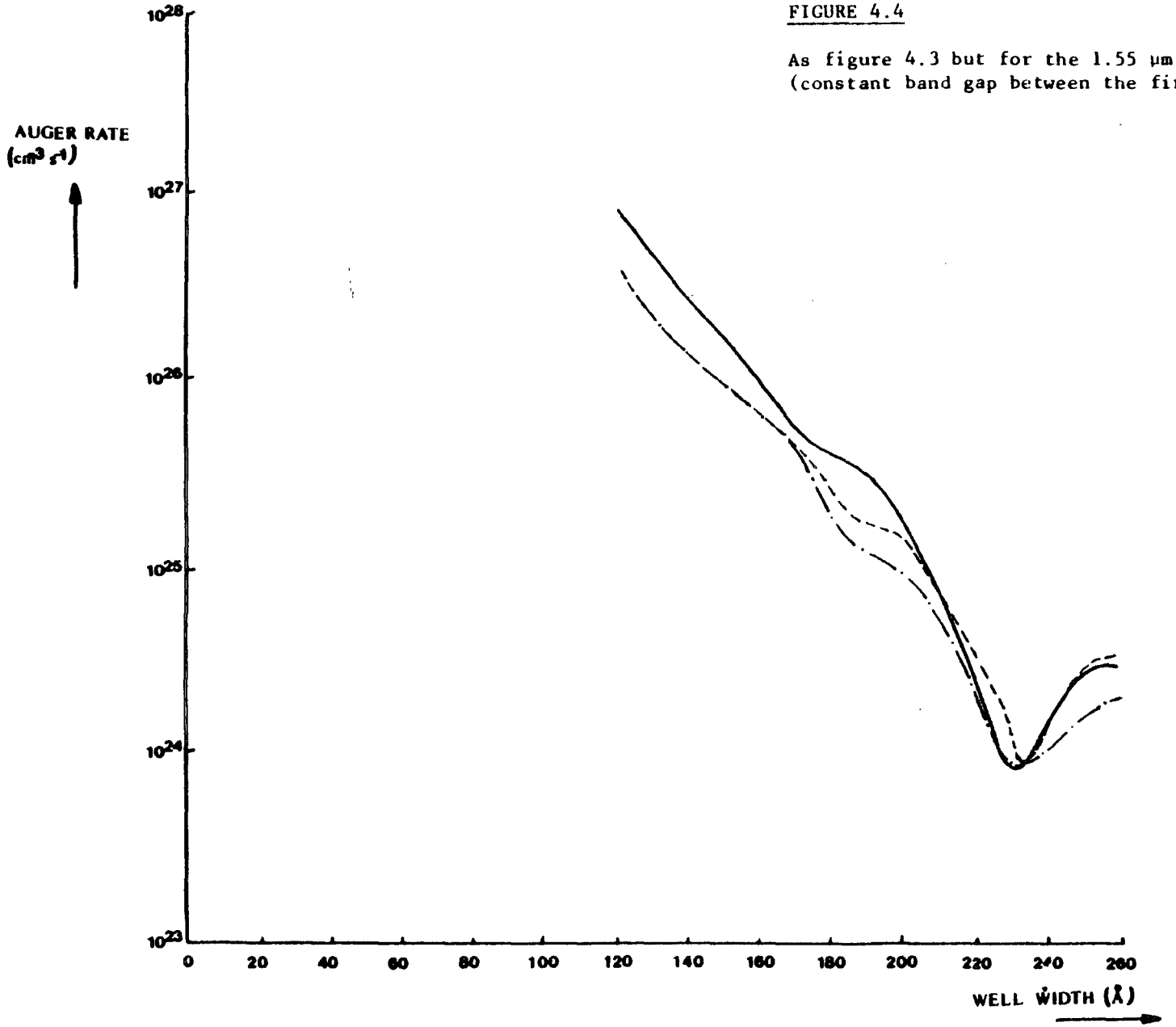

### 4.2.6 DOING THE INTEGRATION OVER UNBOUND SUB-BANDS (THE $E_{c2'}$ INTEGRAL) USING AN ANALYTIC APPROXIMATION

Neglecting, for the moment, the energy dependence of the matrix element through $K_0$ and $K_{\parallel 2'}$, it is seen that the energy integrand is peaked at $\Delta E = 0$ because here energy, and parallel momentum conservation allow transitions involving states which are near the bound sub-band edges, and these states are statistically more likely to contain the required carriers. Figure 4.5 illustrates this peak, and indicates its functional dependence in the energy integrands 4.16 and 4.20.

The basis of an approximate analytical evaluation of the $E_{c2'}$ integral is to evalute the matrix element at the energy of this peak, and remove it from the $E_{c2'}$ integrand. The remaining integration can then be done analytically.

Although the accuracy of this procedure is obviously limited it is useful for checking the full calculation, and for deciding the most appropriate choice of step sizes, etc in the numerical integrations.

FIGURE 4.5

This figure illustrates the $\Delta E = 0$ peak in the non-matrix element part of the energy integrand, and indicates its functional dependence. In particular it indicates the $\Delta E = 0$ peak for the 200Å 1.3 μm InGaAsP/InP system.

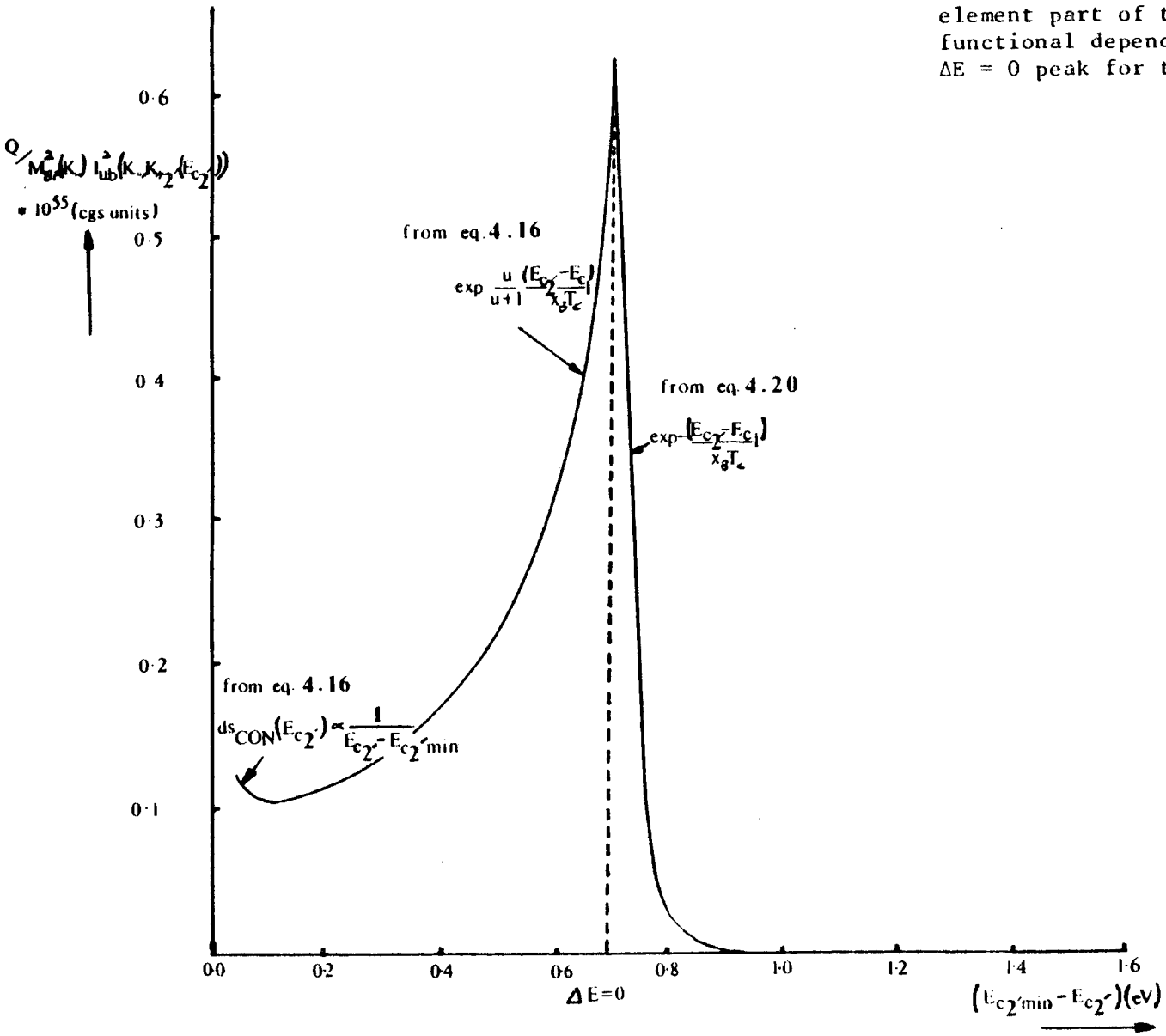


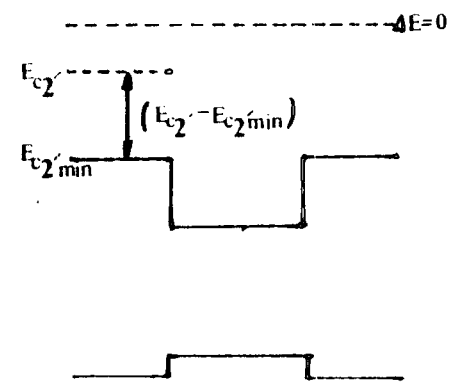

Removing the matrix element from the integrands of 4.16 and 4.20, substituting for $ds_{CON}(E_{c2'})$ and using $\Delta E = E_{c1}+E_{c2}-E_{v1'}-E_{c2'}$ we obtain

$$Q = \frac{\pi^3}{\alpha^3}(x_BT_c)^2 \frac{(\mu+1)}{(2\mu+1)^2}\frac{\ell}{2\pi}\left(\frac{2m}{\hbar^2}\right)^{\frac{1}{2}} M_{BF}^2 I_{ub}^2 \left[ e^{-\frac{\mu}{\mu+1}\frac{E_{c1}}{x_BT_c}} e^{-\frac{(2\mu+1)}{\mu+1}\frac{(E_{c2}-E_{v1'})}{x_BT_c}} \right.$$

$$\int_{E_{c2'min}}^{E_{c2}-E_{v1'}-E_{c1}} \frac{e^{\frac{\mu}{\mu+1}\frac{E_{c2'}}{x_BT_c}}}{(E_{c2'}-E_{c2'min})^{\frac{1}{2}}} dE_{c2'} + (x_BT_c)\frac{2\mu+1}{\mu+1} e^{+E_{c1}/x_BT_c}$$

$$\int_{E_{c2}-E_{v1'}-E_{c1}}^{\infty} e^{-E_{c2'}/x_BT_c} \frac{(E_{c2'}-E_{c1}+E_{v1'}-E_{c2})}{(E_{c2'}-E_{c2'min})^{\frac{3}{2}}} dE_{c2'}$$

$$e^{+E_{c1}/x_BT_c} \int_{E_{c2}-E_{v1'}-E_{c1}}^{\infty} \frac{e^{-E_{c2'}/x_BT_c}}{(E_{c2'}-E_{c2'min})^{\frac{1}{2}}} dE_{c2'} \qquad 4.23$$

Now simplifying this by substituting $x = E_{c2'}-E_{c2'min}$ and using $\Delta E_{max} = E_{c1}+E_{c2}-E_{v1}-E_{c2'min}$

$$Q = \frac{\pi^2}{\alpha^3}(x_BT_c)^2 \frac{(\mu+1)}{(2\mu+1)^2}\frac{\ell}{2}\left(\frac{2m}{\hbar^2}\right)^{\frac{1}{2}} M_{BF}^2 I_{ub}^2 \left[ e^{-\frac{\mu}{(\mu+1)}\frac{E_{c1}}{x_BT_c}} e^{-\frac{2\mu+1}{\mu+1}\frac{E_{c2}-E_{v1'}}{x_BT_c}} \right.$$

$$e^{\frac{\mu}{\mu+1}\frac{E_{c2'min}}{x_BT_c}} \int_{x=0}^{x=\Delta E_{max}} \frac{e^{+\frac{\mu}{(\mu+1)}\frac{x}{x_BT_c}}}{x^{\frac{1}{2}}} dx$$

$$+ x_BT_c \frac{2\mu+1}{(\mu+1)} e^{+E_{c1}/x_BT_c} e^{\frac{-E_{c2'min}}{x_BT_c}} \int_{\Delta E_{max}}^{\infty} \frac{e^{-x/x_BT_c}}{x^{\frac{3}{2}}}(x-\Delta E_{max})\, dx$$

$$\left. + e^{+E_{c1}/x_BT_c} e^{-\frac{E_{c2'min}}{x_BT_c}} \int_{\Delta E_{max}}^{\infty} \frac{e^{-x/x_BT_c}}{x^{\frac{1}{2}}} dx \right] \qquad 4.24$$

The first of these integrals is then solved by expressing it in terms of Dawson's integral. Putting

$$\frac{\mu}{(\mu+1)}\frac{x}{x_BT_c} = y^2 \qquad 4.25$$

gives

$$dx = \frac{(\mu+1)}{\mu} x_B T_c \, dy \qquad 4.26$$

and

$$x^{\frac{1}{2}} = \left(\frac{(\mu+1)}{\mu} x_B T_c\right)^{\frac{1}{2}} y \qquad 4.27$$

Thus the first integral becomes

$$Q_{1st} = \frac{\pi^2}{\alpha^3} (x_B T_c)^2 \frac{(\mu+1)}{(2\mu+1)^2} \frac{\ell}{2} \left(\frac{2m}{\hbar^2}\right)^{\frac{1}{2}} M_{BF}^2 I_{ub}^2 \, e^{-\frac{\mu}{\mu+1} \frac{E_{c1}-E_{c2'min}}{x_B T_c}}$$

$$e^{-\frac{2\mu+1}{\mu+1} \frac{(E_{c2}-Ev_{1'})}{x_B T_c}} \; 2\left(\frac{(\mu+1)}{\mu} x_B T_c\right)^{\frac{1}{2}} \int_{y=0}^{y=\left(\frac{\mu}{\mu+1} \frac{\Delta E_{max}}{x_B T_c}\right)^{\frac{1}{2}}} e^{y^2} \, dy \qquad 4.28$$

$$Q_{1st} = \frac{\pi^2}{\alpha^3} (x_B T_c)^2 \frac{(\mu+1)}{(2\mu+1)^2} \frac{\ell}{2} \left(\frac{2m}{\hbar^2}\right)^{\frac{1}{2}} M_{BF}^2 I_{ub}^2 \, e^{-\frac{\mu}{\mu+1} (E_{c1}-E_{c2'min})}$$

$$e^{-\frac{2\mu+1}{\mu+1} \frac{(E_{c2}-E_{v1})}{x_B T_c}} \; 2\left(\frac{(\mu+1)}{\mu} x_B T_c\right)^{\frac{1}{2}}$$

$$e^{\frac{\mu}{\mu+1} \frac{\Delta E_{max}}{x_B T_c}} \; F\left(\left(\frac{\mu}{\mu+1} \frac{\Delta E_{max}}{x_B T_c}\right)^{\frac{1}{2}}\right) \qquad 4.29$$

where F is Dawson's integral.

To check 4.29 G+R page 317 eg 3.381.1 may be used, it being remembered that $\gamma(\frac{1}{2}, x^2) = 2\int_0^x e^{-t^2} dt = \sqrt{\pi}\,\mathrm{erf}(x)$ where $\gamma$ is the incomplete gamma function. Alternatively G+R page 315 eg 3.361.1 can be used*.

*Unfortunately, this second integral contains a misprint in the 4th edition of G+R. In this edition the square root sign should continue down to include the 'q'.

The second and third integrals are evaluated by applying G+R page 317 eg 3.381.3. The complete result from the evaluation of 4.24 being

$$Q = \frac{\pi^2}{\alpha^3} (x_B T_c)^2 \frac{(\mu+1)}{2(\mu+1)^2} \frac{\ell}{2} \left(\frac{2m}{\hbar^2}\right)^{\frac{1}{2}} M_{BF}^2 I_{ub}^2 \left[ e^{-(E_{c2'min}-E_{c1}+\Delta E_{max})/x_B T_c} \right.$$

$$2\left(\frac{(\mu+1)}{\mu} x_B T_c\right)^{\frac{1}{2}} F\left(\left(\frac{\mu}{\mu+1} \frac{\Delta E_{max}}{x_B T_c}\right)^{\frac{1}{2}}\right)$$

$$+ \frac{1}{x_B T_c} \frac{(2\mu+1)}{(\mu+1)} e^{-(E_{c2'min}-E_{c1})/x_B T_c} \left\{ (x_B T_c)^{3/2} \Gamma\left(\frac{3}{2}, \frac{\Delta E_{max}}{x_B T_c}\right) \right.$$

$$\left. - \frac{\Delta E_{max}}{(x_B T_c)^{\frac{1}{2}}} \Gamma\left(\frac{1}{2}, \frac{\Delta E_{max}}{x_B T_c}\right) \right\} \qquad 4.30$$

$$\left. + e^{-(E_{c2'min}-E_{c1})/x_B T_c} (x_B T_c)^{\frac{1}{2}} \Gamma\left(\frac{1}{2}, \frac{\Delta E_{max}}{x_B T_c}\right) \right]$$

Now this can be approximated. Considering the first term

$F(X') \sim \frac{1}{2X'}$ for large $X'$ (from table 7.5 A+S page 319)

and for worst case here considered

$X' = \left(\frac{\mu}{\mu+1} \frac{\Delta E_{max}}{x_B T_c}\right)^{\frac{1}{2}} \sim 1.4$ (L ~ 260Å in 1.55 μm InGaAsP/InP system)

thus $F(X') \sim 0.46$ (from tables) while $\frac{1}{2X'} \sim 0.36$

Considering the other terms

$$\Gamma(a, X'') \sim X''^{a-1} e^{-X''} \left[1 + \frac{a-1}{X''} + \ldots\ldots\ldots\ldots\right]$$

(from A+S page 263 eg 6.5.32)

So with these approximations

$$Q = \frac{\pi^2}{\alpha^3} (x_B T_c)^3 \; \frac{\ell}{2} \left(\frac{2m}{\hbar^2}\right)^{\frac{1}{2}} M_{BF}^2 I_{ub}^2 \left[ \frac{(\mu+1)^2}{(2\mu+1)^2} \; \mu \; \frac{e^{-(E_{c2}-E_{v1'})/x_B T_c}}{(\Delta E_{max})^{\frac{1}{2}}} + \frac{1}{(2\mu+1)} \; \frac{e^{-(E_{c2}-E_{v1'})/x_B T_c}}{(\Delta E_{max})^{\frac{1}{2}}} + \frac{(\mu+1)}{(2\mu+1)^2} \; \frac{e^{-E_{c2}-E_{v1'})/x_B T_c}}{(\Delta E_{max})^{\frac{1}{2}}} \right] \qquad 4.31$$

which simplifies further to the relatively simple expression

$$Q = \frac{\pi^2}{\alpha^3} (x_B T_c)^3 \; \frac{\ell}{2} \left(\frac{2m}{\hbar^2}\right)^{\frac{1}{2}} M_{BF}^2 I_{ub}^2 \; \frac{1}{\mu} \; \frac{e^{-(E_{c2}-E_{v1'})/x_B T_c}}{(\Delta E_{max})^{\frac{1}{2}}} \qquad 4.32$$

From this the full numerical calculations can be checked and optimised. Taking $(M_{BF}{}^2 . I_{ub}^2)$ as constant in the full numerical calculation the two methods can be made to agree within about 10% which is as good as could be expected in view of the above approximations, and we now proceed to a discussion of the full numerical in the next chapter.

**REFERENCES FOR CHAPTER 4**

4.1 Gradshteyn I S and Ryzhik I M 1980 Table of Integrals, Series and Products (London: Academic).

4.2 Abramowitz and Stegun Handbook of Mathematical Functions (New York: Dover).

# CHAPTER 5 - THE RESULTS

This chapter presents numerical results for the bound-bound and bound-unbound CHCC Auger rate calculations, in an isolated quantum well. It is concerned mainly with the InGaAsP/InP system, but as shall be seen later reference is made to the GaAs/GaAlAs system to assist in the physical interpretation of the numerical results. InGaAsP/InP structures with emission wavelengths of 1.3 μm and 1.55 μm are considered. The alloy composition of InGaAsP being varied with well width to maintain a constant emission wavelength.

The bound-bound and bound-unbound rates are examined, and a physical interpretation of their important features is given. The relative importance of the bound-bound and bound-unbound Auger recombination in the 1.3 μm and 1.55 μm systems is then discussed, and comparisons are made with bulk CHCC Auger calculations. Finally comparisons are made with some other QW CHCC Auger calculations.

## 5.1 THE PARAMETERS FOR THE InGaAsP/InP SYSTEMS

For the 1.3 μm and 1.55 μm InGaAsP/InP structures the alloy composition is varied with well width to keep the quantum well band gap constant.

The required variation is found using the alloy composition dependences of the bulk InGaAsP parameters

from Dutta and Nelson (ref 5.1), a finite square model to determine the bound sub-band levels, and a constant ratio of conduction band discontinuity to valence band discontinuity of 2:1 (see ref 5.2).

Table 5.1 shows the variation of InGaAsP parameters with alloy composition, and figures 5.1 and 5.2 show resultant variation of alloy composition with well width when the energy separation between the first sub-bands is kept constant at respectively, 0.96 eV (corresponding to the 1.3 μm system), and 0.8 eV (corresponding to the 1.55 μm system). From the second of these figures it may be observed that compositional constraints prevent 1.55 μm InGaAsP/InP systems being grown below about 114Å.

**Table 5.1**

This table shows the variation in $In_{1-x}Ga_xAs_yP_{1-y}$ parameters with alloy composition y. The heavy hole band effective mass, light hole band effective mass, intrinsic dielectric constant, and the $\Gamma$ band gap between the bulk spin split-off and bulk heavy hole band '$\Delta$', are found by linear extrapolation between binary values. The $\Gamma$ band gap between the bulk conduction band and bulk heavy hole band, and the conduction band effective mass are found by more direct experimental methods, and the spin split-off mass is given a value typical of binary compounds.

$$\frac{m_{HL}}{m_o}^{\dagger} = (1-y)[0.79x+0.45(1-x)] + y[0.45x+0.4(1-x)]$$

$$\frac{m_{LH}}{m_o}^{\dagger} = (1-y)[0.14x+0.12(1-x)] + y[0.082x+0.026(1-x)]$$

$$\varepsilon_{INT}^{\dagger} = (1-y)[8.4x+9.6(1-x)] + y[13.1x+12.2(1-x)]$$

$$\Delta_{sp}^{\dagger}(eV) = 0.11+0.31y-0.09y$$

$$E_g^{\dagger}(eV) = 1.35-0.72y-0.12y$$

$$\frac{m_c}{m_o}^{\dagger} = 0.080-0.039y$$

$$\frac{m_s}{m_o} = 1.6$$

requirement for lattice matching to $InP^{\dagger}$ $x = \frac{0.4526y}{1-0.031y}$

†= taken from ref 5.1

FIGURE 5.1

This curve shows how the ratio of As to P in InGaAsP must be varied with well width, to keep the separation between the first conduction and first heavy hole bands constant at 0.96 eV (this separation corresponding to the 1.3 μm InGaAsP/InP system)

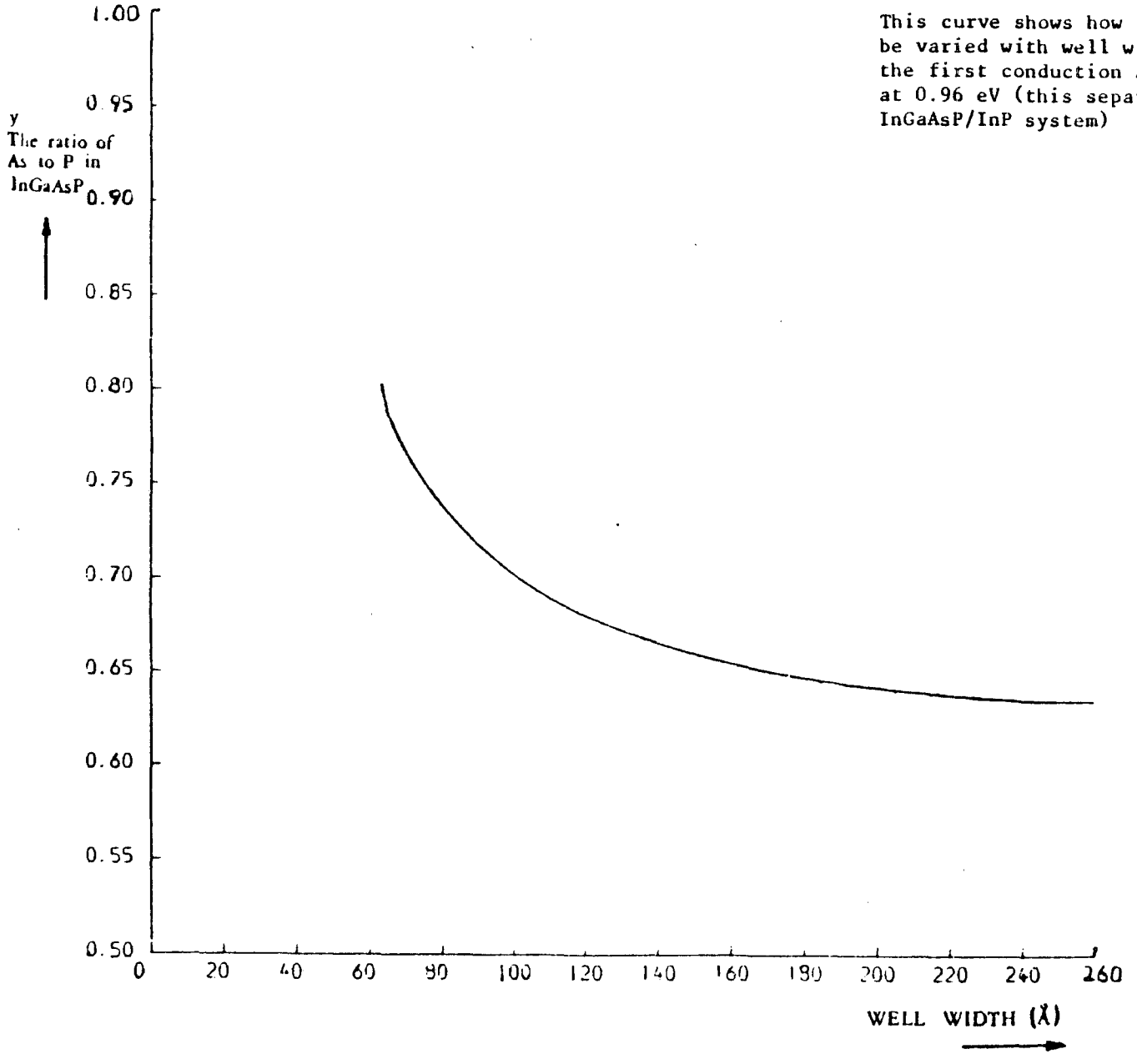

FIGURE 5.2

As for figure 5.2, but with the first sub-bands separated by 0.8 eV (corresponding to the 1.55 μm system)

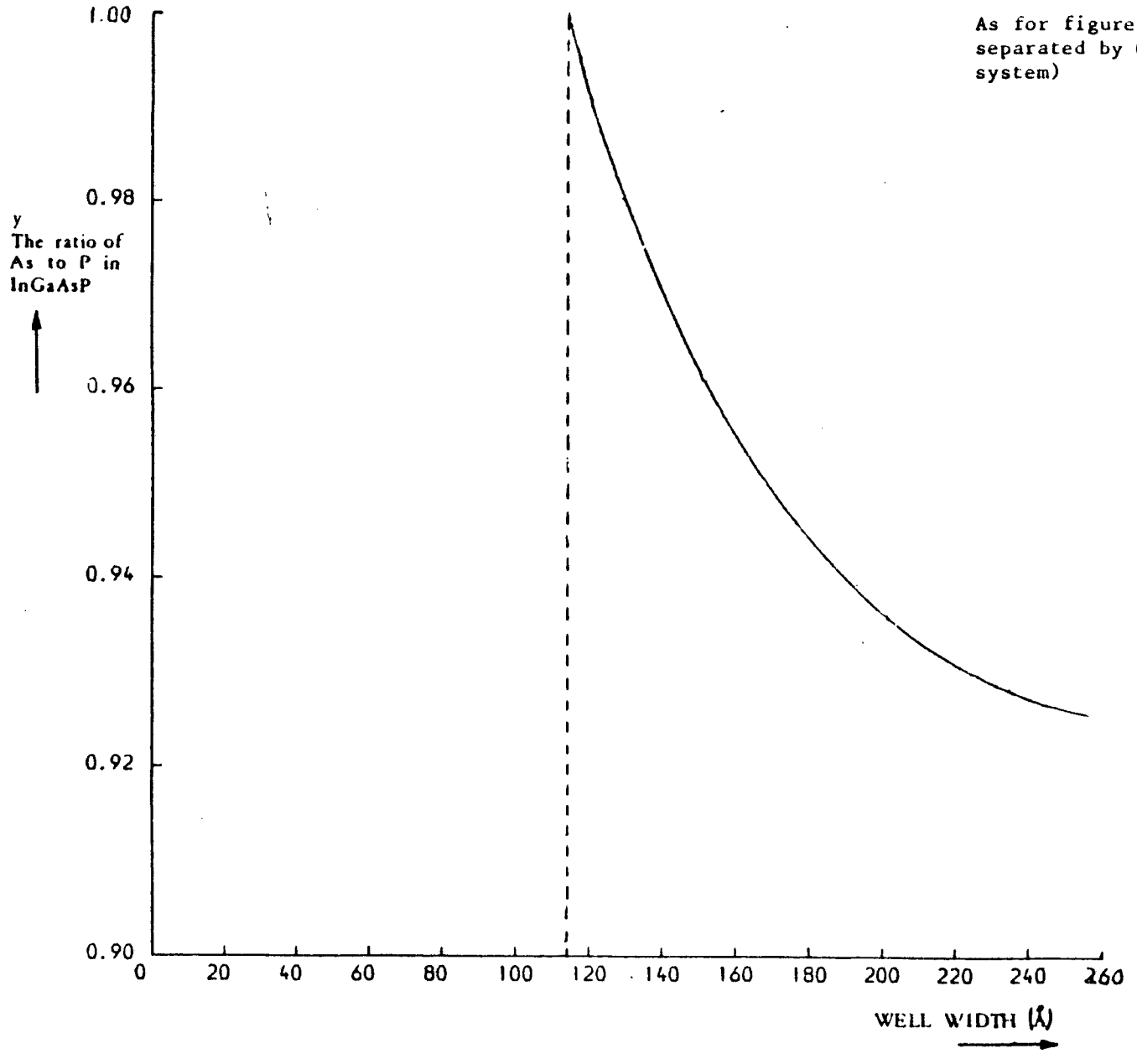

## 5.2 THE BOUND-BOUND CHCC NUMERICAL RESULTS

Using the above parameters, figures 5.3 and 5.4 show respectively for the 1.3 μm and 1.55 μm systems, the variation of the combined bound-bound CHCC Auger rate (that is the resultant of all bound-bound sub-band transitions see equation 3.48) with well width. The figures assume carrier thermalisation, between bound and unbound states, of 10E+18 conduction electrons $cm^{-3}$ and of 10E+18 valence holes (light, heavy, and spin split-off) $cm^{-3}$.

To assist in their interpretation, figures 5.3 and 5.4 also show some important contributions to the combined bound-bound rate. The largest of these contributions is the one where all the carriers remain in the ground electron and hole sub-bands. This is to be expected because the ground sub-bands have the largest populations of carriers. In the other significant processes shown it should be noted that the higher electron sub-bands act only as receivers for the excited electron, they not being sufficiently populated to play any other role. The variation of these important individual contributions with well width is, when the large $K$L matrix element approximation is used, dependent of well width only through the carrier densities, and sub-band energy levels (see earlier figures 2.3, 2.4, 2.6, and 2.7). The values of the contributions shown decrease as higher bands move nearer in energy and

FIGURE 5.3

This figure shows the variation in a 1.3 μm InGaAsP/InP system of the combined (total) bound-bound CHCC Auger rate, and particular contributions to this rate, with well width. The convention used in naming the particular contributions is shown in the insert.

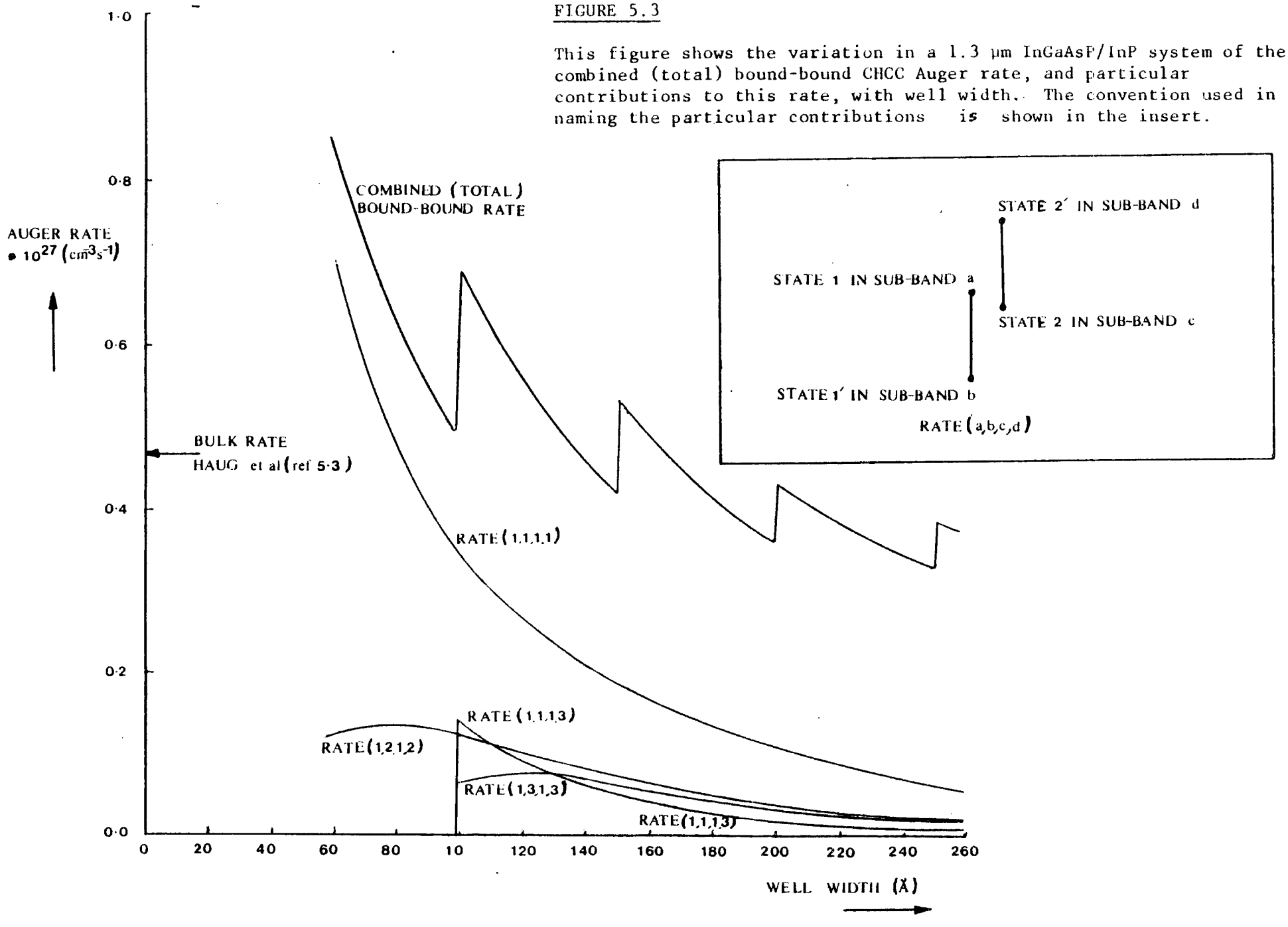

FIGURE 5.4

As figure 5.3 but for the 1.55 μm InGaAsP/InP system

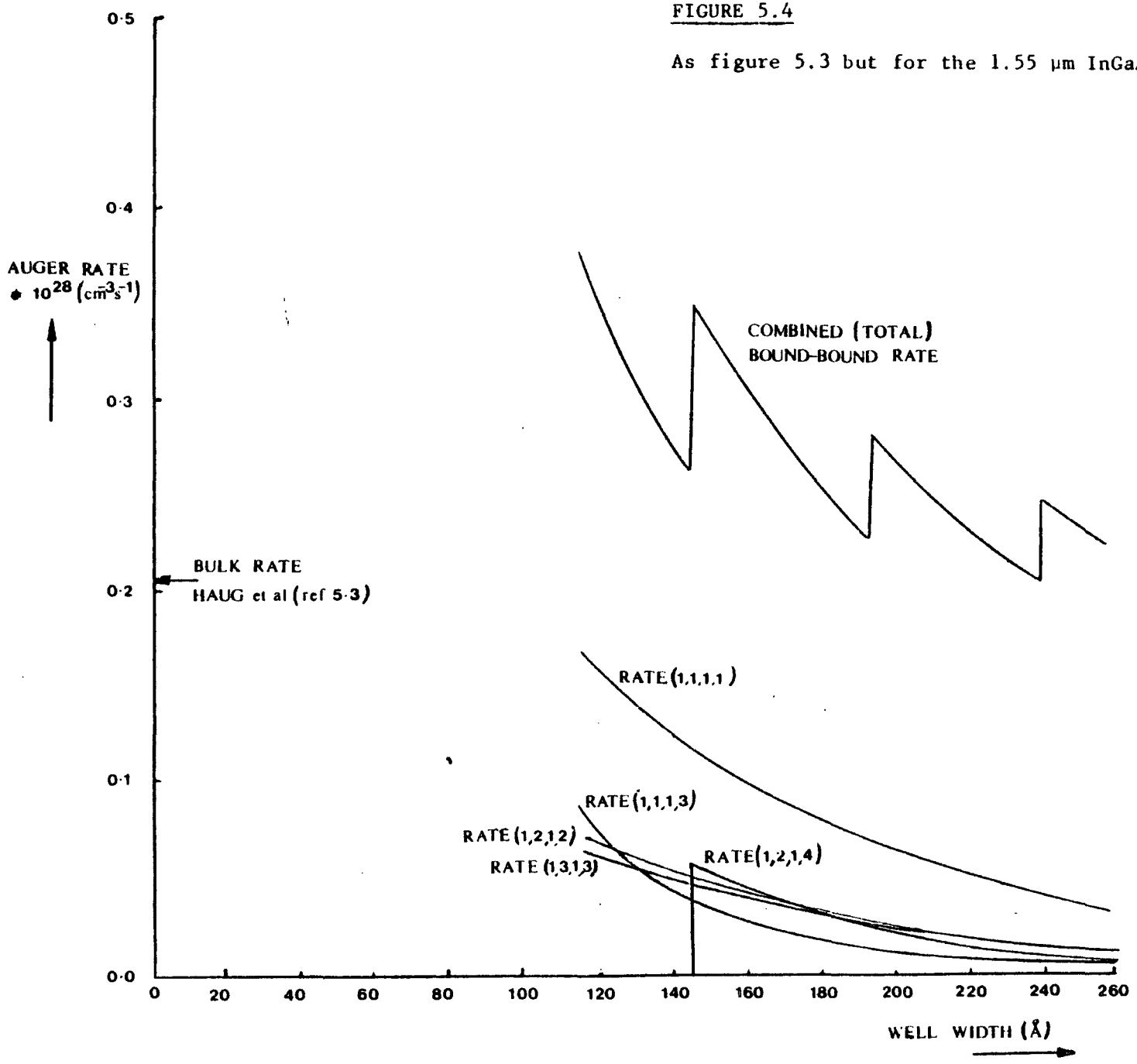

hence take a larger share of the available carriers. This decrease is however tempered (except in the solely first sub-band case) by reductions with well width in the size of the activation energy $\Delta E = E_1 + E_2 - E_{1'} - E_{2'}$. The general trend for the combined bound-bound rate is seen to be downward with increasing well width. The Auger rate curve is, however, punctuated by discontinuities as extra electron sub-bands become bound by the well, and so are available to act as receivers for the promoted (Auger) electron.

## 5.3 THE BOUND-UNBOUND NUMERICAL RESULTS

Figures 5.5 and 5.6 show respectively the variation of the first sub-band bound unbound CHCC Auger rate with well width, in the 1.3 μm and 1.55μm InGaAsP/InP systems with 10E+18 thermalised carriers $cm^{-3}$. By comparing the magnitude of the rate with that for the bound-bound transitions we see that the first sub-band-unbound rate is a significant component of the total Auger rate at small well widths (< 100Å for 1.3μm system). At these small well widths it is found that the first sub-band-unbound process is the only significant bound-unbound contribution. This is because there are few carriers in the other bound states. At large well widths other bound-unbound processes are comparable to the first sub-band contribution but then the rate from each process and their combined effect are small compared to the bound-bound rate. The important features of the bound-unbound rate are 1) it is only comparable with the bound-unbound rate in narrow wells, and 2) it contains oscillations. A qualitative description of these features is now given using the premise that the statistically favoured $\Delta E=0$ condition selects as dominant transitions those involving the unbound sub-band with band bottom corresponding to $\Delta E=0$.

FIGURE 5.5

This figure shows the variation, in a 1.3 μm InGaAsP/InP system, of the first sub-band bound-unbound CHCC Auger rate.

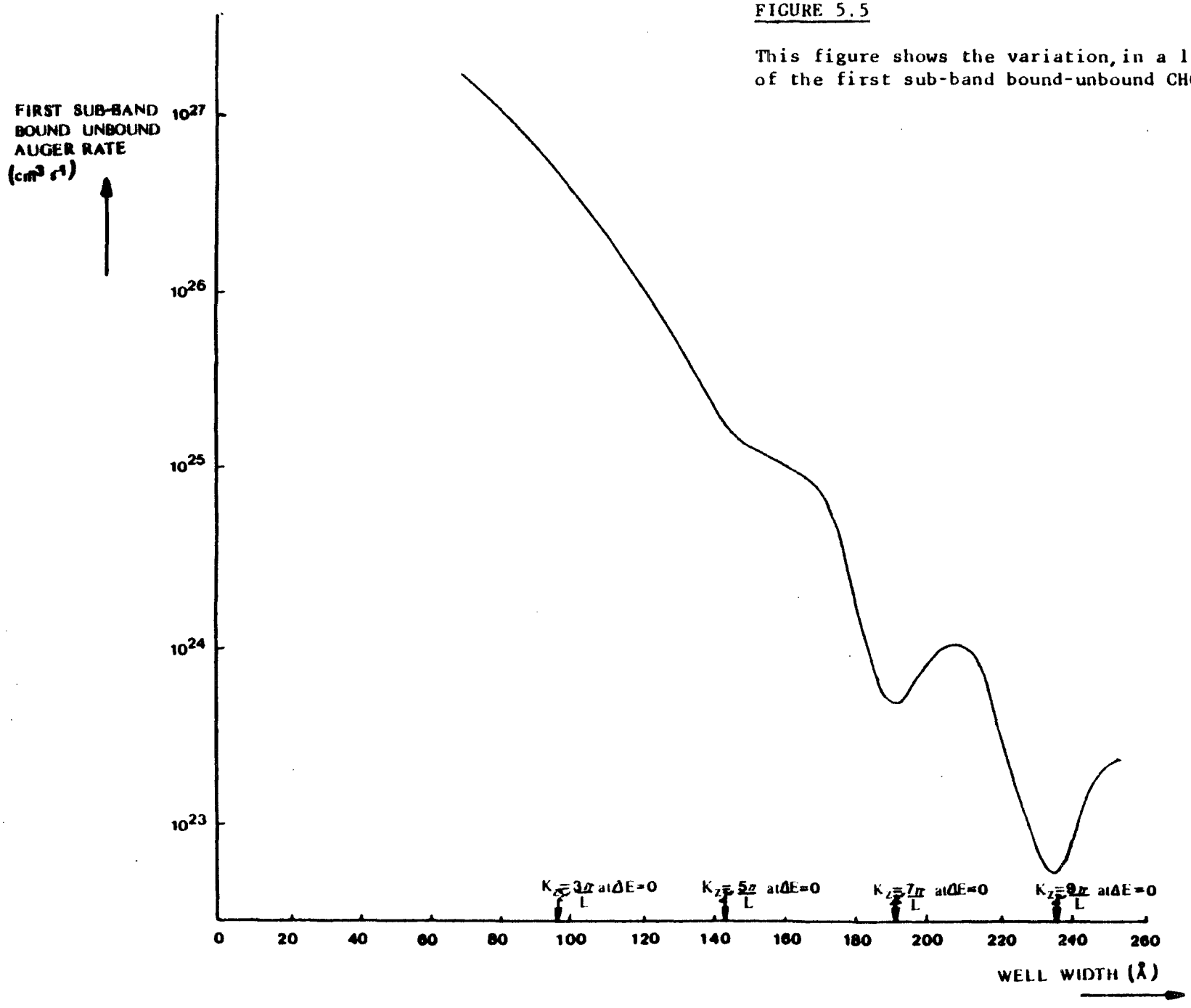

FIGURE 5.6

As figure 5.5 but for the 1.55 μm InGaAsP/InP system

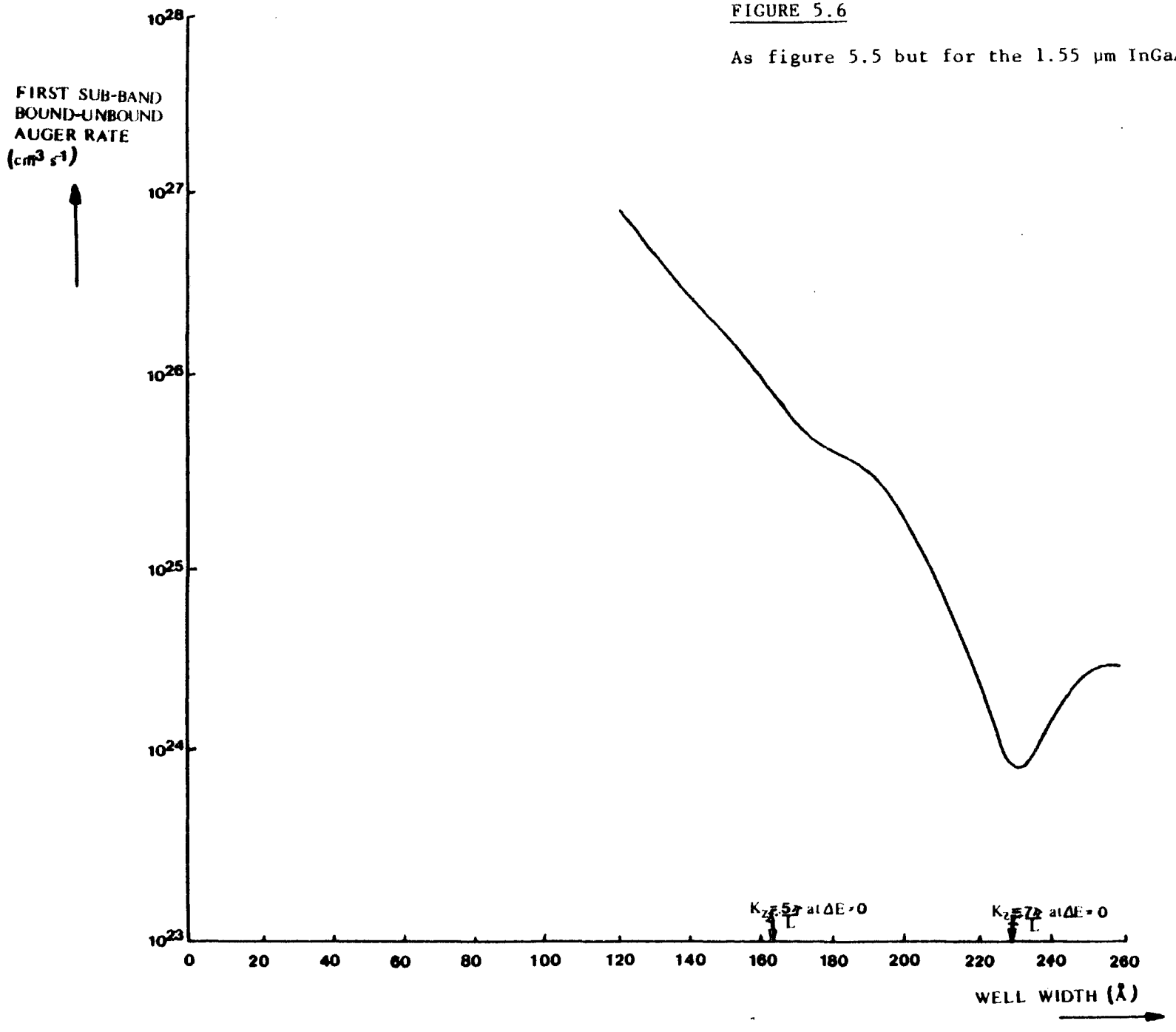

The oscillations seen in Figs 5.5 and 5.6 are not inconsistent with the assumption that the unbound state sub-band is fixed by the $\Delta E=0$ condition. On these grounds we would expected minima to occur when the well width is such that the unbound state perpendicular wavevector $K_{z2'} = \frac{5\pi}{L}, \frac{7\pi}{L}, \frac{9\pi}{L}$ etc (see Appendix 3 with KL large ?). Unfortunately the graphs are not conclusive because the $\Delta E=0$ peak in the InGaAsP/InP systems is not very sharp and is not very good at picking out the transitions discussed above.

The factors affecting the variation of the bound-unbound rate with well width are :1) changes in the size of the $\Delta E=0$ peak; 2) changes in the width of the $\Delta E=0$ peak; 3) the dependences of the effective density of states on well width, 4) the factor of L which appears when the Auger rate is expressed per unit volume rather than per unit area; and 5) the general decrease in wavefunction overlap between the bound and unbound states as the envelope function of the unbound state selected by the $\Delta E=0$ condition gets a larger perpendicular wavevector and hence more envelope function oscillations across the well. At the end of the next section the relative importance of these factors is investigated and it is shown that the fifth factor accounts for most of the rapid decrease in the results.

It is interesting to note that the discontinuities appearing in the bound-bound Auger rate vs well width curve (Figs 5.3 and 5.4) do not have any counterpart in the bound-unbound curve. The discontinuities come about because a new bound state is created in the important region of space - that is, in the well where the recombining carriers are localized. The new bound state is then available to receive the excited electron and can make a significant contribution to the Auger rate. However binding a new state has a negligible effect on the continuum of unbound states, their density being determined by the boundary conditions at the boundaries of the infinite system. It should be noted that the total number of states per unit volume does not change when a new state is bound - only one state is bound but the volume is infinite.

## 5.4 A TEST OF THE EXPLANATION OF THE NUMERICAL BOUND-UNBOUND RESULTS USING THE GaAs/GaAlAs SYSTEM

### PARAMETER REQUIREMENTS

The requirements for choosing a set of parameters with which to test the interpretation of the behaviour in Figs 5.5 and 5.6 , are 1) they should give a sharp $\Delta E=0$ peak, and 2) they should give weight to large K transitions so that the large K approximations will hold.

For the first requirement the choice of parameters is suggested by the functional dependences indicated in figure 4.5 . A sharp $\Delta E=0$ peak can either be achieved by increasing '$\mu$' the ratio of the conduction band mass to the valence band mass, or increasing $\Delta E_{max}$. $\Delta E_{max}$ depends on the difference between the effective band gap $\Delta Eg$, and the effective conduction band discontinuity '$E_{c2min} - E_{c1}$'.

Guidance upon the second requirement can be obtained from expression in Appendix 4. Detailed examination of the integrand shows that the integral is dominated by the behaviour at large K if the quantum well energy gap is large.

**GaAs PARAMETERS**

Figures 5.7, and 5.8 show that the requirements needed to test the numerical result against the premise are fulfilled in the GaAs/GaAlAs system, where the ratio of the conduction effective mass to heavy hole effective mass is taken as 0.067 to 0.45, the bulk GaAs band gap is taken as 1.42 eV, and the conduction band discontinuity is 85% of the difference between the bulk GaAs band gap and bulk GaAlAs band gap (ref 5.2). Figure 5.7 shows that as required the $\Delta E=0$ condition is defined by a sharp peak in the GaAs/GaAlAs system. Figure 5.8 compares, similarly to Figs 4.3 and 4.4, the full numerical calculation of the bound-unbound Auger rate with the rate when small K values are omitted, and hence shows that the integral is dominated by the behaviour of the integrand at large K.

**THE INTERPRETATION OF THE GaAs/GaAlAs RESULTS**

Figure 5.8 shows that the oscillations in the numerical results are compatible with the premises, ie compatible with the interpretation in Section (5.3) based on the values of K for the unbound states involved in the dominent transitions.

Further, numerical investigations have shown that, as suggested earlier, the increased oscillation of the unbound wavefunction defined by $\Delta E=0$ accounts for most of

FIGURE 5.7

As figure 4.5 but for the GaAs/GaAlAs system with a 200Å wide well.

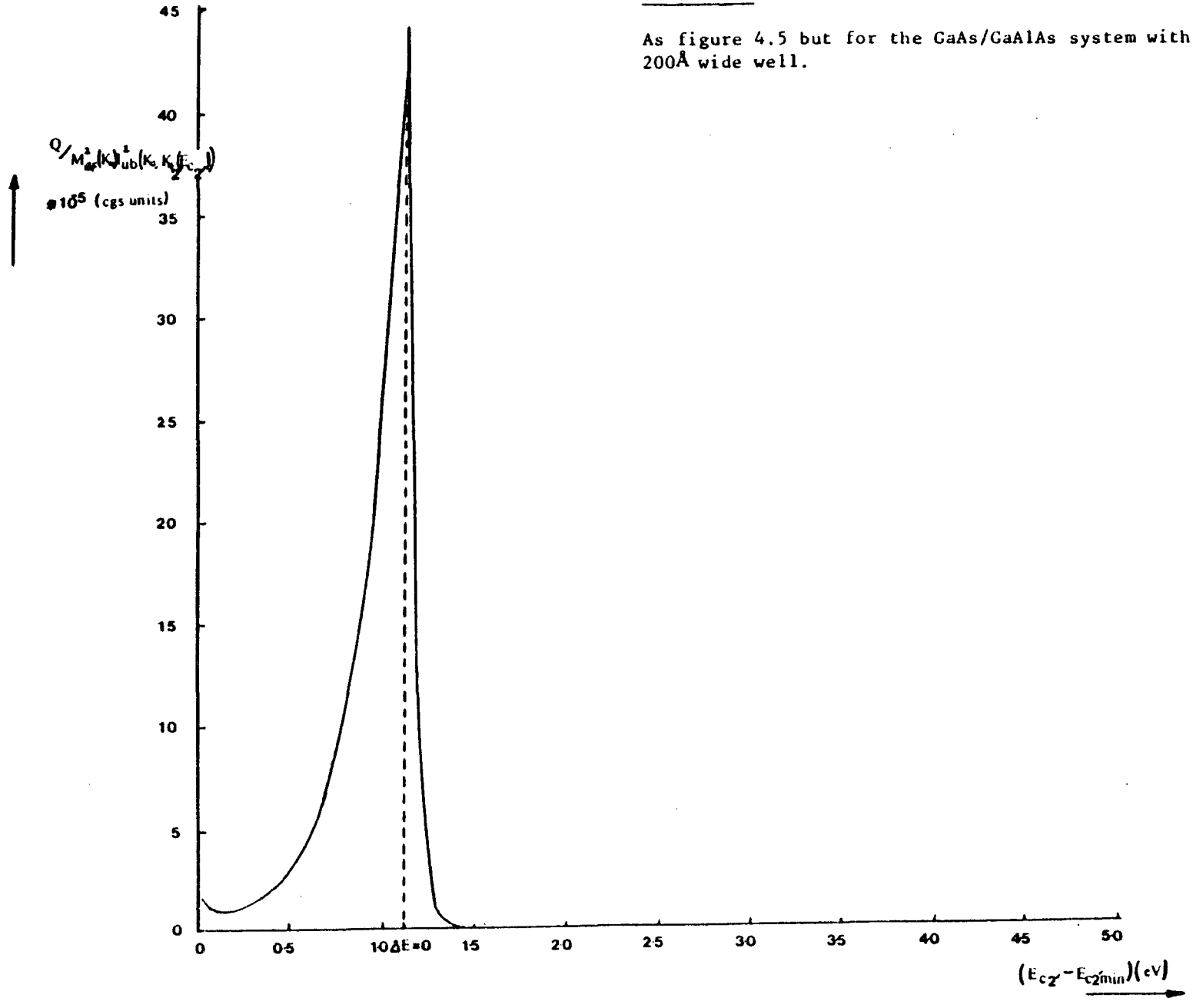

FIGURE 5.8

As figures 4.3 and 4.4 but for the GaAs/GaAlAs system.

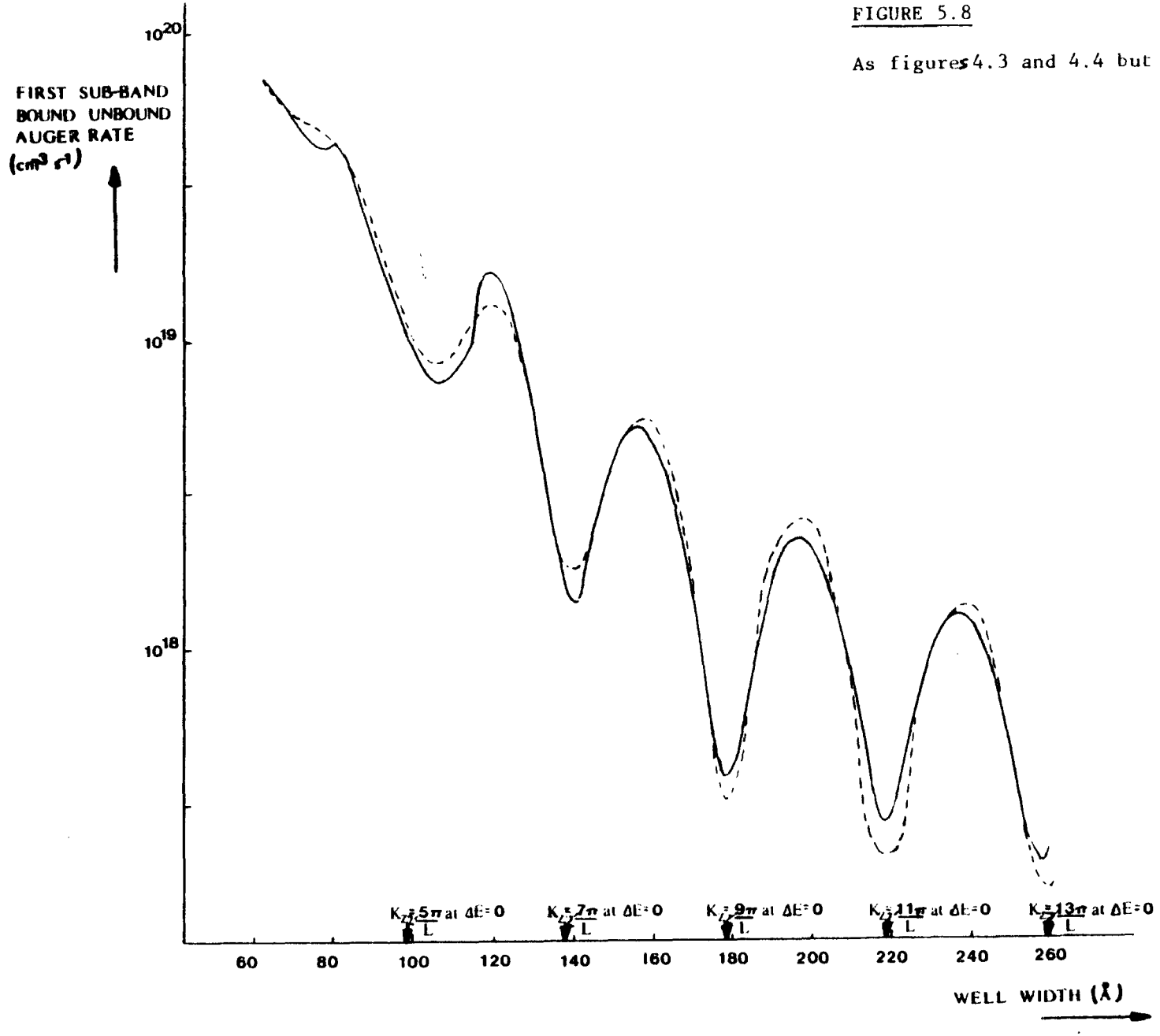

the rapid decrease in the rate. However even in the GaAs/GaAlAs system the blurring caused by the width of the $\Delta E=0$ peak is still significant, and must be taken into account to get good numerical agreement between the approximation and the full the numerical results.

However, with GaAs/GaAlAs parameters we have established an interpretation of the numerical results, by showing them to be consistent with a simple explanations in terms of the $\Delta E=0$ statistical peak.

## 5.5 UNBOUND-UNBOUND PROCESSES

Because of the carrier distributions assumed processes other than where colliding electrons and hole are bound are unlikely on statistical grounds. Therefore unbound-unbound processes have not been considered, they being neglected as insignificant.

## 5.6 THE COMBINED RESULTS

Figures 5.9 and 5.10 show the variation of the combined bound-bound, and first sub-band bound-unbound CHCC Auger rate with well width in the 1.3 μm and 1.55 μm InGaAsP/InP systems. First the relative importance of the first sub-band bound-unbound rate in the 1.3 μm system is explained. Then comparisons are made between QW results and bulk CHCC Auger rate calculations.

### 5.6.1 THE RELATIVE IMPORTANCE OF THE FIRST SUB-BAND BOUND-UNBOUND RESULTS IN THE InGaAsP/InP STRUCTURES

The relative importance of the first sub-band bound-unbound result in the 1.3 μm InGaAsP/InP system compared to the 1.55 μm InGaAsP/InP system is easily explained on the basis of the discussion in the previous sections.

In the 1.55 μm system the well must be grown relatively wide because of compositional constraints. Because the well is relatively deep, many (at least three) bound sub-bands are always within the well. Consequently the similarities

FIGURE 5.10

As figure 5.9 but for the 1.55 μm InGaAsP/InP system

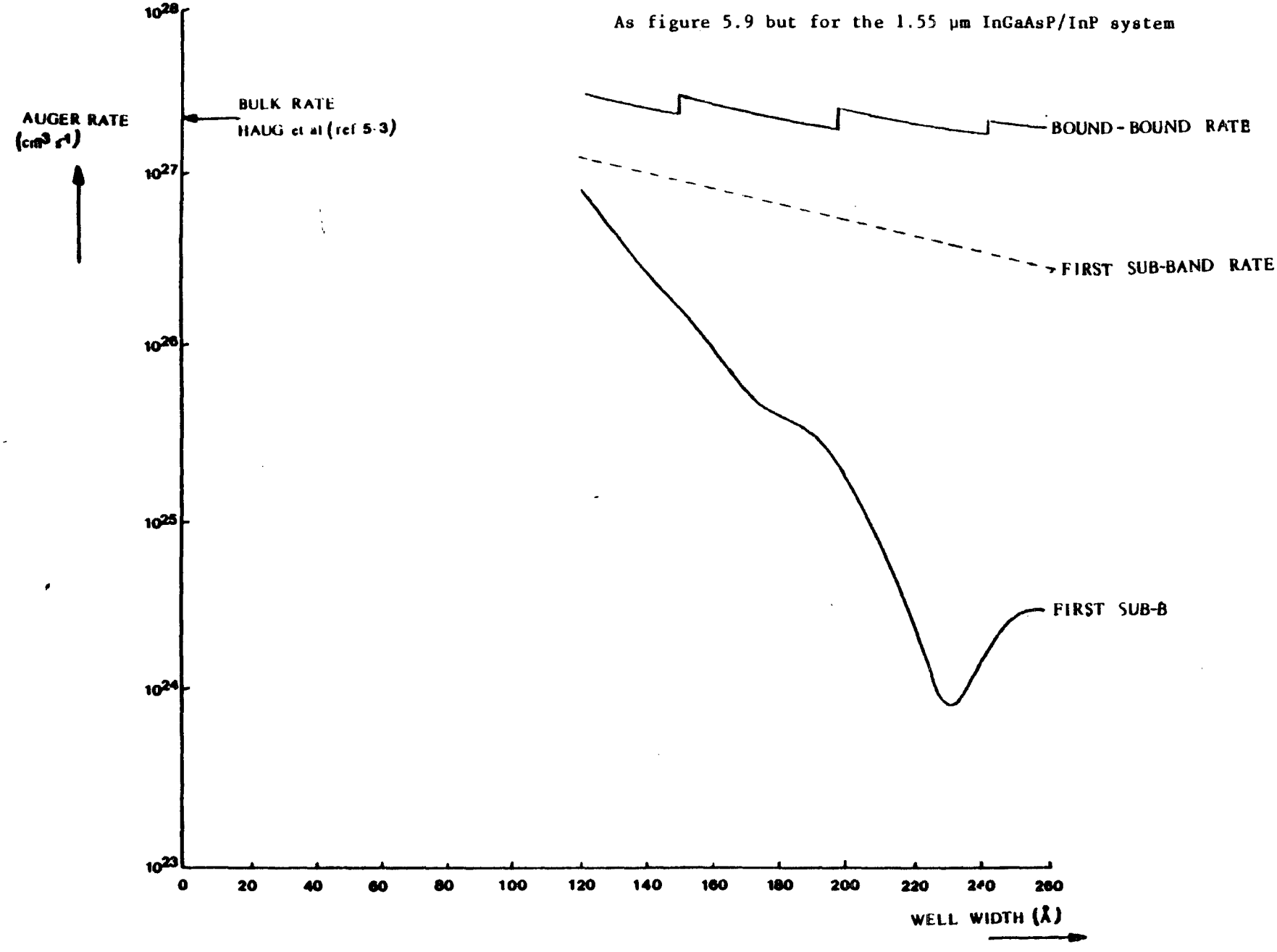

FIGURE 5.9

The variation of the combined bound-bound, and first sub-band bound-unbound CHCC Auger rate with well width in the 1.3 μm InGaAsP/InP system. The bulk rate which shares most in common with the QW calculations (ie that taken from ref 5.3) is also shown for comparison.

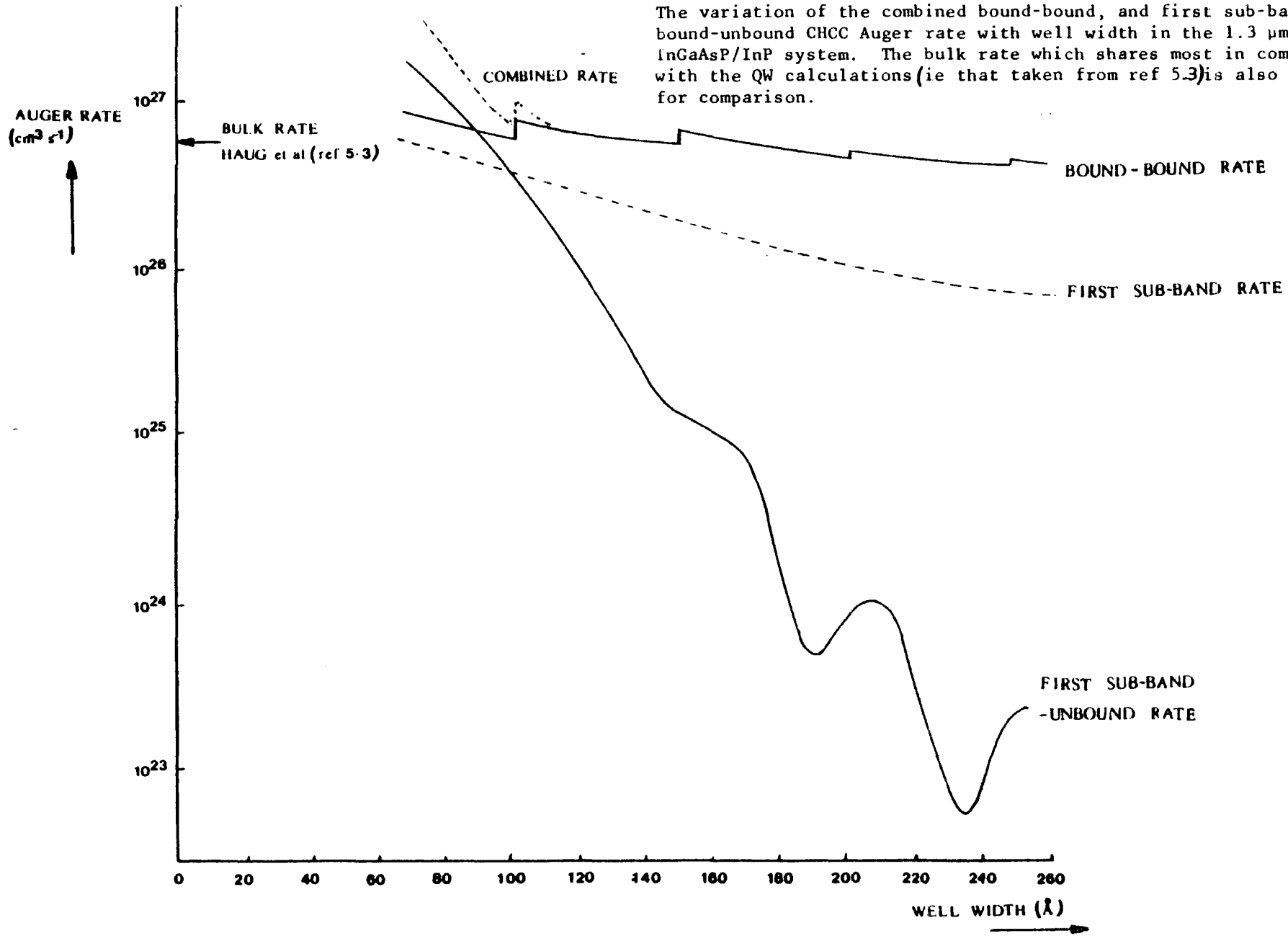

between the first bound state envelope function and envelope functions belonging to unbound states involved in dominant transitions, are less than in the 1.3 μm system. Hence the first sub-band bound-unbound matrix elements are generally smaller, and the first sub-band bound-unbound rate less important than in the 1.3μm system.

### 5.6.2 COMPARISON OF THE COMBINED RESULTS WITH BULK CHCC AUGER RATE CALCULATIONS

Several calculations of the CHCC Auger rate in bulk semiconductors exist. To make a sensible comparison with the quantum well results we should consider those calculations employing the same major assumptions and approximations as this thesis - that is the use of isotropic parabolic bands, and the evaluation the Bloch function overlap integrals using Beattie and Smith's effective mass sum rule (see next chapter). Figure 5.11 compares some well known bulk results with the quantum well calculation. It shows that the QW rate at intermediate and wide wells is similar to the bulk calculation it is most closely related to ie Haug et al (ref 5.3). This similarity is now confirmed by reverting to using just the first sub-band bound-bound results.

FIGURE 5.11

A comparison of the QW results with various bulk calculations. The parameters used are those of the 1.55 μm InGaAsP/InP system. Similar results have been obtained for the 1.3 μm InGaAsP/InP system and for the GaAs/GaAlAs system.

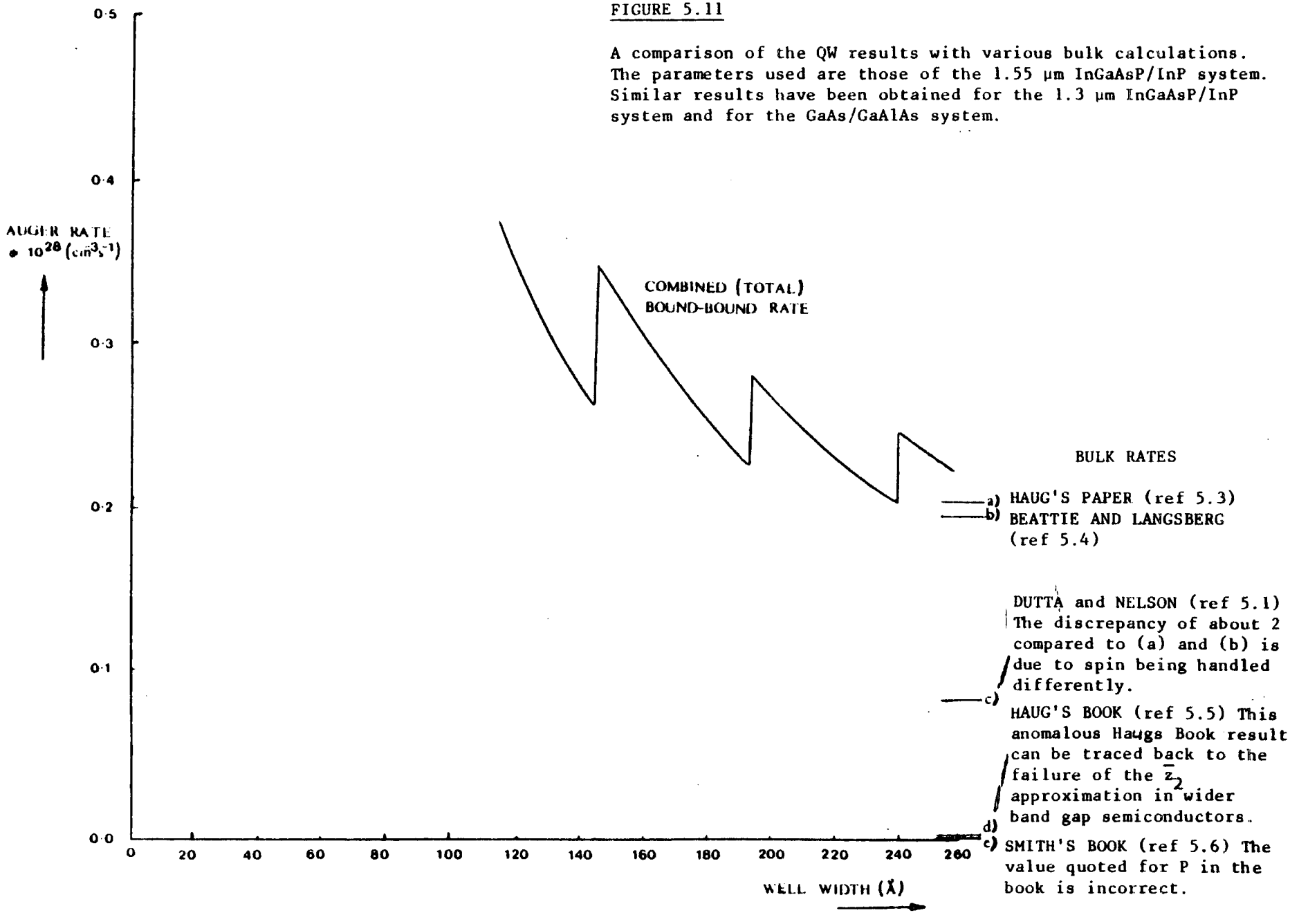

## A SIMPLE COMPARISON OF THE QUANTUM WELL AND BULK AUGER RATES

In intermediate width wells reasonable guidance about the size of the QW Auger recombination rate can be obtained by considering just the first sub-band bound-bound processes, and assuming all injected carriers reside in the first electron and hole sub-bands. With these approximations the ratio of the QW CHCC Auger rate $R_{QW}$ to the bulk CHCC Auger rate $R_{BULK}$ (due to Haug et al (ref 5.3)) can be shown to be

$$\frac{R_{QW}}{R_{BULK}} = \frac{9\sqrt{\pi}}{8} \frac{2\mu+1}{\mu+1} \left(\frac{x_B T_c}{E_a}\right)^{\frac{1}{2}}$$

where for convenience we define an activation energy '$E_a$' by

$$E_a = \left(\frac{\mu}{\mu+1}\right) Eg$$

It is seen that apart from a factor of the order of unity the ratio of the recombination rates is given by $\left(\frac{x_B T_c}{E_a}\right)$. The ratio is small when $E_a$ is much larger than $x_B T_c$. However, it is in such circumstances that the Auger recombination is negligible because the carriers cannot obtain sufficient energy from thermal agitation to participate in Auger recombination either in the bulk or a quantum well. When $E_a$ and $x_B T_c$ are of comparable size, then the Auger recombination is significant and the rates in a quantum well and in the bulk are the same order of magnitude.

## 5.7 THE SIGNIFICANCE OF THE RESULTS

Here some tentative conclusions about device optimisation are made and we speculate about the temperature dependence of the CHCC Auger contribution to the threshold current in a quantum well laser.

Any conclusions about device optimisation for low threshold currents will, in view of the approximations (such as taking parabolic bands), and the uncertainties in parameters (such as the overlap integrals between the cell periodic parts of the Bloch functions) be qualitative rather than quantitative. It only being meaningful to base conclusions upon the comparison between the QW Auger rate and a similarly calculated bulk rate. Assuming Auger recombination makes a significant contribution to the threshold current in bulk DH InGaAsP/InP lasers, then InGaAsP/InP QW lasers with wide and intermediate width wells must be designed to take full advantage of the lower threshold carrier densities which the gain expression 1.7 allows. In particular the optical properties of the system (such as optical confinement) should be optimised so that the threshold carrier concentration is low, and hence Auger recombination is unimportant.

For narrow wells, in particular those where bound-unbound transitions are important, any similar reductions in threshold current density will have less effect, because

the QW CHCC Auger rate for a given thermalised carrier concentration, is significantly greater than the bulk CHCC Auger rate.

The temperature dependence of the CHCC Auger contribution to the threshold current depends upon well width. The various Auger recombination processes have different exponential temperature dependences, and there is a redistribution of carriers between sub-bands as temperature and well width. Further investigations of these dependences is identified as a area for future work. However, one might expect, from the analytical analysis of Chapter 4 (see in particular eg 4.32) that the temperature dependence of CHCC Auger recombination will be greater in narrow wells because of the exponential factor in 4.32 is small. Interestingly the size of this exponential factor depends on the conduction band discontinuity.

## 5.8 COMPARISON OF THE RESULTS WITH OTHER QUANTUM WELL CHCC AUGER RECOMBINATION CALCULATIONS

Here two other calculations of QW CHCC Auger recombination are briefly discussed. Dutta assumes that the carriers involved remain in the first electron and hole sub-bands. He has obtained independently an expression for the rate similar in many respects to the expression derived in this thesis for the first sub-band rate in the large KL approximation. Unfortunately his treatment of the matrix element seems to contain an error in that a factor of $1/(2\pi)^2$ is missing from the transformation of $\delta(\underline{K}_1+\underline{K}_2-\underline{K}_{1'}-\underline{K}_{2'})\ \delta(\underline{K}_1+\underline{K}_2-\underline{K}_{1'}-\underline{K}_{2'})$ to $\frac{A}{(2\pi)^2}\delta(\underline{K}_1+\underline{K}_2-\underline{K}_{1'}-\underline{K}_{2'})$. Hence Dutta's equation A6 should contain a extra factor of $(2\pi)^2$. In one respect Dutta's calculations go beyond the present work in that he allows (see ref 5.7) the possibility of using Fermi-Dirac statistics by solving part of the summaton over first sub-band states numerically.

Chiu et al (ref 5.8) investigates CHCC Auger recombination numerically. The paper does not contain any details of the calculation and precise information upon the approximations used has not been forthcoming, and it is therefore difficult to make detail comments upon Chiu et al's work. He does however find that the QW Auger rate in a 200Å well at 300K is around two orders of magnitude less than the bulk rate at 300K. A result which is completely at variance with the calculations of this thesis and those of Dutta.

**REFERENCES FOR CHAPTER 5**

5.1 Dutta N K and Nelson R J 1982 J. Appl. Phys 53 74.

5.2 Chin R, Holonyak N, Kirchoefer S W, Kolbas R M and Rezek E A 1979 Appl Phys Lett 34 862.

5.3 Haug A, Kerkhoff D and Lochmann W 1978 Physica Status Solidi (b) 89 357.

5.4 Beattie A R and Landsberg P T 1959 Proc. R. Soc. A249 16.

5.5 Haug A 1972 Theoretical Solid State Physics Vol 2 (Oxford: Pergamon).

5.6 Smith R A 1978 Semiconductors (Cambridge).

5.7 Dutta N K 1983 J. Appl Phys 54 1236.

5.8 Chiu L C and Amnon Yariv 1982 IEEE J. Quantum Electron QE-18 No 10 1406.

See also

Smith C, Abram R A and Burt M G 1985 Superlattices and Microstructures Vol 1 No 2 page 119.

# CHAPTER 6 - THE OVERLAP INTEGRALS BETWEEN THE CELL PERIODIC PARTS OF THE WAVEFUNCTIONS WHICH APPEAR IN AUGER CALCULATIONS

In this chapter it is shown how the overlap integrals between the cell periodic parts of the wavefunctions which appear in Auger calculations (see Chapters 3 and 4) may be evaluated using a 15 band K.p method. Unfortunately the results presented here are not yet at a stage where they may be substituted in the expressions of Chapters 3 and 4. However even at this early stage it can be seen that they represent significant modifications to previous band to band Auger rate calculations both for the well and the bulk. The overlaps obtained using the 15 K.p band method differ considerable from conventional overlap estimates but are in good agreement with results from a pseudopotential method. Since these differences were first noticed when preliminary estimates of the overlaps were made for the (001) direction, the (001) results are presented immediately after the K.p method has been introduced. These (001) results are then justified, because their differences from conventional estimates of the overlaps. Next the results for other directions are considered, and the similarities between these results and some obtained by a pseudopotential method are shown. Finally to illustrate the difficulties in simply substituting the overlaps discussed in this chapter into the expressions of chapters 3 and 4 some results are presented for non-parallel wavevectors.

## 6.1 AN INTRODUCTION TO K.P THEORY

In this section we shall review, for completeness and to establish some notation, how within the one electron approximation and using the Hartree hamilton, an exact matrix equation describing the one electron energies and wavefunctions for the entire zone may be obtained, if sufficient is known about the zone centre states.

Using one electron Bloch wavefunctions $\psi_{nK} = e^{-iKr} U_{nK}(r)$ one gets from the Schrodinger equation

$$H_K U_{nK}(r) = E_{nK} U_{nK}(r) \qquad 6.1$$

where

$$H_K \equiv e^{-iKr} H e^{+iKr} \qquad 6.2$$

Now expanding the periodic parts of the wavefunctions in terms of the zone centre periodic parts $U_{m_o}(r)$, and using orthonormality equation 6.1 becomes

$$\sum_m c_{mn} \int_{\substack{\text{UNIT}\\\text{CELL}}} U_{m_o}(r) H_K U_{n_o}(r) d^3r = c_{nn} E_{nK} \qquad 6.3$$

Expanding $H_K$ in terms of K gives

$$\sum_m c_{mn} \int_{\substack{\text{UNIT}\\\text{CELL}}} U_{m_o}(r)[H - iK.[r,H] - \frac{1}{2} \sum_{\substack{\mu=x,y,z\\ v=x,y,z}} K\mu K_v[r\mu,[r_v,H] + \ldots\ldots] \qquad 6.4$$

$$U_{n_o}(r) d^3r = c_{nn} E_{nK}$$

which may now be simplified if the Hartree hamilton is used. ( $iK \cdot [r,H]$ becoming $2K.p$ , $\frac{1}{2} K_\mu K_\nu [r_\mu,[r_\nu,H]]$, becoming $K^2$ ( using Cardona atomic units, ref 6.2 ) and higher commutators becoming zero.) If other hamiltons are used, Kane (ref 6.1) shows the form of the commutators and concludes that only minor changes to the results occur. One reason for this is that for the Hartree-Fock hamilton at least $iK.[r,H]$ has the same symmetry as $2K.p$ and is determined empirically. Here only the Hartree hamilton with the addition of K independent spin orbit interaction is considered

ie

$$H_K = H + 2K.p + K^2 \qquad 6.5$$

where, using Cardona atomic units

$$H = -\nabla^2 + V(r) + \frac{1}{c^2} [(\nabla V \wedge P).\sigma] \qquad 6.6$$

Hence combining 6.4 and 6.5 one gets a matrix equation (to be discussed later) which allows the energy bands and wavefunctions to be determined at any point in the zone if sufficient information is available about the zone centre energy eigenvalues and eigenvectors.

## 6.2 THE (001) DIRECTION

### 6.2.1 THE 15*15 HAMILTON AND THE FITTING OF PARAMETERS

Initially equation 6.4 is solved for K values along the (001) direction because this reduces, by symmetry considerations, the amount of information needed about the zone centre states. Cardona and Pollak (refs 6.2 and 6.3) build this information up in a systematic way. Here only the philosophy of Cardona and Pollak's approach is outlined. For details of how particular matrix elements are determined the reader is referred to the original series of papers, by Cardona, Pollak, Broerman and Higgenbotham (refs 6.2 to 6.5).

First Cardona and Pollak establish using only the symmetry properties of the octahedral group the number and type of zone centre states to be used. The zone centre states used are the irreducible representations of the octahedral group which of course have the same symmetry properties as the zone centre periodic parts of the Bloch functions. An indication of which zone centre states, need be considered, is then obtained by considering the combinations of plane waves which have the same symmetry properties as the periodic $U_{n_0}$'s. The lowest energy plane waves satisfying the symmetry requirements are the $\frac{2\pi}{a}$ [0,0,0], $\frac{2\pi}{a}$ [1,1,1], $\frac{2\pi}{a}$ [2,0,0], and $\frac{2\pi}{a}$ [2,2,0] waves. Now since the energy gap between the $\frac{2\pi}{a}$ [2,0,0] and $\frac{2\pi}{a}$ [2,2,0] waves is large and from

perturbation theory the amount of interaction between states depends inversely on the energy gap separating them, zone centre states corresponding to $\frac{2\pi}{a}$ [2,2,0] waves and higher are neglected. The symmetries of the states corresponding to the remaining waves are then found by considering the character tables for the plane waves. Hence one gets an irreducible set of 15 zone centre states as follows

$$|\Gamma_{2'}^{lower}>,\ |Z_{25'}^{lower}>,\ |\Gamma_{12'}^{(1)}>,\ |Z_{25}^{upper}>,\ |\Gamma_{2'}^{upper}>,\ |X_{25'}^{lower}>,\ |y_{15}>$$

$$|Y_{25'}^{upper}>,\ |Y_{25'}^{lower}>,\ |x_{15}>,\ |X_{25'}^{upper}>,\ |Z_{15}>,\ |\Gamma_{1}^{upper}>,\ |\Gamma_{1}^{lower}>$$

and $|\Gamma_{12}^{(2)}>$

where $\Gamma_{2'}$ is invariant under the zincblende symmetry operations but changes sign under the remaining operations of the diamond group, $Z_{25'}$ transforms as xy, $\Gamma_{12}^{(1)}$ as $\sqrt{3}$ $(x^2-y^2)$, $Z_{15}$ as z, $\Gamma_{12}^{(2)}$ as $3z^2-r^2$, and $\Gamma_1$ is invarient under the operations of the diamond group. Each basis state must now arbitrarily be assigned a spin and phase. Spin is assigned so that it is quantized in the (001) z direction,

$$\sigma_z|\uparrow> = |\uparrow> \qquad \sigma_z|\downarrow> = -|\downarrow>$$
$$\sigma_y|\uparrow> = i|\downarrow> \qquad \sigma_y|\downarrow> = -i|\uparrow>$$
$$\sigma_x|\uparrow> = |\downarrow> \qquad \sigma_x|\downarrow> = +|\uparrow> \qquad 6.7$$

and phase is assigned in order that the momentum matrix elements in equation 6.4 are real, ie even-parity states are taken as purely real and odd-parity states as purely imaginary.

The Ge crystal potential is next turned on and the matrix elements for these states are determined. The diagonal matrix elements are determined both experimentally by cyclotron resonance and theoretically by O.P.W and pseudopotential calculations. During these determinations of the zone centre diagonal matrix elements (ie $U_{m_o}$ 's energies) spin orbit interactions are ignored because they are explicitly included in the hamilton to be solved. The zone centre diagonal matrix elements used are then:

$\Gamma_{25'}^{lower} \sim 0.00$

$\Gamma_{2'}^{lower} \sim 0.0728$

$\Gamma_{15} \sim 0.232$

(eigenvalues in rydbergs)

$\Gamma_{1}^{upper} \sim 0.571$

$\Gamma_{1}^{lower} \sim 0.966$

$\Gamma_{12'} \sim 0.770$

$\Gamma_{25}^{upper} \sim 1.25$

$\Gamma_{2'}^{upper} \sim 1.35$

The sizes of the off diagonal matrix elements are found by a mixture of experimental determination and band fitting so that the resultant band structure agrees with non-zone centre results, the number of parameters which must be considered being considerably reduced by the application of group theory. In the (001) direction the only non-zero momentum matrix elements for states of the same spin are:

$$2i < \Gamma_{25'}^{lower} | p | \Gamma_{2'}^{lower} > \equiv P = 1.360$$

$$2i < \Gamma_{25'}^{lower} | p | \Gamma_{15} > \equiv Q = 1.070$$

$$2i < \Gamma_{25'}^{lower} | p | \Gamma_{12'} > \equiv R = 0.8049$$

$$2i < \Gamma_{25'}^{lower} | p | \Gamma_{2'}^{upper} > \equiv P'' = 0.1000$$

$$2i < \Gamma_{25'}^{upper} | p | \Gamma_{2'}^{lower} > \equiv P' = 0.1715$$

$$2i < \Gamma_{25'}^{upper} | p | \Gamma_{15} > \equiv Q' = -0.752$$

$$2i < \Gamma_{25'}^{upper} | p | \Gamma_{12'} > \equiv R' = 1.4357$$

$$2i < \Gamma_{25}^{upper} | p | \Gamma_{2'}^{upper} > \equiv P''' = 1.6231$$

$$2i < \Gamma_{1}^{upper} | p | \Gamma_{15} > \equiv T = 1.2003$$

$$2i < \Gamma_{1}^{lower} | p | \Gamma_{15} > \equiv T' = 0.5323$$

States with opposite spins cannot interact except through the spin orbit interaction. Those which do interact are:

| | Ge value | GaAs value | InP value |
|---|---|---|---|
| $\langle \uparrow Z_{25}^{lower} \| H_{50} \| X_{25}^{lower} \downarrow \rangle = -\frac{1}{3}\Delta_{25'}$ | $= -\frac{1}{3}(0.0213)$ or | $-\frac{1}{3}(0.0213)$ or | $-\frac{1}{3}(0.0274)$ |
| $\langle \uparrow iY_{15} \| H_{50} \| iZ_{15} \downarrow \rangle = -i\frac{\Delta}{3}15$ | $= -\frac{i}{3}(0.0265)$ or | $-\frac{i}{3}(0.0265)$ or | $-\frac{i}{3}(0.0381)$ |

and equivalent by symmetry matrix elements. Hence along the (001) direction with kx and ky equal to zero the matrix can be seperated into two 15 by 15 blocks, and this is the advantage of working in a high symmetry direction such as the (001) direction.

Having found the parameters for Ge the matrix for GaAs or InP is determined by the addition of an antisymmetric potential $V^-$ to the crystal potential of Ge. This is equivalent to using the tetrahedral group to determine which matrix elements are zero rather than the octahedral group. The additional momentum matrix elements in the zincblende structure are:

| | | value in GaAs | value in InP |
|---|---|---|---|
| $\langle \Gamma_{15} \| V^- \| \Gamma_{25}^{lower} \rangle$ | $\equiv v_1^-$ | $= 0.12652$ | $0.13973$ |
| $\langle \Gamma_2^{lower} \| V^- \| \Gamma_1^{upper} \rangle$ | $\equiv v_2^-$ | $= -0.24791$ | $-0.22161$ |
| $\langle \Gamma_{2'}^{lower} \| V^- \| \Gamma_1^{lower} \rangle$ | $\equiv v_3^-$ | $= 0.38210$ | $0.26413$ |

$$< \Gamma_{15} | V^- | \Gamma_{25}^{upper} > \equiv V_4^- = 0.12297 \qquad 0.15348$$

$$< \Gamma_{2'}^{upper} | V^- | \Gamma_1^{upper} > \equiv V_5^- = -0.34820 \qquad -0.28018$$

$$< \Gamma_{2'}^{upper} | V^- | \Gamma_1^{lower} > \equiv V_6^- = 0.0 \qquad 0.0$$

and the additional spin orbit interaction matrix elements are:

| | value in GaAs | value in InP |
|---|---|---|
| $< Z_{25'}^{lower} \uparrow \| H_{50} \| iY_{15} \downarrow > = \frac{\Delta^-}{3}$ | = 0.00507/3 | 0.02922/3 |

and similar. ( The sizes of these new matrix elements being determined by fitting to known experimental GaAs and InP energy gaps, details of which are given in refs 6.3, to 6.5.)

Having above discussed the size and the parameters of the matrix equation 6.4. Figure 6.1 shows the complete 001 matrix which must be diagonalised to give the eigenvectors required for the overlap integrals.

| | $\lvert i\Gamma^1_{2'}\uparrow\rangle$ | $\lvert Z^1_{25'}\uparrow\rangle$ | $\lvert i\Gamma^{(2)}_{12'}\uparrow\rangle$ | $\lvert Z^u_{25'}\uparrow\rangle$ | $\lvert i\Gamma^u_{2'}\downarrow\rangle$ | $\lvert X^1_{25'}\downarrow\rangle$ | $\lvert iY_{15}\downarrow\rangle$ | $\lvert X^u_{25'}\downarrow\rangle$ | $\lvert Y^1_{25'}\downarrow\rangle$ | $\lvert iX_{15}\downarrow\rangle$ | $\lvert Y^u_{25'}\downarrow\rangle$ | $\lvert iZ_{15}\uparrow\rangle$ | $\lvert\Gamma^u_1\uparrow\rangle$ | $\lvert\Gamma^1_1\uparrow\rangle$ | $\lvert i\Gamma^{(1)}_{12}\uparrow\rangle$ |
|---|---|---|---|---|---|---|---|---|---|---|---|---|---|---|---|
| $\langle i\Gamma^1_{2'}\uparrow\rvert$ | $E(\Gamma^1_{2'})+K^2$ | $PK_z$ | | $P'K_z$ | | | | | | | | | $-iV^-_2$ | $-iV^-_3$ | |
| $\langle Z^1_{25'}\uparrow\rvert$ | | $K^2$ | $\sqrt{2}\,RK_z$ | | $P''K_z$ | $\frac{-\Delta_{25'}}{3}$ | $\frac{-\Delta^-}{3}$ | | $\frac{+i\Delta_{25'}}{3}$ | $\frac{-i\Delta^-}{3}$ | | $iV^-_1$ | | | |
| $\langle i\Gamma^{(2)}_{12'}\uparrow\rvert$ | | | $E(\Gamma_{12'})+K^2$ | $\sqrt{2}R'K_z$ | | | | | | | | | | | |
| $\langle Z^u_{25'}\uparrow\rvert$ | | | | $E(\Gamma^u_{25'})+K^2$ | $P\,K_z$ | | | | | | | $iV^-_4$ | | | |
| $\langle i\Gamma^u_{2'}\downarrow\rvert$ | | | | | $E(\Gamma^u_{2'})+K^2$ | | | | | | | | $-iV^-_5$ | $-iV^-_6$ | |
| $\langle X^1_{25'}\downarrow\rvert$ | | | | | | $K^2$ | $QK_z-\Delta^-/3$ | | $\frac{i\Delta_{25'}}{3}$ | $iV^-_1$ | | $\frac{-i\Delta^-}{3}$ | | | |
| $\langle iY_{15}\downarrow\rvert$ | | | | | | | $E(\Gamma_{15})+K^2$ | $Q'K_z$ | $-iV^-_1$ | $\frac{-i\Delta_{15}}{3}$ | $-iV^-_4$ | $\frac{-i\Delta_{15}}{3}$ | | | |
| $\langle X^u_{25'}\downarrow\rvert$ | | | | | | | | $E(\Gamma^u_{25})+K^2$ | | $-V^-_4$ | | | | | |
| $\langle Y^1_{25'}\downarrow\rvert$ | | | | | | | | | $K^2$ | $+\Delta^-/3\;QK_z$ | | $\frac{\Delta^-}{3}$ | | | |
| $\langle iX_{15}\downarrow\rvert$ | | | | | | | | | | $E(\Gamma_{15})+K^2$ | $Q'K_z$ | $\frac{-\Delta_{15}}{3}$ | | | |
| $\langle Y^u_{25'}\downarrow\rvert$ | | | | | | | | | | | $E(\Gamma^u_{15})+K^2$ | | | | |
| $\langle iZ_{15}\uparrow\rvert$ | | | | | | | | | | | | $E(\Gamma_{15})+K^2$ | $TK_z$ | $T'K_z$ | |
| $\langle\Gamma^u_1\uparrow\rvert$ | | | | | | | | | | | | | $E(\Gamma^u_1)+K^2$ | | |
| $\langle\Gamma^1_1\uparrow\rvert$ | | | | | | | | | | | | | | $E(\Gamma^1_1)+K^2$ | |
| $\langle i\Gamma^{(1)}_{12}\uparrow\rvert$ | | | | | | | | | | | | | | | $E(\Gamma^{(1)}_{12})+K^2$ |

FIGURE 6.1

The upper right hand corner of the hermitian 15 by 15 matrix when Kx and Ky are zero.

### 6.2.2 THE RESULTS IN THE (001) DIRECTION

The overlaps which are of interest for the CHCC Auger process are those between the initial and final states of the recombining electron. Since each eigenvector is doubly degenerate because of spin, for each interaction four overlaps need to be considered. However, because of the way the matrix can be split into two 15 by 15 matries, two overlaps are exactly zero, and the other two are similar and may be found by solving the 15 by 15 matrices. The results shown are for one of these non-zero overlaps, or at the risk being pedantic, are obtained by squaring each overlap, dividing by two, and then taking the square root (this operation being used to define a quantity equivalent to the overlap integral originally used by Landsberg).

For wavevectors corresponding to the threshold condition the conduction band - conduction band overlap is found to be around 0.7 which agrees well with the usual approximation of taking it as unity.

On the other hand the conduction band - heavy hole band overlap does not agree well with the usual approximations (refs 6.6 to 6.10). In figure 6.2 it is shown how the modulus of the overlap between the zone centre conduction band and the heavy hole band varies as the heavy hole wavevector which is taken to lie along the (001) axis is increased. These overlaps are significantly smaller than

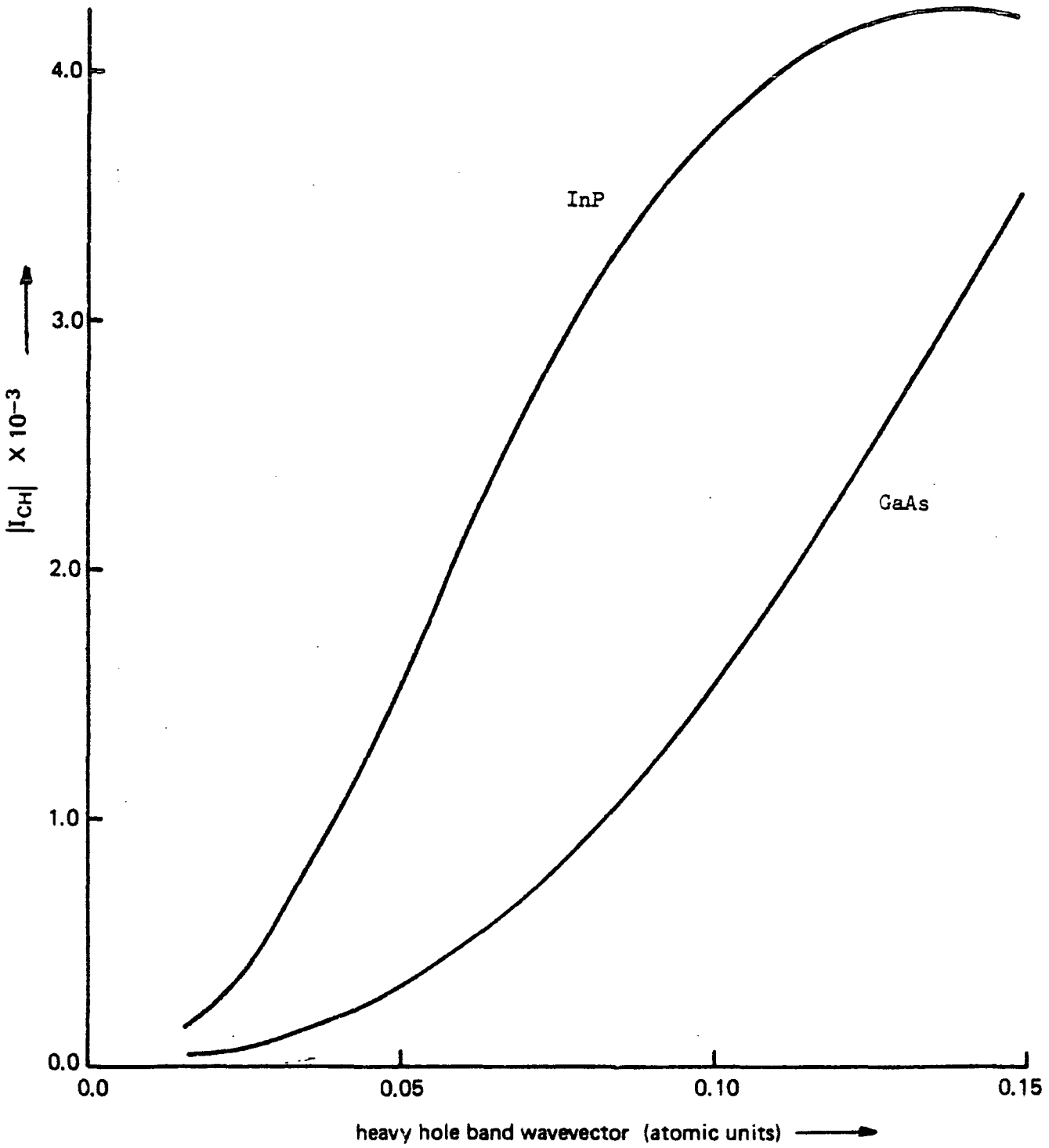


FIGURE 6.2

This figure shows the variation in the modulus of the overlap integral between the cell periodic parts of the conduction and heavy hole wavefunctions $|I_{CH}|$, as the heavy hole wavevector, lying in the (001) direction, is increased (the conduction band wavevector being taken as zero).

predicted by the usual effective mass sum rule overlap estimates, and this has important consequences for theoretical estimates of the CHCC Auger recombination rate. At threshold for the CHCC process in GaAs and InP the wavevector transfers are respectively 0.085 and 0.073 atomic units if parabolic bands are assumed. Thus it can be seen from figure 6.2 that the overlap moduli along the (001) direction are approximately 0.00011 for GaAs and 0.00028 for InP. But using the effective mass sum rule prescription of Beattie and Smith (ref 6.7) one finds the overlap moduli to be 0.63 for GaAs and 0.63 for InP. While using the Antoncik and Landsberg prescription for using the effective mass sum rule (ref 6.6) gives threshold overlap moduli of 0.46 for GaAs and 0.42 for InP. The size of the overlaps obtained from this preliminary study are therefore two to three orders of magnitude smaller than those customarily used. It is therefore clearly necessary to show how the results were checked and to investigate the discrepancies between them and other estimates of overlap integrals (ref 6.11).

### 6.2.3 CHECKING THE RESULTS

Apart from the obvious checks of the 15 band $\vec{k}\cdot p$ results against the published Ge, GaAs, and InP data from Cardona and Pollak two further types of checks have been carried out. These were the checking of zone centre zincblende eigenvectors and matrix elements against first order perturbation theory expectations, and the application of the effective mass sum rule (refs 6.6 and 6.12) to the results. As will be seen later in this chapter these two checks take on an importance beyond the simple confirmation of the consistency of the 15 band calculations. The first is of use in providing the zincblende basis matrix elements for a comparison between 15 band results and those of the four band Kane model (ref 6.13) and the second is of use in showing the failure of the Beattie-Smith and Antoncik-Landsberg effective mass sum rule approximations for the overlap integrals.

The zone centre, zincblende eigenvectors in the absence of the spin orbit interaction are found by diagonalising the matrix of the asymmetrical potential $V^-$ in the basis of Ge zone centre states in the absence of spin interaction. The machine output for the conduction band and heavy hole band, zincblende eigenvectors in the Ge basis is

$$|c\rangle = |S\rangle = |\Gamma_1^{\text{lower cond.GaAs}}\rangle = 0.81|i\Gamma_{2'}^{\text{lower}}\rangle + 0.13|\Gamma_{2'}^{\text{upper}}\rangle + 0.49i|\Gamma_1^{\text{upper}}\rangle + 0.30i|\Gamma_1^{\text{lower}}\rangle \qquad 6.8$$

$$|H\rangle = |X_{15}^{GaAs} + iY_{15}^{GaAs}\rangle \text{ where } |X_{15}^{GaAs}\rangle = 0.91|X_{25'}^{\text{lower}}\rangle + 0.41\, i|iX_{15}\rangle + 0.04|X_{25'}^{\text{upper}}\rangle$$

and these compare well with first order perturbation theory estimates of

$$|c> = |s> = |\Gamma_1^{\text{lower cond.GaAs}}> = 0.85|i\Gamma_{2'}^{\text{lower}}> +0.0\ |\Gamma_{2'}^{\text{upper}}> +0.42i|\Gamma_1^{\text{upper}}> +0.31i|\Gamma_1^{\text{lower}}>$$

$$|H> = |X_{15}^{GaAs}+Y_{15}^{GaAs}> \text{ where } |X_{15}^{GaAs}> = 0.88|X_{25'}^{\text{lower}}> +0.48i|iX_{15}> +0.0\ |X_{25}^{\text{upper}}> \qquad 6.9$$

From which the matrix elements of matrix 6.4 in terms of the zincblende, zone centre eigenvectors in absence of spin interaction, basis can now be found. Considering for example a spin orbit interaction matrix element between GaAs valance band states

$$i < Z_{15}^{GaAs}\uparrow|H_{SO}|X_{15}^{GaAs}\downarrow> = \{< Z_{15}^{GaAs}|Z_{25}^{\text{lower}}> < Z_{25}^{\text{lower}}|Hy|X_{25'}^{\text{lower}}> + < Z_{15}^{GaAs}|iZ_{15}> < iZ_{15}|Hy|X_{25'}^{\text{lower}}>\} < X_{25'}^{\text{lower}}|X_{15}^{GaAs}> + \{< Z_{15}^{GaAs}|Z_{25'}^{\text{lower}}> < Z_{25}^{\text{lower}}|Hy|iX_{15}> + < Z_{15}^{GaAs}|iZ_{15}> < iZ_{15}|Hy|iX_{15}>\} < iX_{15}|X_{15}^{GaAs}>$$

now using the previous values $\Delta_{25}$ and $\Delta_{15}$ for Ge spin orbit interactions and the above expressions for $|\Gamma_{15}^{GaAs}>$ gives

$$i < Z_{15}^{GaAs}\uparrow|H_{SO}|X_{15}^{GaAs}\downarrow> = -i6.114 \times 10^{-3}$$

which again agrees with machine output.

The second category of checks on the 15 band K.p results involves the application of the effective mass sum rule, which may be written as

$$\sum_{m\neq n} (E_m(K) - E_n(K)) \left| I_{nm}(K)_{r=q}^{m=q'} \right|^2 = \left(1 + \frac{m}{m_n}\right)(q - q')^2$$

where the $I_{nm}$ is the overlap between eigenvector n and another eigenvector m and the other symbols have their usual meaning. This tests successfully the self consistency of the eigenvectors and eigenvalues and if the diagonalisation is working correctly it will always work providing the q-q' is small enough for first order perturbation of the wavefunctions to work. The results show that with the wavevectors of interest the use of perturbation theory is questionable but more importantly from the point of view of comparison with other overlap estimates the contributions of the different $I_{nm}$'s is not as guessed in the Beattie-Smith and Antonĉcik-Landsberg estimates.

### 6.2.4 COMPARISON WITH CONVENTIONAL ESTIMATES AND REASONS FOR THE DISCREPANCIES

Effective mass sum rule estimates of conduction band-heavy hole band overlap depend on the assumption that this overlap is the major contributor to the conduction band mass (Beattie and Smith) or the major contributor to the heavy hole band mass (Antoncik and Landsberg). It is found however that this is not the case. For instance, for the conduction band sum rule with K = 0.01, q = 0 and q' = 0.001 atomic units, the retention of only the terms involving the light hole and spin split-off valence bands results in only a 3% error for GaAs and less than a 1% error for InP, in estimating the conduction band effective mass. While for the heavy hole band sum rule with K = 0.05, q = 0 and q' = 0.001 the retention of only contributions from the two bands in the lowest triplet of the conduction band accounts for 99% of the contributions to the heavy hole effective mass. These results are not however too surprising in view of the fact that Kane's 4 band model gives the effective mass of the heavy hole band with the wrong sign unless these higher bands are included.

In fact the 15 band K.p (001) results are readily understandable in terms of Kane's 4 band model and corrections thereto. Kane's 4 band model gives the zone centre conduction band eigenvector and the heavy hole valence band eigenvector as $|S\downarrow\rangle$ and $|X_{15}^{GaAs} + iY_{15}^{GaAs}\uparrow\rangle$, or $|S\uparrow\rangle$

and $| X_{15}^{GaAs} - iY_{15}^{GaAs} \downarrow >$ respectively. Hence the overlap between them is zero due to spin. Now as can be seen from the equations 6.8, 6.9 and the matrix of figure 6.1 the 15 band eigenvectors retain the same form as Kane's eigenvectors. That is the heavy hole eigenvector and the conduction eigenvector do not mix directly because the spin orbit interaction does not couple them directly. Further symmetry can be used to show that as the heavy hole eigenvector increases, then the second order perturbation (ie linear $K$) coupling via $|Z_{25'}^{lower}>$ or $|Z_{15}>$ is also zero. To illustrate this second point a matrix formulation of Lowdin's technique may be used for folding down Kane's extended hamilton matrix H (ref 6.1). This is now done. Kane's extended hamilton matrix H is written

$$H-E = \begin{pmatrix} A & C \\ \tilde{C}^* & B \end{pmatrix}$$

where A contains the interactions between the original 4 (8) states, B contains the interactions between the new additional states, and C contains the interactions between the original and new states. (The states of A and B being chosen so that the interactions in C are small compared to the energy separations between states interacting in C.) Multiplying the above matrix by S

$$S = \begin{pmatrix} I & -A^{-1}C \\ -B^{-1}\tilde{C}^* & I \end{pmatrix}$$

gives

$$(H-E)S = \begin{pmatrix} A-CB^{-1}\tilde{C}^{*} & 0 \\ 0 & B-\tilde{C}^{*}A^{-1}C \end{pmatrix}$$

Hence the eigenvectors $U_K$ can be found from

$$\sum_K (A - CB^{-1}\tilde{C}^{*})_{jK} \; U_K = 0$$

where

$$(CB^{-1}\tilde{C}^{*})_{jK} \simeq \sum_{\ell}^{B} H_{j\ell} \frac{1}{E_{\ell}-E} H_{\ell K}$$

the true eigenvalue E in $CB^{-1}\tilde{C}^{*}$ being replaced by its approximate value ie the appropriate diagonal element of A. Now to get in $CB^{-1}\tilde{C}^{*}$ a linear term in K we must take in a momentum matrix element as one off diagonal matrix element and a spin orbit interaction matrix element as the other off diagonal matrix element. But combinations of this form can be shown to be zero using the symmetry operations of the tetrahedral group. That is in the (001) direction there is no linear K term in the overlap and therefore the overlap might be expected to be small. Thus it has been established that our directly obtained overlaps are not incomparible with predictions obtained directly from Kane's model.

Now while considering the comparison of the preliminary results with other estimates of the overlap integrals two further estimates which are based upon Kane's 4 band model should be mentioned.

The first of these is due to Takeshima, Sugimura, and Dutta and Nelson (refs 6.8 6.9 and 6.10). Little information is available about this estimate and in the absence of further information it is suggested (ref 6.14) that they may have obtained it by takingthe conduction band - heavy hole band overlap they use as the average Kane's conduction band -light hole band and conduction band -heavy hole band overlaps.

$$|\phi_{CH}|^2 = \frac{1}{2}\left\{|\langle\phi_c(0)|\phi_H(K)\rangle|^2 + |\langle\phi_c(0)|\phi_L(K)\rangle|^2\right\}$$

where

$$\langle\phi_c(0)|\phi_H(K)\rangle \simeq 0$$

and from ref 6.13

$$|\phi_L(K)\rangle = a_L(K)|iS\uparrow\rangle + b_L(K)|-(X_{15}^{GaAs} + iY_{15}^{GaAs}\uparrow/\sqrt{2}\rangle + c_L(K)|Z_{15}^{GaAs}\uparrow\rangle$$

$$|\phi_c(0)\rangle = a_c(0)|iS\uparrow\rangle$$

with to first order in K (reverting to Kane's units for consistency with his paper)

$a_c = 1$

$$a_L \simeq KP\,\frac{2\Delta}{3}\Big/N_L \quad , \quad b_L = -\frac{\sqrt{2}}{3}\,\Delta E_G/N_L \quad , \quad c_L = -E_G\,\frac{2\Delta}{3}\Big/N_L$$

$$\left(P = -i\left(\frac{\hbar}{m}\right) < S|p_z|Z_{15}^{GaAs} >,\ \Delta = \frac{3\hbar i}{4m^2c^2} < X_{15}^{GaAs}|\ \frac{\partial V}{\partial X}p_y - \frac{\partial V}{\partial Y}p_x\ |Y_{15}^{GaAs} >\right.$$

and $N_L$ a normalising constant)

$$|< \phi_c(0)|\phi_L(K) >|^2 = \frac{2}{3}\ \frac{K^2P^2}{E_G^{\ 2}} = \frac{2}{3}\,\frac{K^2}{E_G}\ \frac{\hbar^2}{2m}\ E_p \text{ with } E_p = \frac{\hbar^2p^2}{2m}$$

and therefore

$$|\phi_{CH}|^2 = \frac{1}{3}\ \frac{E_p}{E_G}\ \frac{\hbar^2}{2m}$$

In the absence of any justification for this (their expression) the author can just assume that they are trying to account in an arbitrary way for the mixing of light and heavy hole bands caused by impurities within the semiconductor. Some circumstantial evidence (ref 6.15) existing that the size of the overlaps depends on impurity concentration.

The second Kane related expression for the conduction band - heavy hole band overlap is due to Beattie and Smith (ref 6.7 and 6.16). To derive it they assume that the system is above threshold and that the eigenvectors are non-parallel. They then give, using Kane's 4 band model, an unweighted average over the angle between the eigenvectors of the overlap. This is obviously incomparable with the 15 band K.p (001) results but does indicate that a

significant increase in the overlap is possible when one moves away from the threshold condition. In section 6.3.3 the overlap for non-parallel wavevectors is investigated, and with this information and information about wavevectors which are parallel but not in the (001) direction it is hoped, that eventually from this work a weighted average overlap can be obtained and substituted into the threshold Auger results of Chapters 3 and 4. In the next section initial calculations towards this eventual end are described.

## 6.3 EXTENSION OF THE CALCULATION TO OTHER WAVEVECTOR DIRECTIONS

### 6.3.1 EXTRA MATRIX ELEMENTS DEPENDENT ON Kx AND Ky

Using group theory the additional matrix elements which appear when Kx and Ky are non-zero can be found. Figure 6.3 shows these additional matrix elements. Their sizes are again taken from Pollak, Higgenbotham and Cardona (ref 6.4).

The presence of these extra matrix elements prevents the splitting of the 30 by 30 matrix into two 15 by 15 matricies, and so it is this larger matrix which must be diagonalised to find the overlaps.

### 6.3.2 RESULTS WITH THE WAVEVECTORS PARALLEL

Figures 6.4 and 6.5 show how the modulus squared of the conduction band-heavy hole band overlap varies as the heavy hole wavevector rotates between (001) and (011) in the zy plane. The conduction band wavevector is set to zero and to be consistent with section 6.2.1 the modulus of the overlap squared is found by squaring each of the four conduction band-heavy hole band overlaps (there being four because the spin-orbit interaction splits each band not in a symmetry direction into two bands) then adding the squares and dividing by two. Also shown on the graphs are pseudopotential calculations by Brand of the same overlaps (ref 6.17 and 6.18).

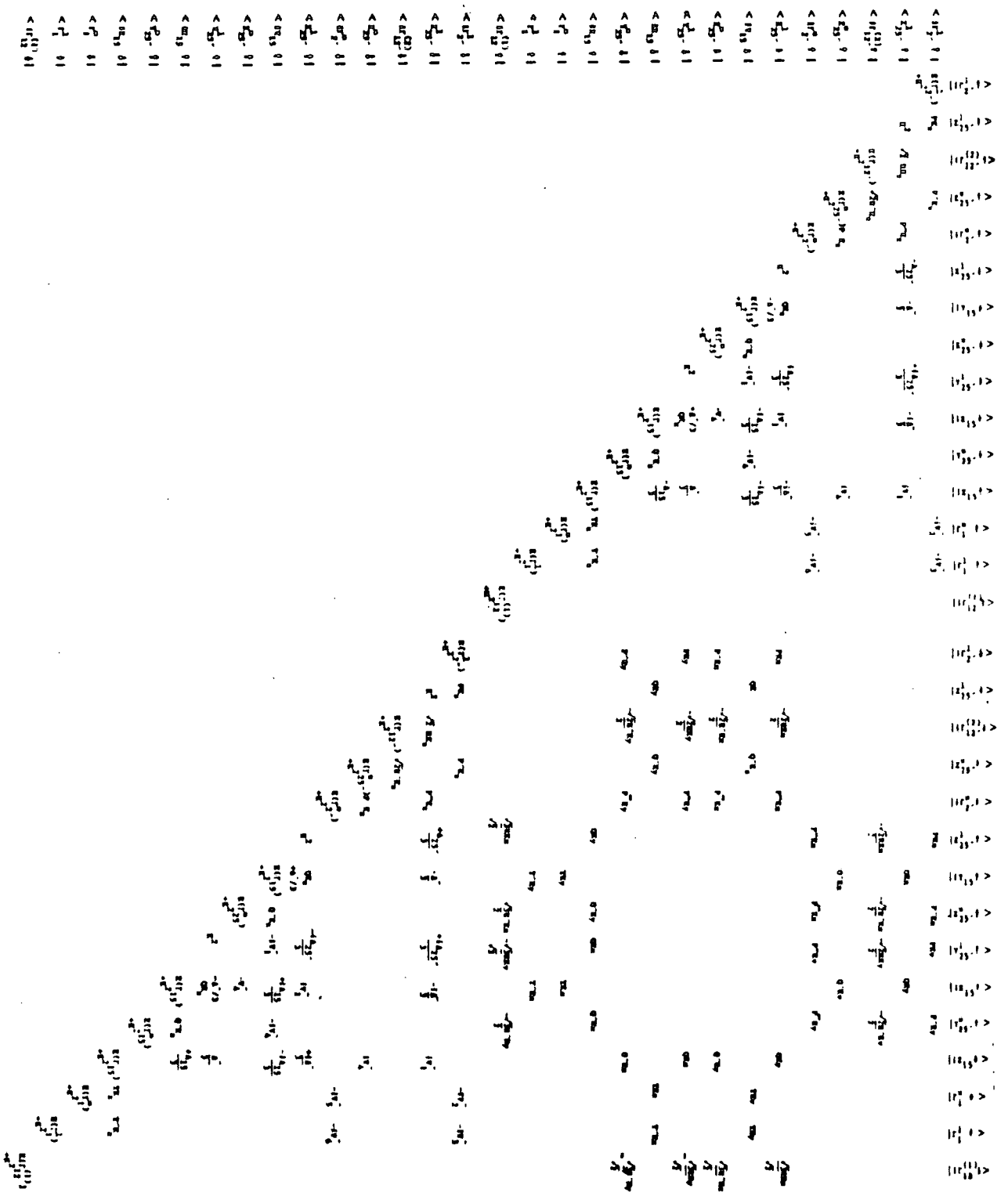

FIGURE 6.3

The upper right hand corner of the hermitian 30 by 30 matrix when Kx and Ky are non-zero.

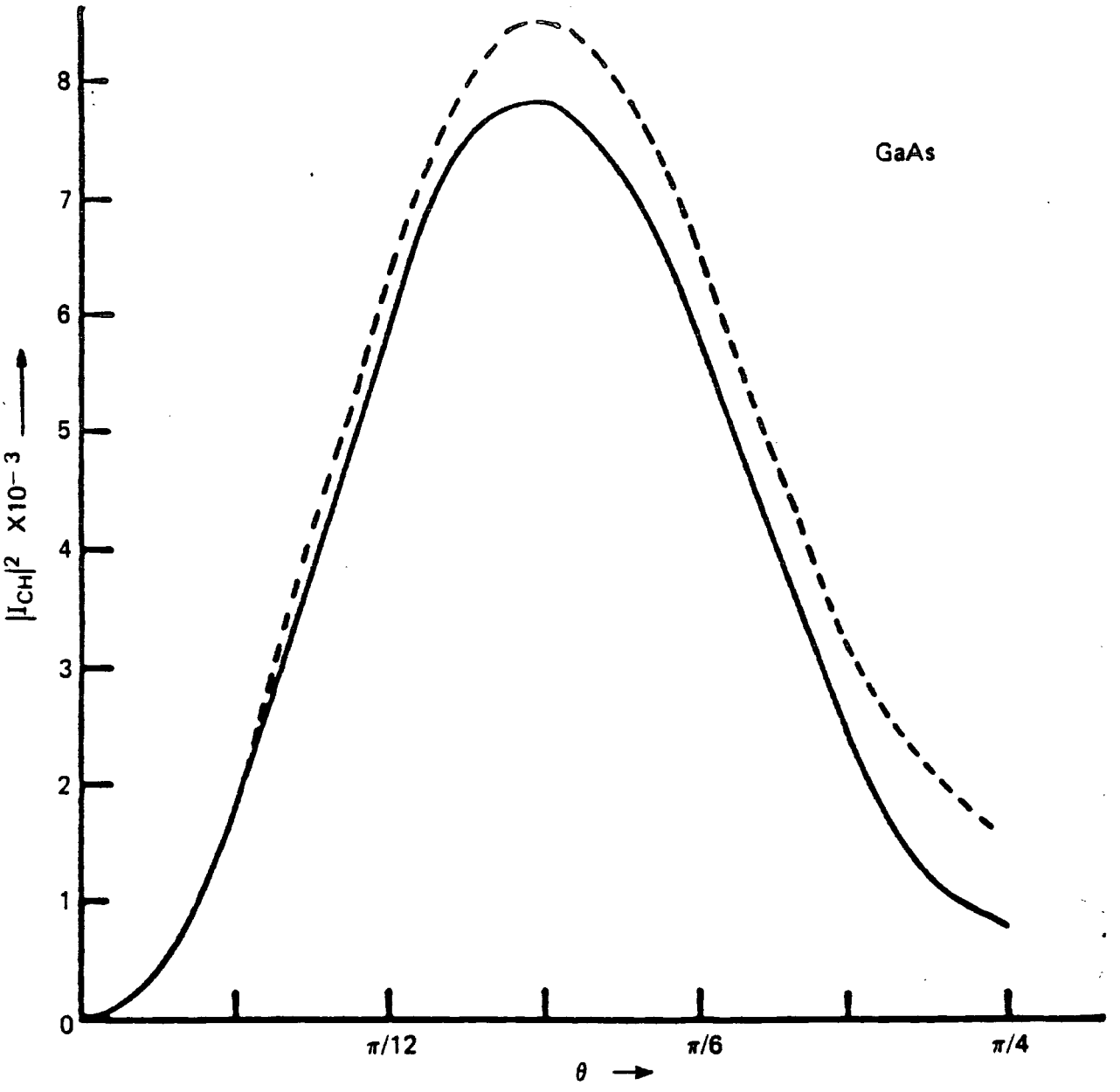


FIGURE 6.4

This figure shows, for GaAs, $|I_{CH}|^2$ as a function of θ, the angle the heavy hole wavevector makes with the z axis in the yz plane. The conduction band wavevector is taken as zero, and the heavy hole band wavevector as $0.2\left(\frac{2\pi}{a}\right)$ where a is the lattice spacing. The solid curve shows the 15 band K.p results and the dashed curve shows nonlocal pseudopotential results.

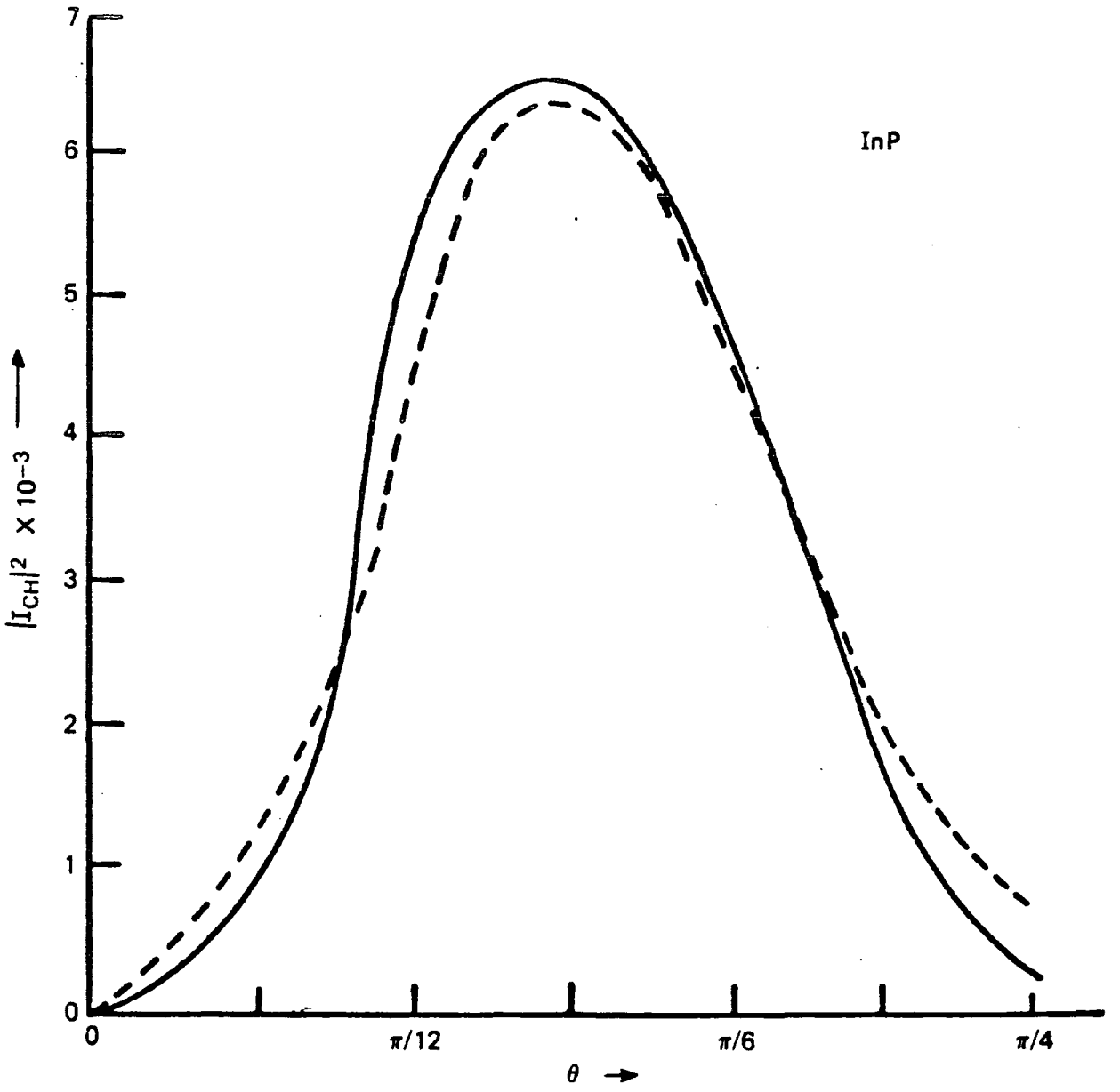


FIGURE 6.5

As figure 6.4 but for InP.

Rotation of the heavy hole wavevector has little effect on the shape of the graphs. Further rotations in the zy plane repeat, because of the crystal symmetry, the same pattern, and rotations around the (001) direction in the xy plane only modify the shown size of the overlap squared for a particular angle to the (001) axis by a few percent.

Brand has found empirical fits to these results (ref 6.19). He shows that the curves shown in figures 6.4 and 6.5 may be fitted by

$$I^2(CK_1, HK_1) = \beta \sin^2 4\theta \quad \text{with } \beta = 0.683 \text{ from pseudopotentials}$$

$$\text{and } \beta = 0.625 \text{ from 30 band K.}p.$$

$\theta$ being measured from the (001) axis and the heavy hole wavevector being taken as reasonably large. For smaller heavy hole wavevectors the numerical results show the relative size of the overlap in the (011) direction increases. But this is not a serious problem and should one wish to make the simplifying assumption that for a QW grown on the 001 plane the conduction band wavevector is exactly zero, then most of the integrals needed to incorporate the above empirical expression into the analytical calculations can be found in G+R.

Brand has also found an empirical fit for variation of the peak overlap with heavy hole wavevector magnitude. The peak overlap occurs midway between the (001) and (011)

directions. Figures 6.6 and 6.7 show how the size of this peak overlap decreases with decreasing heavy hole wavevector. Also shown on figures 6.6 and 6.7 is the effect of taking a small anti-parallel conduction wavevector. This more closely mimics the threshold condition and also gives a better fit to the empirical linear K relationship

$$\Gamma^2(CK_1, HK_{1'}) = \beta(K_1 - K_{1'})^2$$

(for which the coefficient $\beta$ is very different from the coefficient which could be obtained from an application of one of the effective mass sum rule estimations).

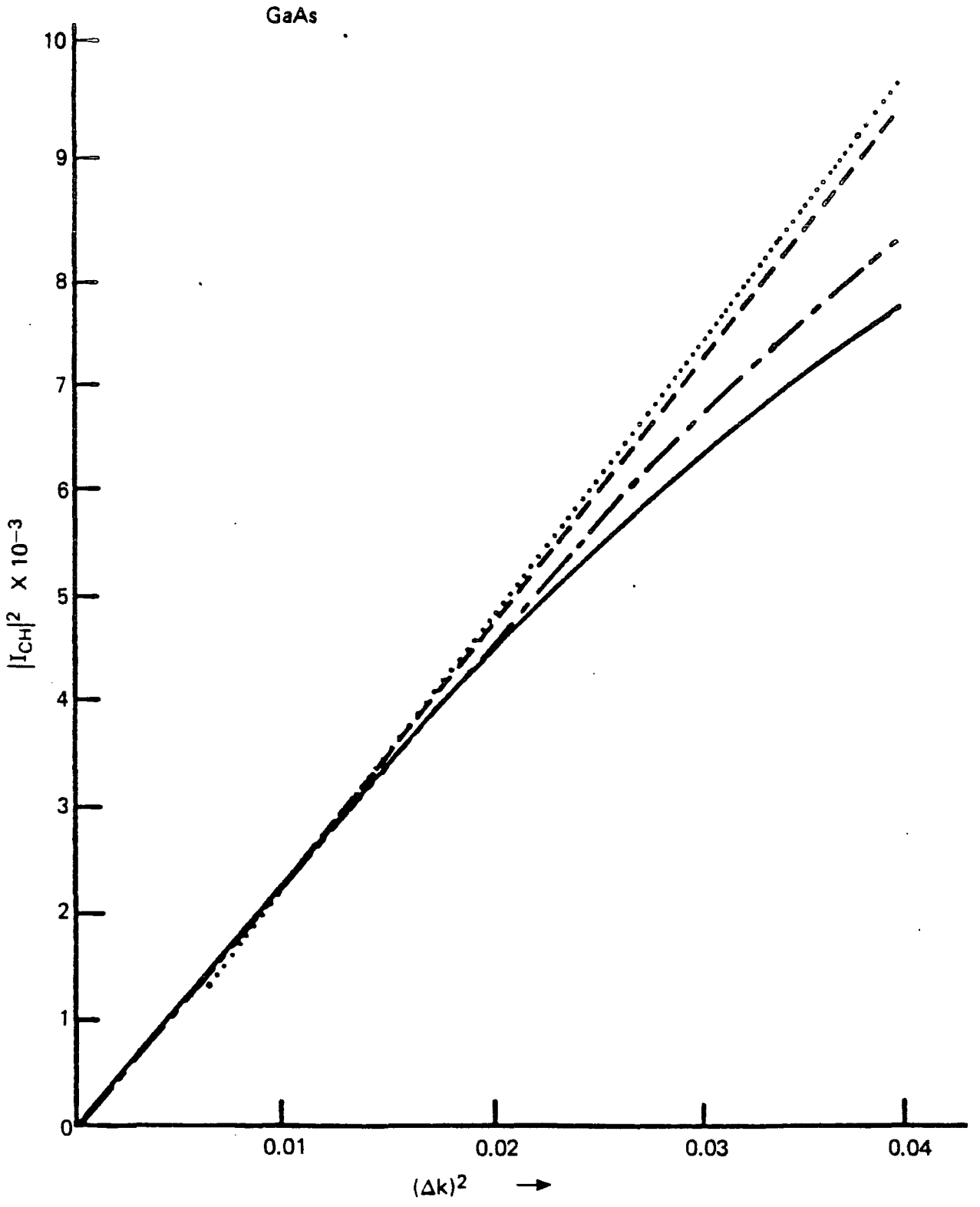


FIGURE 6.6

This figure shows, for GaAs, $|I_{CH}|^2$ as a function of the square of the difference $\Delta K = |\underline{K}_H - \underline{K}_c|$ between the heavy hole and conduction band wavevectors, $\underline{K}_H$ and $\underline{K}_c$. The wavevectors are taken to lie midway between (001) and (011) and are measured in units of $\frac{2\pi}{a}$. The solid curve shows the 15 band K.p results with $\underline{K}_c = 0$. The dotted-dashed curve shows nonlocal pseudopotential results with $\underline{K}_c = 0$. The dotted curve shows the 15 band K.p results with $\underline{K}_c = -0.05 \left(\frac{2\pi}{a}\right)$. And the dashed curve shows the nonlocal pseudopotential results with $\underline{K}_c = -0.05 \left(\frac{2\pi}{a}\right)$.

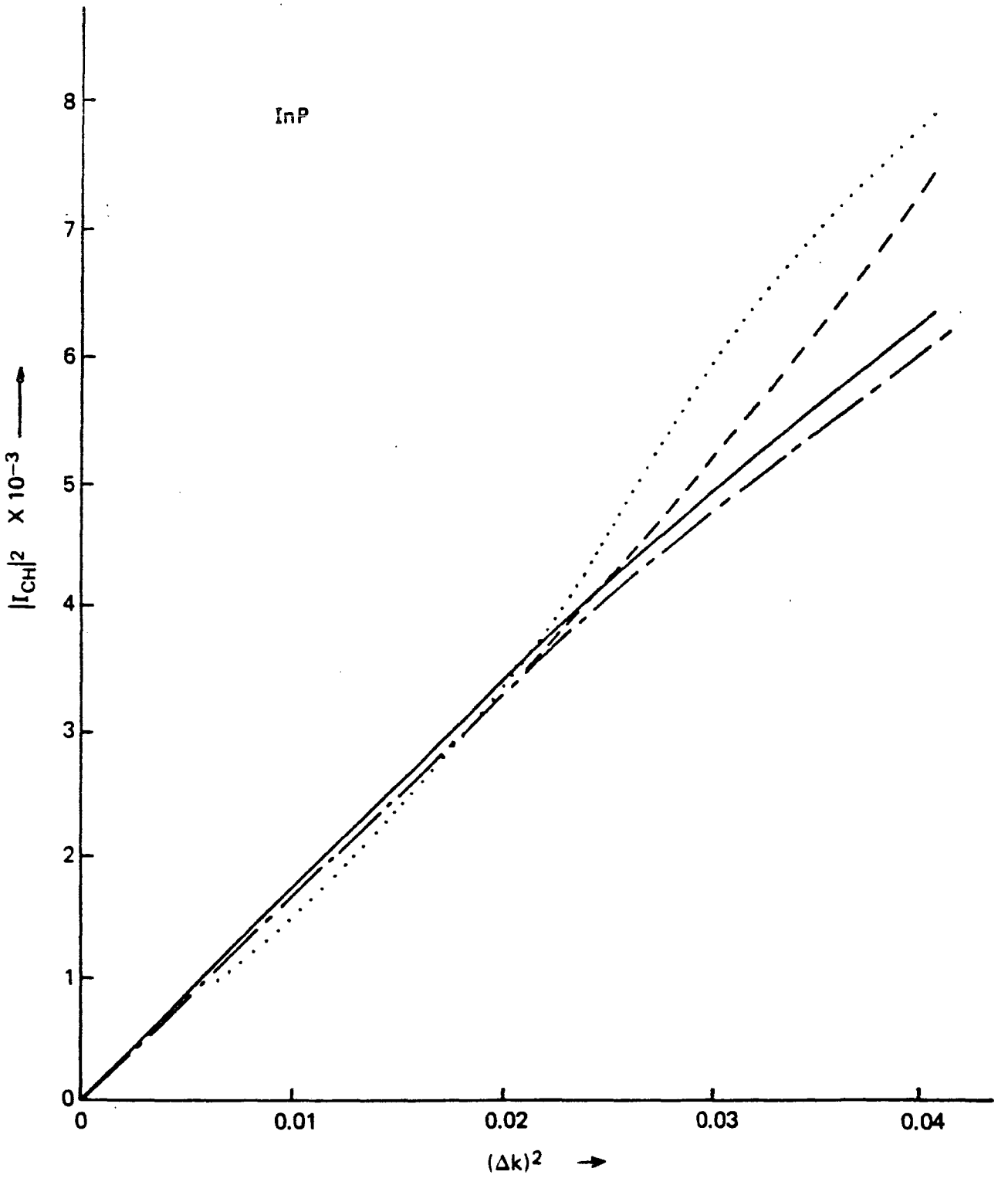


FIGURE 6.7

As figure 6.6 but for InP.

### 6.3.3 RESULTS WITH NON-PARALLEL WAVEVECTORS

In the results presented in this section the conduction band wavevector is taken to lie along the (001) direction with a small fixed magnitude, and the heavy hole wavevectors which has a large fixed magnitude, is rotated in between (001) and (011) in the zy plane. The modulus squared of the overlap is then plotted against the angle which the heavy hole wavevector makes with the (001) axis. Figures 6.8 and 6.9 show the behaviour of the overlap modulus squared in GaAs and InP respectively and compare the 15 band K.p results with pseudopotential results. As with the parallel wavevector results the agreement between the 15 band K.p and the pseudopotential results is good and their sizes are considerably smaller than predicted by conventional effective mass sum rule estimates.

The next level of approximation after the effective sum rule estimates, is to use the Kane's 4 band model to estimate the overlaps. In Kane's 4 band model the conduction band states $|\phi_{c\alpha}>$ and $|\phi_{c\beta}>$ with wavevector along the (001) direction are of the form

$$|\phi_{c\alpha}> = a_c|iS\downarrow> + b_c|(X_{15}^{GaAs} - iY_{15}^{GaAs})/\sqrt{2}\uparrow> + c_c|Z_{15}^{GaAs}\downarrow>$$

$$|\phi_{c\beta}> = a_c|iS\uparrow> - b_c|(X_{15}^{GaAs} + iY_{15}^{GaAs})/\sqrt{2}\downarrow> + c_c|Z_{15}^{GaAs}\uparrow>$$

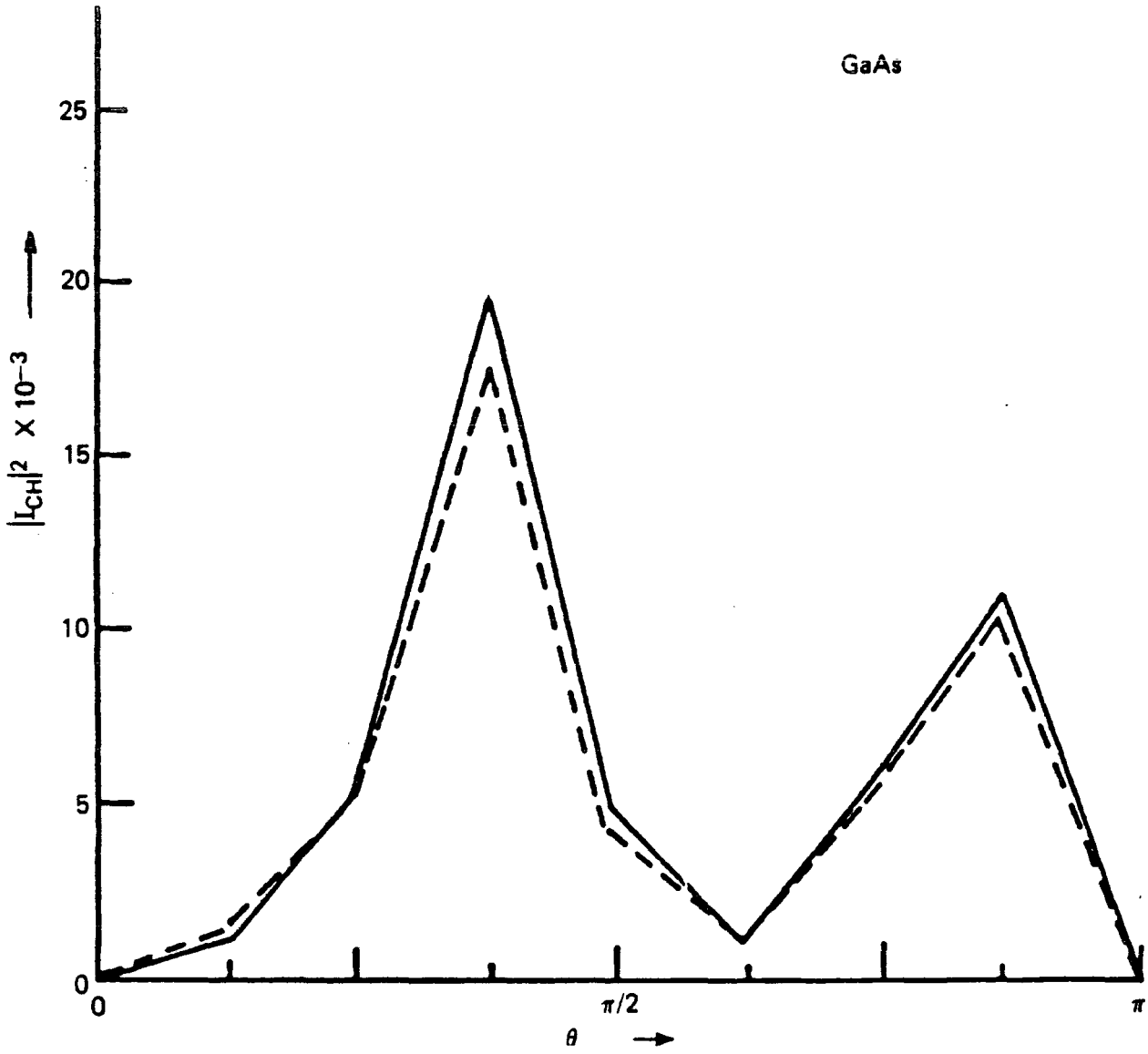


FIGURE 6.8

This figure compares the K.p (solid curve) and the pseudopotential (dashed curve) results for $|I_{CH}|^2$ as a function of the angle θ between the heavy hole and conduction band wavevectors. The conduction band wavevector is taken to be in the (001) direction and to be 0.015 $\left(\frac{2\pi}{a}\right)$. While the heavy hole band wavevector is taken as 0.15 $\left(\frac{2\pi}{a}\right)$. GaAs parameters are used.

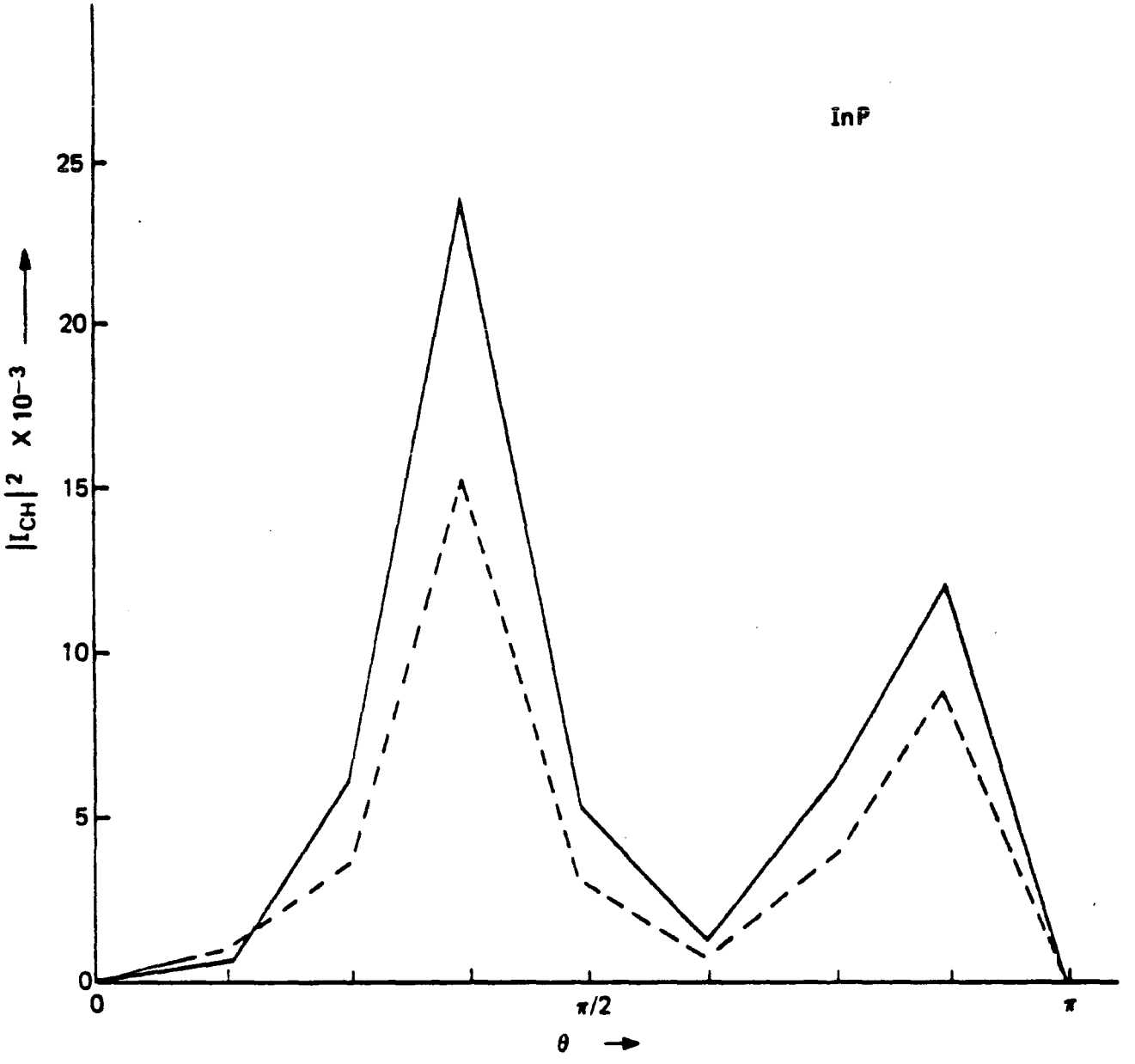


FIGURE 6.9

As figure 6.3 but for InP.

while the heavy hole states $|\phi_{H\alpha}>$ and $|\phi_{H\beta}>$ are given by

$$|\phi_{H\alpha}> = |(X_{15}^{GaAs} + iY_{15}^{GaAs})'/\sqrt{2}\ \uparrow'>$$

$$|\phi_{H\beta}> = |(X_{15}^{GaAs} - iY_{15}^{GaAs})'/\sqrt{2}\ \downarrow'>$$

where the primed quantities are given by

$$|\uparrow'> = \cos\theta/2|\uparrow> + \sin\theta/2|\downarrow>$$

$$|\downarrow'> = -\sin\theta/2|\uparrow> + \cos\theta/2|\downarrow>$$

$$X_{15'}^{GaAs'} = (\cos\theta)X_{15}^{GaAs} - (\sin\theta)Z_{15}^{GaAs}$$

$$Y_{15'}^{GaAs'} = Y_{15}^{GaAs}$$

$$Z_{15}^{GaAs'} = (\sin\theta)X_{15}^{GaAs} + (\cos\theta)Z_{15}^{GaAs}$$

Using these in the same way as in early steps of Beattie and Smith's 4 (8) band averageing procedure

$$|\phi_{H\alpha}> = \frac{\cos}{\sqrt{2}}\theta/2\ |(X_{15}^{GaAs}\cos\theta + iY_{15}^{GaAs} - Z_{15}^{GaAs}\sin\theta)\uparrow>$$

$$+ \frac{\sin}{\sqrt{2}}\theta/2\ |X_{15}^{GaAs}\cos\theta + iY_{15}^{GaAs} - Z_{15}^{GaAs}\sin\theta)\downarrow>$$

and

$$|\phi_{H\beta}> = -\frac{\sin}{\sqrt{2}}\theta/2\ |(X_{15}^{GaAs}\cos\theta - iY_{15}^{GaAs} - Z_{15}^{GaAs}\sin\theta)\uparrow>$$

$$+ \frac{\cos}{\sqrt{2}}\theta/2\ |(X_{15}^{GaAs}\cos\theta - iY_{15}^{GaAs} - Z_{15}^{GaAs}\sin\theta)\downarrow>$$

thus

$$|<\phi_{c\alpha}|\phi_{H\alpha}>|^2 = |<\phi_{c\beta}|\phi_{H\beta}>|^2 = |b_c + \sqrt{2}_c|^2 \sin^4\left(\frac{\theta}{2}\right) \cos^2\left(\frac{\theta}{2}\right)$$

$$|<\phi_{c\alpha}|\phi_{H\beta}>|^2 = |<\phi_{c\beta}|\phi_{H\alpha}>|^2 = |b_c + \sqrt{2}\, c_c|^2 \sin^2\left(\frac{\theta}{2}\right) \cos^4\left(\frac{\theta}{2}\right)$$

giving the average overlap squared

$$|I_{CH}|^2_{average} = \frac{1}{2}\left[2|<\phi_{c\alpha}|\phi_{H\alpha}>|^2 + 2|<\phi_{c\alpha}|\phi_{H\beta}>|\right]$$

$$= \frac{1}{4}\ |b_c + \sqrt{2}\, c_c|^2 \sin^2\theta \qquad 6.10$$

which Beattie and Smith now average over $\theta$. Here however equation 6.10 is retained for comparison with the 15 band K.p results. ( The coefficients $a_c$, $b_c$, and $c_c$ being found by solving Kane's (ref 6.13) cubic equation (10) exactly using the zincblende parameters found during the checking of the 001 results (see section 6.2.3).) The comparison of the Kane model predictions (from equation 6.10) and with the more exact 15 K.p results are shown in figures 6.10 and 6.11. These again show that the simpler estimate of the overlap is inadequate.

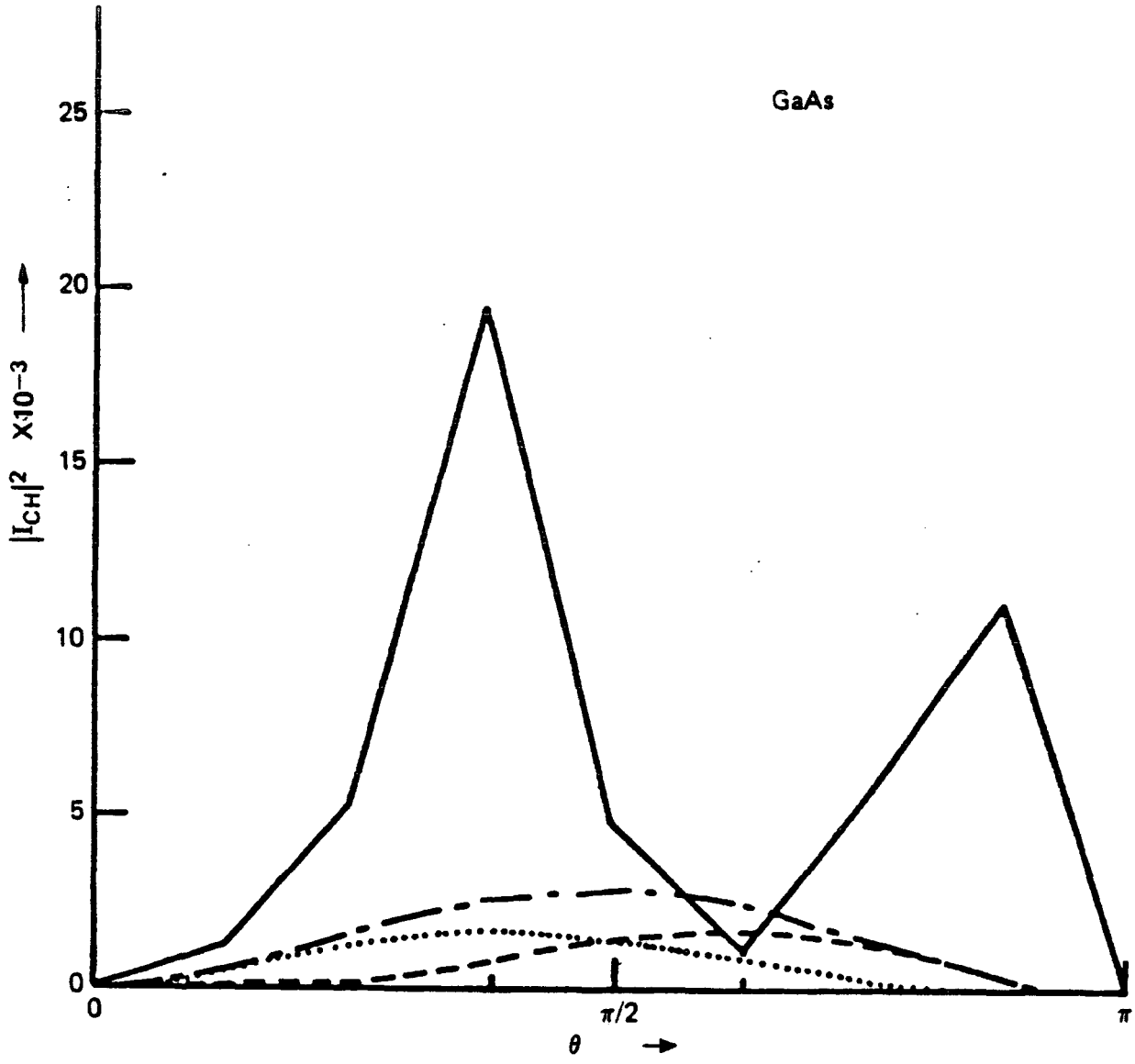


FIGURE 6.10

This figure shows $|I_{CH}|^2$ as a function of θ, the angle between heavy hole and conduction band wavevectors. The conduction band wavevector $K_c = 0.015\left(\frac{2\pi}{a}\right)$ is taken to lie along the z axis and the heavy hole wavevector $K_H$ is taken as equal to $0.15\left(\frac{2\pi}{a}\right)$. The solid curve shows the 15 band K.p results and the dotted dashed curve shows the Kane 4 band results. The contributions to the Kanes 4 band results are shown by the dashed curve (results for equal 'spin indices') and the dotted curve (different 'spin indices'). GaAs parameters are used.

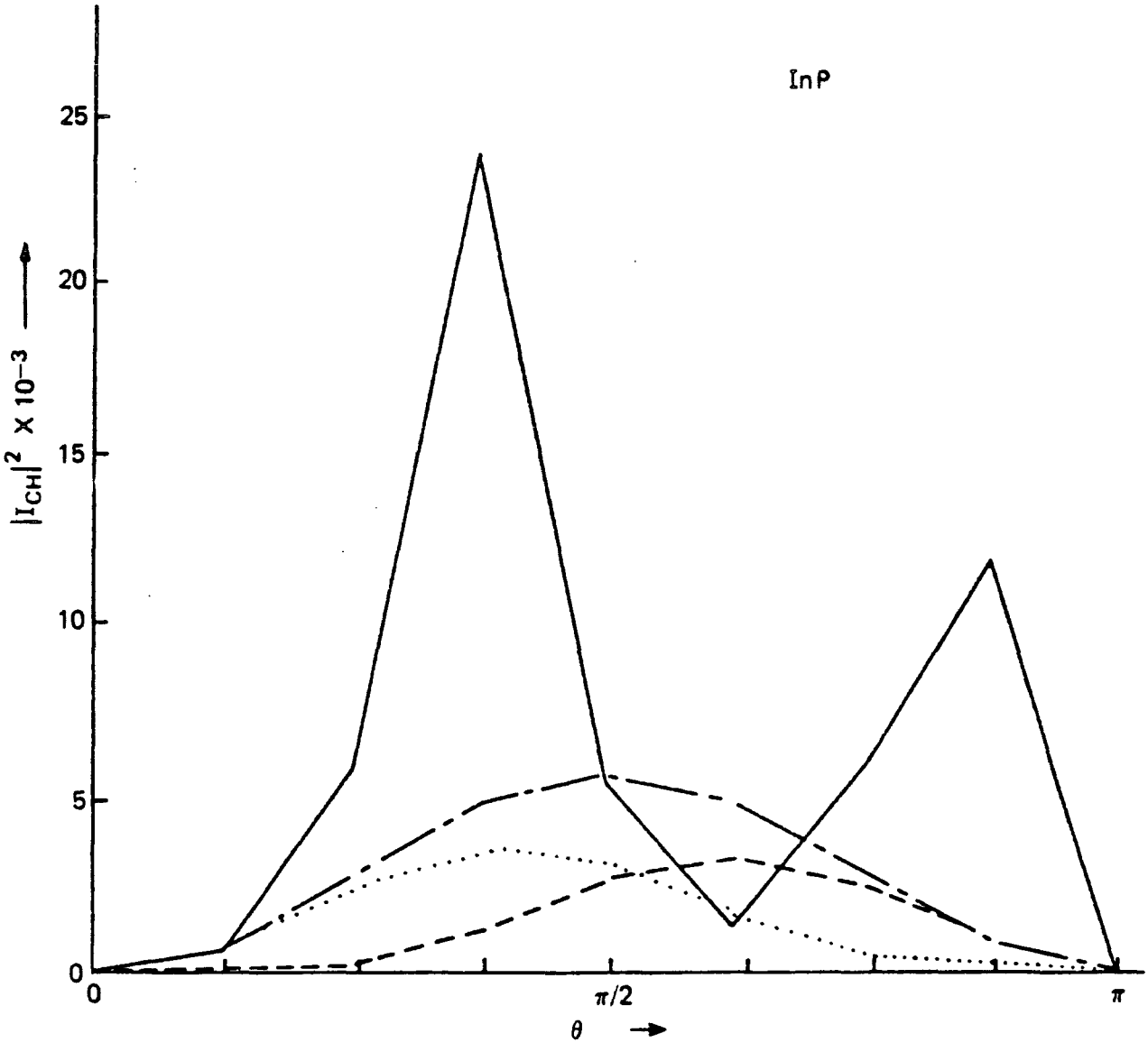


FIGURE 6.11

As figure 6.10 but for InP.

## 6.4 THE SIGNIFICANCE OF THE RESULTS FOR THEORETICAL AUGER RATE CALCULATIONS

In view of the above results the usual procedure of estimating the overlap integral squared at threshold, using conventional methods, and then using this to evaluate the Auger rate is obviously inadequate. Both the use of wavevectors corresponding to the threshold condition and the size of the overlap integral found using them are questionable.

Anisotropy destroys the condition that wavevectors should be exactly parallel at threshold. But even so the comparative size (in some cases bigger) non-parallel wavevectors compared with the parallel wavevectors makes it desirable to perform the whole Auger calculation numerically to see if the threshold condition is in fact strong enough to justify its use. Assuming that it is strong enough we are then left with the problem of finding a sensibly weighted average overlap to use.

Conventional effective mass sum rule and 4 band Kane derived overlap estimates do not agree with the more accurate 15 band K.p or pseudopotential estimates. The highly anistropic nature of these more accurate results make estimating an average difficult. However from the peak values of overlap squared it can be seen that such an average is going to be around two orders of magnitude down on conventional estimates. This supports the earlier

criticisms of the effective mass sum rule estimates, and also goes part way to explaining the present discrepancy between the measured Auger recombination rate in p-type InGaAsP and present theoretical predictions. Su et al (ref 6.15) having reported a measured Auger rate an order of magnitude lower than its predicted value by Dutta and Nelson (ref 6.10), and Sugimura (ref 6.9). Using the 15 band overlaps changes this theoretical overestimate of almost an order of magnitude into an underestimate of around an order of magnitude, and therefore it seems apparent that the simple treatment of Auger recombination at present popularly used (see for example ref 6.10) is not sufficient for reliable predictions of phenomenon, such as the temperature sensitivity of a semiconductor laser, which depend on a knowledge of the absolute size of the Auger recombination rate. It becomes necessary to consider for example the possible mixing, by inhomogeneities (dopants, compositional fluctuations, stains etc), of light and heavy hole band wavefunctions, the differences between lattice and carrier temperatures, and the correct (non-parabolic) band structure of the semiconductor.

**REFERENCES FOR CHAPTER 6**


6.1 Kane E O 1966 Semiconductors and Semimetals (ed R K Willardson and A C Beer) 1 75 (New York: Academic Press)

6.2 Cardona M and Pollak F H 1966 Phys. Rev 142 530

6.3 Cardona M, Pollak F H and Broerman J G 1965 Phys. Lett. 19 276

6.4 Pollak R H, Higgenbotham C W and Cardona M 1966 J. Phys. Soc. Japan 21 (suppl.) 20

6.5 Pollak F H and Cardona M 1966 J. Phys. Chem. Solids 27 423

6.6 Antoncik E and Landsberg P T 1963 Proc. Phys. Soc 82 337

6.7 Beattie A R and Smith G 1967 Phys. Status Solidi 19 557

6.8 Takeshima M 1978 J. Appl. Phys. Lett. 49 6118

6.9 Sugimura A 1981 Appl. Phys. Lett, 39 21

6.10 Dutta N and Nelson R J 1982 J. Appl. Phys. 53 74

6.11 Burt M G and Smith C 1984 J. Phys. C: Solid State Phys. 17 L47

6.12 Langsberg P T 1965 Lectures in Theoretical Physics, Boulder Vol 8A Ed. Brittin W E

6.13 Kane E O J. Phys. Chem. Solids 1 249

6.14 Burt M G 1982 Electron. Lett. 18 806

6.15 Su C B. Schlafer J, Manning J, and Olshansky R 1982 Electron. Lett. 18 595

6.16 Beattie A R 1983 Private Communication

6.17 Burt M G, Brand S, Smith C and Abram R A 1984 J. Phys. C: Solid State Phjys. 17 (1984) 6385

6.18 Brand S, Burt M G, Smith C and Abram R A 1985 Proc 17th Int. Conf. on the Physics of Semiconductors (San Francisco 1984) (Berlin: Springer)

6.19 Brand S and Abram R A 1984 J Phys C. Solid State Phys 17 L201

## APPENDIX 1 - THE THRESHOLD CONDITION FOR DIRECT BAND TO BAND CHCC AUGER RECOMBINATION

During the discussion of non-parabolicity (see section 2.1.3) and the interaction matrix element

$\langle \psi_{\substack{\text{INITIAL}\\\text{SYSTEM}\\\text{STATE}}} | H' | \psi_{\substack{\text{FINAL}\\\text{SYSTEM}\\\text{STATE}}} \rangle$ (see sections 2.4.1 and 2.4.2)

estimates of the most probable size of the in-plane wavevectors are made. These estimates are based on the sharp maximum in P (subject to energy and momentum conservation) which occurs because of its exponentials. This sharp maximum is referred to as the threshold condition for direct band to band CHCC Auger recombination, and the size of the in-plane wavevectors which correspond to it are found in essentially the same way as the bulk (ref 2.4), except that an effective band gap rather than the bulk band gap is used to define $K_G$.

We have

$$P = e^{-(E_1-\mu_c)/x_BT_c}\, e^{-(E_2-\mu_c)/x_BT_c}\, e^{+(E_{1'}-\mu_v)/x_BT_c} - e^{-(E_{2'}-\mu_c)/x_BT_c} \qquad \text{A1.1}$$

Neglecting the last term because $E_{2'}$ is large one must maximise

$$-(E_1-\mu_c) - (E_2-\mu_c) + (E_{1'}-\mu_v) \qquad \text{A1.2}$$

to get the maximum value of P. Expressing this in terms of the magnitude of wavevectors in the plane of the well

(using isotropic masses and parabolic bands)

$$2\Gamma_c - \Gamma_v - E_{c1} - E_{c2} + E_{v1'} - \frac{\hbar^2}{2m_c^*}(K_{\parallel 1}^2 + K_1^2 + \mu K_{\parallel 1'}^2) \qquad \text{A1.3}$$

$$\text{where } \mu = \frac{m_c^*}{m_{HH}^*}$$

From which it can be seen that for the most probable case the wavevectors must be parallel to each other. ( The parallel condition depending in particular on the isotropic mass assumption.) The parallel wavevectors are now related by writing $K_{\parallel 1} = aK_{\parallel 1'}$ and $K_{\parallel 2} = bK_{\parallel 2'}$.

Hence energy conservation gives

$$K_{\parallel 2'}^2 = (a^2 + b^2 + \mu)K_{\parallel 1'} + K_G^2 \qquad \text{A1.4}$$

where

$$K_G = (E_{c1} + E_{c2} - E_{v1'} - E_{c2'}) \frac{2m_c^*}{\hbar^2} = \Delta E \frac{2m_c^*}{\hbar^2} \qquad \text{A1.5}$$

and in-plane wavevector conservation (anticipating section 2.4.4) gives

$$K_{\parallel 2'} = (a + b + 1)K_{\parallel 1'} \qquad \text{A1.6}$$

Combining A1.4 and A1.6

$$K_{\parallel 1'}^2 = \frac{K_G^2}{1 + 2ab + 2a + 2b - \mu} \qquad \text{A1.7}$$

From which it follows that we must maximise

$$2\mathcal{P}_c - \mathcal{P}_v - E_{c2'} - \frac{\hbar^2}{2m_c^*} K_G \left( \frac{a^2 + b^2 + \mu}{1 + 2ab + 2a + 2b - \mu} + 1 \right) \qquad \text{A1.8}$$

This is done by differentiation with respect to 'a' and 'b' and yields

$$K_{\parallel 1} = -\mu K_{\parallel 1'}, \; K_{\parallel 2} = -\mu K_{\parallel 1'} \text{ and } K_{\parallel 2'} = (2\mu+1)K_{\parallel 1'} \qquad \text{A1.9}$$

which are the threshold wavevector relationships for wavevector components in the plane of the well.

In general the size of the coefficients depend on the in-plane E-K **relationships** used, but with isotropic bands the major conclusions remain the same ie the wavevector components in the plane of the well are similar for the colliding electrons and small compared to the Auger electron's in-plane wavevector.

## APPENDIX 2 - CHECKS ON THE BOUND-BOUND MATRIX ELEMENTS

### CHECK 1 : DOING THE FIRST qz INTEGRAL APPROXIMATELY

**a) FOR LARGE KL**

If KL >> 1 then in equation 3.5 $e^{-iK|Z_1-Z_2|} \rightarrow \frac{2}{K}\,\delta(Z_1-Z_2)$

giving

$$I_b' = \frac{8\pi}{L^2K^2}\int_0^L \sin\frac{n_1\pi}{L}z_1 \sin\frac{n_{1'}\pi}{L}z_1 \sin\frac{n_{2'}\pi}{L}z_2 \sin\frac{n_2\pi}{L}z_1\,\delta(z_1-z_2)dz_1dz_2 \qquad \text{A2.1}$$

$$I_b' \simeq \frac{2\pi}{L^2K^2}\int_0^L (\cos(n_1-n_{1'})\frac{\pi z}{L} - \cos(n_1+n_{1'})\frac{\pi z}{L})(\cos(n_2-n_{2'})\frac{\pi z}{L}-\cos(n_2+n_{2'})\frac{\pi z}{L}\,dz \qquad \text{A2.2}$$

$$I_b' \simeq \frac{\pi}{K^2L}\cdot\Big[\delta|n-n_{1'}|,|n_2-n_{2'}|(1+\delta_{n_1-n_{1'},0})+\delta|n_1+n_{1'}|,|n_2-n_{2'}|-\delta|n_1-n_{1'}|, \qquad \text{A2.3}$$
$$|n_2+n_{2'}| + \delta|n_1+n_{1'}|,|n_2-n_{2'}|\Big]$$

ie the same as 3.14

**b) FOR SMALL KL**

If KL << 1 then 3.5 may be approximated with K = 0. Hence

$$I_b' \simeq \frac{4\pi}{KL^2}\int_0^L \sin\frac{n_1\pi}{L}z_1 \sin\frac{n_{1'}\pi}{L}z_1dz_1\int_0^L \sin\frac{n_2\pi}{L}\sin\frac{n_2\pi}{L}z_2dz_2 \qquad \text{A2.4}$$

$$I_b' = \frac{\pi}{K}\,\delta_{n_1,n_{1'}}\,\delta_{n_2,n_{2'}} \qquad \text{A2.5}$$

which is as expected from 3.18.

**CHECK 2 : DOING THE $z_1$ AND $z_2$ INTEGRALS FIRST**

Considering for clarity, only the first sub-band process, we have from G+R page 476 eq 3.892.1

$$\int_0^L e^{iq_z z} \sin^2 \frac{\pi}{L} dz = \frac{L}{12} \frac{e^{iq_z L/2}}{\bar{B}(2 + q_z L/2\pi, 2 - q_z L/2\pi)} \qquad \text{A2.6}$$

$$= \frac{L}{2} \frac{e^{iq_z L/2}}{\Gamma(2 + \frac{q_z L}{2\pi})\ \Gamma(2 - \frac{q_z L}{2\pi})} \qquad \text{A2.7}$$

where $\bar{B}$ = Beta function and $\Gamma$ = Gamma function.

Using this to carry out the $z_1$ and $z_2$ integrals

$$I_b' = \int_{-\infty}^{+\infty} \frac{1}{K^2 + q_z^2} \left\{\Gamma(2 + \frac{q_z L}{2\pi})\ \Gamma(2 - \frac{q_z L}{2\pi})\right\}^{-2} dq_z \qquad \text{A2.8}$$

Now for convenience introducing the variable $X = q_z L/2$ gives

$$I_b' = \int_{-\infty}^{+\infty} \left(\frac{L}{2\pi}\right) \frac{1}{\left(\frac{KL}{2\pi}\right)^2 + X^2} \left\{\Gamma(2+X)\ \Gamma(2-X)\right\}^{-2} dX \qquad \text{A2.9}$$

to which approximations can now be made

**THE LARGE KL APPROXIMATION**

If KL >> $2\pi$ it is observed that $\left\{\Gamma(2+x)\ \Gamma(2-x)\right\}^{-2}$ peaks at $x = 0$ and is small outside the range $-2 < x < 2$. Using this

$$I_b' \simeq \frac{L}{2\pi}\left(\frac{2\pi}{KL}\right)^2 \int_{-\infty}^{-\infty} \left\{\Gamma(2+X)\ \Gamma(2-X)\right\}^{-2} dX \qquad \text{A2.10}$$

and using G+R page 656 eq 6.414.6

$$I_b' \simeq \frac{3\pi}{LK^2} \text{ as expected} \qquad \text{A2.11}$$

**THE SMALL KL APPROXIMATION**

If KL << $2\pi$ is it observed that $\left\{\Gamma(2+x)\ \Gamma(2-x)\right\}^{-2}$ is small outside the range $-2 < x < 2$ and is approximately 1 inside the range. Hence

$$I_b' \simeq \frac{L}{2\pi} \int_{-2}^{+2} \frac{1}{\left(\frac{KL}{2\pi}\right)^2 + X^2}\, dX = \frac{2}{K} \arctan\left(\frac{4\pi}{KL}\right) \qquad \text{A2.12}$$

$$I_b' \simeq \frac{\pi}{K} \text{ as expected} \qquad \text{A2.13}$$

**CHECK 3 : OBTAINING THE LARGE KL RESULTS DIRECTLY FROM 2.87, 2.88, AND 2.89**

2.87, 2.88 and 2.89 give when the perpendicular wavevector dependence of the periodic parts of the Bloch wavefunctions are neglected

$$I_b' = \frac{1}{M_{BF}} \int_{-\infty}^{+\infty} \frac{1}{K^2 + q_z^2} \left\{1',1\right\}\left\{2',2\right\} dq_z \qquad \text{A2.14}$$

Considering again just the first sub-band process

$$I_b' \doteq \frac{1}{K} \int_{-\infty}^{+\infty} \left(\frac{2}{L}\right)^2 (2H(q_z) - H(q_z + \frac{2\pi}{L}) - H(q_z - \frac{2\pi}{L}))\ (2H(-q_z) - H(q_z + \frac{2\pi}{L}) - H(q_z - \frac{2\pi}{L}))\ dq_z \qquad \text{A2.15}$$

where it is observed that as $L \to \infty$ the H's peak sharply at the zero's of their arguments.

Multiplying this out and dropping terms such as $\int_{-\infty}^{+\infty} H(q_z \pm \frac{2\pi}{L})\ H(-q_z)\ dq_z$ and $\int_{-\infty}^{+\infty} H(q_z + \frac{2\pi}{L}) H(-q_z + \frac{2\pi}{L})\ dq_z$ because they may be shown to be zero by complex integration leaves

$$I_b' \doteq \frac{1}{K^2} \int_{-\infty}^{-\infty} \left(\frac{2}{L}\right)^2 \left[4\bar{H}^2(q_z) + \bar{H}^2(q_z + \frac{2\pi}{L}) + \bar{H}^2(q_z - \frac{2\pi}{L})\right] dq_z \qquad \text{A2.16}$$

$$I_b' \doteq \frac{1}{K^2} \int_{-\infty}^{+\infty} \left(\frac{2}{L}\right)^2 6\bar{H}^2(q_z)\ dq_z \quad \text{where } \bar{H}(x) = H(+x)\ e^{-ixL/2} \quad \text{or } \bar{H}(x) = H(-x)\ e^{+ixL/2} \qquad \text{A2.17}$$

Now from 2.90

$$\bar{H}(x) = \frac{\sin \frac{xL}{2}}{x/2} \qquad \text{A2.18}$$

and

$$\int_{-\infty}^{+\infty} \left( \frac{\sin \frac{q_z L}{2}}{q_z/2} \right)^2 dq_z \rightarrow 2\pi L \text{ as } L \rightarrow \infty \qquad \text{A2.19}$$

(from

$$\int_{-\infty}^{+\infty} \frac{\sin^2 Lx}{x^2 + c^2} dx = \int_{-\infty}^{+\infty} \frac{1 - \cos 2Lx}{x^2 + c^2} dx = \int_{-\infty}^{+\infty} \left( \frac{1}{x^2 + c^2} - \frac{\cos 2Lx}{x^2 + c^2} \right) dx \qquad \text{A2.20}$$

$$= \frac{\pi}{c} \left[ 1 - e^{-2Lc} \right] \qquad \text{A2.21}$$

$$\rightarrow 2\pi L \text{ as } c \rightarrow 0 \quad ) \qquad \text{A2.22}$$

Therefore

$$I_b' \simeq \frac{1}{K^2} \left( \frac{2}{L} \right)^2 .6.2\pi L \qquad \text{A2.23}$$

$$I_b' \simeq \frac{3\pi}{K^2 L} \text{ as expected} \qquad \text{A2.24}$$

## APPENDIX 3 - CHECKS ON THE EVALUATION OF THE UNBOUND MATRIX ELEMENT

Several alternative routes may be taken between 4.6 and 4.13.

Here three types of check on the evaluation of $I_{ub'}$ are made. First it is indicated that $z_1$ integrals may be done a different way. Then it is shown that 4.10 tends, with suitable modifications, to the approximate results of Chapter 3. Finally $I'_{ub}$ is also checked by side stepping 4.6, and doing the $q_z$ integral approximately. (The approximations thus obtained then being shown to be consistent with approximations obtained directly from 4.10 and 4.2.)

### CHECK 1 : ALTERNATIVE MEANS OF DOING THE $z_1$ INTEGRALS

When $n_1 = n_{1'} = 1$ in 4.6 the first two $z_1$ integrals may be done using G+R page 478 eq 3.895.2 (with $K \neq 0$), and the third may be done using G+R page 372 eqs 3.631.1 and 3.631.8. Although the result of the third integration

$$I_{ub'}\Big|_{n_1=n_{1'}=1} \begin{pmatrix}\text{THIRD}\\ \text{INTEGRAL}\end{pmatrix} = \left(\frac{2}{L}\right)^{3/2}\left\{\frac{a\pi L}{(K^2+B^2)}\;\frac{\sin(BL/2)}{12\;\bar{B}(2+(BL/2\pi),2-(BL/2\pi))}\right.$$

$$+\frac{a\pi L}{(K^2+A^2)}\;\frac{\sin(AL/2)}{12\;\bar{B}(2+(AL/2\pi),2-(AL/2\pi))}$$

$$\left.+\frac{a'\pi L}{(K^2+A^2)}\;\frac{\cos\;(AL/2)}{12\;\bar{B}(2+(AL/2\pi),2-(AL/2\pi))}+\frac{a'\pi L}{K^2+B^2}\;\frac{\cos(BL/2)}{12\;\bar{B}(2+(BL/2\pi),2-(BL/2\pi))}\right\}$$

where $\bar{B}$=Beta function

appears somewhat different to 4.9 it may be shown to be identical to 4.9 either numerically, or analytically by integrating G+R page 949 eq 8.381.4.

**CHECK 2 - OBTAINING THE APPROXIMATIONS OF CHAPTER 3 FROM $I'_{ub}$ OF Eq 4.5**

By taking $\alpha = \left(\frac{2}{L}\right)^{\frac{1}{2}}$ and a = 0, giving the promoted (Auger) electron the parity of the corresponding bound state, and setting $K_{z2'}$ equal to its possible discrete values (ie $\frac{\pi}{L}, \frac{2\pi}{L}, \frac{3\pi}{L}, \frac{4\pi}{L}, \frac{5\pi}{L}$ etc) it is possible to show that 4.5 reduces to the approximate values of $I'_b$ in Chapter 3. Apart from checking 4.5 these reductions have also been used to check various computer programs and the alternative $z_1$, $z_2$ first approach to 4.2.

**THE FIRST SUB-BAND PROCESS**

When $K_{z2'} = \frac{\pi}{L}$ and KL is large the leading terms in 4.10 are

$$I'_{ub} \simeq \left(\frac{2}{L}\right)^2 \frac{\pi L}{2K^2} \left\{\frac{1}{\Gamma(2)\Gamma(2)} + \frac{1}{\Gamma(3)\Gamma(1)}\right\} \qquad \text{A3.1}$$

Hence the expected result is obtained ie

$$I'_{ub} \simeq \frac{3\pi}{K^2 L}$$

Considering again the first sub-band result but now with KL << 1

$$I_{ub}' \simeq \left(\frac{2}{L}\right)^2 \frac{\pi}{K} \left\{ \frac{1}{K^2} \left[ \frac{KL/2}{\Gamma(2)\Gamma(2)} - \frac{KL}{2} \right] + \frac{L}{4\pi^2} \left[ \frac{KL/2}{\Gamma(3)\Gamma(1)} + \frac{KL}{2} \right] \right. \qquad \text{A3.2}$$

Because of the cancellation we go to the next order in the exponential of the first part. Hence with the second part neglected

$$I_{ub}' \simeq \frac{2}{L}^{2} \frac{\pi}{K} \frac{1}{K^2} \left[ \frac{KL/2}{\Gamma(2)\Gamma(2)} - \frac{KL-K^2L^2/2}{2} \right] \qquad \text{A3.3}$$

$$I_{ub}' \simeq \frac{\pi}{K}$$

Again as expected from Chapter 3.

**THE SECOND SUB-BAND PROCESS - WITH $K_{z2'} = \frac{2\pi}{L}$ AND $K_{z1} = K_{z1'} = K_{z2} = \frac{\pi}{L}$**

When the promoted Auger state is given odd parity with respect to the centre of the well then from both from 4.10 and the parity considerations of section 2.4.3.1 it is seen that $I_{ub}'$ is zero as hoped for.

**THE THIRD SUB-BAND PROCESS - WITH $K_{z2'} = \frac{3\pi}{L}$ AND**

**$K_{z1} = K_{z1'} = K_{z2} = \frac{\pi}{L}$**

Taking KL >> 1

$$I_{ub}' \simeq \left(\frac{2}{L}\right)^2 \frac{\pi}{K} \left\{ \frac{1}{K^2} \left[ \frac{-KL/2}{2} - \frac{2}{\left(\frac{K^2L^2}{\pi^2}\right)} \right] + \frac{1}{K^2} \left[ \frac{2}{\left(\frac{K^2L^2}{\pi^2}\right)} \right] \right\} \qquad \text{A3.4}$$

$$I_{ub}' \simeq - \frac{\pi}{LK^2} \qquad \text{A3.5}$$

as required.

**CHECK 3 - DOING THE FIRST $q_z$ INTEGRAL APPROXIMATELY**

In this set of checks 4.6 is side stepped, and the resulting approximations to $I'_{ub}$, and conclusions about the behavior of $I'_{ub}$, are shown to be consistent with expectations from both 4.10 and the alternative $z_1$, $z_2$ first approach to 4.2.

a) **LARGE K**

Suppose $K \to \infty$ then 4.2 becomes (see for example check 1 of Appendix 2)

$$I'_{ub} - \left(\frac{2}{L}\right)^{3/2} \frac{2\pi}{K^2}\left(\int_0^L a' \sin^2 \frac{\pi z}{L} \sin \frac{n_1 \pi z}{L} \sin K_{z2'} dz + \int_0^L a \sin^2 \frac{\pi z}{L} \sin \frac{n_1 \pi z}{L} \cos k_{z2'} z \, dz\right) \qquad \text{A3.6}$$

$$(n_1 = n_2 = 1)$$

Apply the trigonometrical product formulae

$$I'_{ub} \simeq \left(\frac{2}{L}\right)^{3/2} \frac{2\pi}{K^2} \frac{1}{2}\left(\int_0^L a' \sin^2 \frac{\pi z}{L} \cos\left(\frac{n_1 \pi}{L} - K_{z2'}\right) z dz - \int_0^L a' \sin^2 \frac{\pi z}{L} \cos\left(\frac{n_1 \pi}{L} + K_{z2'}\right) z \, dz\right.$$

$$\left. + \int_0^L a \sin^2 \frac{\pi}{L} z \sin\left(\frac{n_1 \pi}{L} - K_{z2'}\right) z \, dz + \int_0^L a \sin^2 \frac{\pi}{L} z \sin\left(\frac{n_1 \pi}{L} + K_{z2'}\right) z \, dz\right) \qquad \text{A3.7}$$

Now using G+R page 372 eq's 3.631.8 and 3.631.1

$$I'_{ub} \simeq \left(\frac{2}{L}\right)^{3/2} \frac{\pi L}{K^2} \left[\frac{a' \cos(\frac{n_1 \pi}{L} - K_{z2'})L/2 + a \sin \frac{n_1 \pi}{L} - K_{z2'})L/2}{12\, B(2 + (\frac{n_1 \pi}{L} - K_{z2'})L/2\pi,\ 2 - (\frac{n_1 \pi}{L} - K_{z2'})L/2\pi}\right.$$

$$\left. + \frac{a \sin(\frac{n_1 \pi}{L} + K_{z2'})L/2 - a' \cos(\frac{n_1 \pi}{L} + K_{z2'})L/2}{12\, B(2 + (\frac{n_1 \pi}{L} + K_{z2'})L/2\pi,\ 2 - (\frac{n_1 \pi}{L} + K_{z2'})L/2\pi}\right] \qquad \text{A3.8}$$

which may itself be checked when $n_1' = 1$ by again using G+R page 372 eq's 3.631.8 and 3.631.1, but this time without the trigonometrical product formulae.

Particular values of the $I'_{ub}$ are now considered and it is found that because the unbound state (unlike the bound state) can choose its parity to suit the requirements of the other states, $I'_{ub}$ has non-zero values when $K_{z1} = K_{z1'} = K_{z2} = \frac{\pi}{L}$ and $K_{z2'} = \frac{2\pi}{L}, \frac{4\pi}{L}, \frac{6\pi}{L}$ etc. Further when $K_{z1} = K_{z1'} = K_{z2} = \frac{\pi}{L}$ and $K_{z2'} = \frac{3\pi}{L}$ then $I'_{ub}$ is non-zero, but when $K_{z1} = K_{z1'} = K_{z2'} = \frac{\pi}{L}$ and $K_{z2'} = \frac{5\pi}{L}, \frac{7\pi}{L}, \frac{9\pi}{L}$ etc. then $I'_{ub}$ is zero.

These results are consistent with results obtained directly from 4.10 and also not inconsistent with results obtained by doing the $z_1$, $z_2$ integrals first. To see this second point, the origin is placed at the centre of the well to take advantage of the parity

$$I'_{ub} = \left(\frac{2}{L}\right)^{3/2} B' \int_{-\infty}^{+\infty} \frac{dq_z}{K^2 + q_z^2} \int_{-\frac{L}{2}}^{+\frac{L}{2}} \cos\left(\frac{2\pi}{L} z_1\right) \cos q_z z_1 \, dz_1$$

$$\int_{-\frac{L}{2}}^{+\frac{L}{2}} \cos \frac{\pi}{L} z_2 \cos K_{z2'} z_2 \cos q_z z_2 \, dz_2 \qquad \text{A3.9}$$

then the $z_1$ and $z_2$ integrals are evaluated before the $q_z$ integral

$$I'_{ub} = \left(\frac{2}{L}\right)^{3/2} B' \int \frac{dq_z}{K^2+q_z^2} \left\{ \frac{1}{q_z} \sin \frac{q_z L}{2} + \frac{1}{2} \frac{\sin(\pi + q_z L/2)}{\left(\frac{2\pi}{L} + q_z\right)} + \frac{1}{2} \frac{\sin(\pi - q_z L/2)}{\left(\frac{2\pi}{L} - q_z\right)} \right\}$$

$$\left\{ \frac{1}{2} \frac{\sin\left(\frac{\pi}{2} + \frac{K_{z2}L}{2} - \frac{q_z L}{2}\right)}{\frac{\pi}{L} + K_{z2} - q_z} + \frac{1}{2} \frac{\sin\left(\frac{\pi}{2} - \frac{K_{z2}}{2} + \frac{q_z L}{2}\right)}{\frac{\pi}{L} - K_{z2} + q_z} + \frac{1}{2} \frac{\sin\left(\frac{\pi}{L} + \frac{K_{z2}}{2} + \frac{q_z L}{2}\right)}{\frac{\pi}{L} + K_{z2} + q_z} \right.$$

$$\left. + \frac{1}{2} \frac{\sin\left(\frac{\pi}{2} - \frac{K_{z2}}{2} - \frac{q_z L}{2}\right)}{\frac{\pi}{L} - K_{z2} - q_z} \right\} \qquad \text{A3.10}$$

Now when $K_{z2'} = \frac{3\pi}{L}$ similar terms appear in both brackets and a non-zero $I'_{ub}$ is expected. But when $K_{z2'} = \frac{5\pi}{L}$ the terms become less similar, and it becomes more difficult to confirm the above conclusions about the behavior of $I'_{ub}$

b) **SMALL K**

**Using the K = 0 approximation (see again appendix 2 check 1b) to do the first $q_z$ integral approximately**

$$I'_{ub} = \left(\frac{2}{L}\right)^{3/2} \frac{\pi}{K} \int_0^L \sin\frac{\pi z_1}{L} \sin\frac{n_{1'}\pi}{L} z_1 \, dz_1 \left\{ \int_0^L a' \sin\frac{\pi}{L} z_2 \sin K_{z2'} z_2 \, dz_2 + \int_0^L a \sin\frac{\pi z_2}{L} \cos K_{z2'} z_2 \, dz_2 \right\} \qquad \text{A3.11}$$

Now again using G+R page 372 eqs 3.631.8 and 3.631.1

$$I'_{ub} = \frac{\pi}{K} \frac{\sin n_{1'}\pi/2 \, (a' \sin K_{z2'}L/2 + a \cos K_{z2'}L/2)}{\Gamma\left(\frac{3+n_{1'}}{2}\right)\Gamma\left(\frac{3-n_{1'}}{2}\right)\Gamma\left(\frac{3+n_{2'}}{2}\right)\Gamma\left(\frac{3-n_{2'}}{2}\right)}$$

So when $K_{z1'} = \frac{\pi}{L}$ and $K_{z2'} = \frac{2\pi}{L}, \frac{4\pi}{L}, \frac{6\pi}{L}$ etc. then $I'_{ub}$ is non-zero, and when $K_{z1'} = \frac{\pi}{L}$ and $K_{z2'} = \frac{3\pi}{L}, \frac{5\pi}{L}, \frac{7\pi}{L}$ then $I'_{ub}$ is zero.

Again these results are both consistent with immediate observations from 4.13 and not inconsistent with possible interpretations of 4.27. That is interpretations where small K selects small $q_z$ through the $\frac{1}{K^2+q_z^2}$ term and it is observed that the second bracket of 4.48 is zero at $q_z = 0$ when $K_{z2'} = \frac{3\pi}{L}, \frac{5\pi}{L}, \frac{7\pi}{L}$ etc.

**APPENDIX 4 - PART 1 - DOING THE $E_{c2'}$ INTEGRAL FIRST FOR THE BOUND-UNBOUND CALCULATION**

The integral to be considered is

$$Q = \frac{\pi^3 (x_B T_c)}{\alpha^2 (\mu+1)} M_{BF}^2 I_{ub}^{2} ds_{CON} (E^+_{c2'min}) \int_0^\infty \int_{E_{c2'min}}^\infty e^{-(E_{c2'}-E_{c1})/x_B T_c} \left\{ 1 - erf\sqrt{\frac{\alpha}{x_B T_c}} \left( \frac{\Delta E}{2\alpha K} + \frac{(2\mu+1)}{(\mu+1)} \frac{K}{2} \right) \right\} dE_{c2'} \, K \, dK \qquad \text{A4.1}$$

For the first part

$$\int_{E_{c2'min}}^\infty e^{-E_{c2'}/x_B T_c} dE_{c2'} = x_B T_c \, e^{-E_{c2'min}/x_B T_c} \qquad \text{A4.2}$$

For the second part the variable is changed to X where

$$X = -\sqrt{\frac{\alpha}{x_B T_c}} \left( \frac{E_{c1} + E_{c2} - E_{v1'} - E_{c2'}}{2\alpha K} + \frac{2\mu+1}{\mu+1} \frac{K}{2} \right) \qquad \text{A4.3}$$

So

$$E_{c2'} = 2\alpha K \left( \sqrt{\frac{x_B T_c}{\alpha}} X + \frac{(2\mu+1)}{(\mu+1)} \frac{K}{2} \right) + E_{c1} + E_{c2} - E_{v1'} \qquad \text{A4.4}$$

and

$$dE_{c2'} = 2\sqrt{\alpha \, x_B T_c} \; K \, dX \qquad \text{A4.5}$$

Hence the second integral becomes

$$Q_{2nd} = \frac{\pi^3}{\alpha^2(\mu+1)} (x_B T_c)\, M_{BF}^2\, I_{ub}^2\, ds_{CON}\, (E^+_{c2'min}) \int_0^\infty \int_{E_{c2'min}}^\infty (-2\sqrt{\alpha x_B T_c}\, K)$$

$$e^{-2\alpha K \frac{X}{\alpha\, x_B T_c} + \frac{(2\mu+1)}{(\mu+1)} \frac{K}{2} x_B T_c}$$

$$e^{-(E_{c2} - E_{v1'})/x_B T_c}\, \mathrm{erf}(-X)\, dX\, KdK \qquad \text{A4.6}$$

Now using A+S page 304 eqs 7.435 and 7.436 with $a = -2\sqrt{\alpha\, x_B T_c}\; K$ and $b = -1$ and evaluating between the given limits, gives

$$Q_{2nd} = \frac{\pi^3}{\alpha^2(\mu+1)} (x_B T_c)^2\, M_{BF}^2\, I_{ub}^2\, ds_{CON}\, (E^+_{c2'min}) \int_0^\infty$$

$$\Bigg( e^{(\alpha K^2 - \frac{\alpha(2\mu+1)}{(\mu+1)} K^2 - E_{c2} + E_{v1'})/x_B T_c} - e^{-(E_{c2'min} - E_{c1})/x_B T_C}$$

$$\mathrm{erf}\left\{\frac{\alpha}{x_B T_c}\left(\frac{\Delta E_{max}}{2\alpha K} + \frac{2\mu+1}{\mu+1}\frac{K}{2}\right)\right\} e^{(\alpha K^2 - \frac{\alpha(2\mu+1)}{\mu+1} K^2 - E_{c2} + E_{v1'})/x_B T_c}$$

$$\mathrm{erfc}\left\{\frac{\alpha}{x_B T_c}\left(\frac{\Delta E_{max}}{2\alpha K} + \frac{2\mu+1}{\mu+1}\frac{K}{2} - K\right)\right\} KdK \qquad \text{A4.7}$$

where $\Delta E_{max}$ is defined for convenience by

$$\Delta E_{max} = E_{c1} + E_{c2'} - E_{v1} - E_{c2'min} \qquad \text{A4.8}$$

ie the maximum $\Delta E$ for a given set of participating bound sub-bands

Collecting all the terms together

$$Q = \frac{\pi^3}{\alpha^2(\mu+1)} (x_B T_c)^2 M_{BF}^2 I_{ub}^2 \, ds_{CON}(E^+_{c2'min}) \int_0^\infty \left( e^{-(E_{c2'min} - E_{c1})/x_B T_c} \right.$$

$$\left. \operatorname{erfc}\left\{ \sqrt{\frac{\alpha}{x_B T_c}} \left( \frac{\Delta E_{max}}{2\alpha K} + \frac{(2\mu+1)}{(\mu+1)} \frac{K}{2} \right) \right\} \right.$$

$$\left. + e^{-(\alpha K^2 \frac{\mu}{\mu+1} + E_{c2'} - E_{v1'})/x_B T_c} \left( 1 + \operatorname{erf}\left\{ \frac{\alpha}{x_B T_c} \left( \frac{\Delta E_{max}}{2\alpha K} - \frac{K}{2(\mu+1)} \right) \right\} \right) \right) . \, K dK$$

A4.9

(this equation will be referredto in Chapter 5)

From G+R page 651 eq 6.297.1 the first part of A4.9 becomes

$$\frac{\pi^3 (x_B T_c)^3}{\alpha^2} M_{BF}^2 I_{ub}^2 \, ds_{CON}(E^+_{c2'min}) \frac{(\mu+1)}{(2\mu+1)^2} e^{-(E_{c2'min} - E_{c1})/x_B T_c} e^{-\frac{(2\mu+1)}{(\mu+1)} \frac{\Delta E_{max}}{x_B T_c}}$$

A4.10

For the second part of A4.9, equation A4.23 can be anticipated to give

$$\frac{\pi^3}{\alpha^2} (x_B T_c)^3 M_{BF}^2 I_{ub}^2 \, ds_{CON}(E^+_{c2'min}) e^{-(E_{c2} - E_{v1'})/x_B T_c} \left( \frac{1}{\mu} - \frac{(\mu+1)}{(2\mu+1)\mu} e^{-\frac{2\mu}{\mu+1} \frac{\Delta E_{max}}{x_B T_c}} \right)$$

A4.11

The full solution is therefore, after some rearrangement

$$Q = \frac{\pi^3}{\alpha^3} (x_B T_c)^3 M_{BF}^2 I_{ub}^2 \, ds_{CON}(E^+_{c2'min}) e^{-(E_{c2'min} - E_{c1})/x_B T_c} \left[ \frac{1}{\mu} e^{-\Delta E_{max}/x_B T_c} - \frac{(\mu+1)^2}{(2\mu+1)^2 \mu} e^{\frac{(2\mu+1)}{(\mu+1)} \frac{\Delta E_{max}}{x_B T_c}} \right]$$

A4.12

**which** can now be used to optimise and check the numerical integrations, and to check sections 4.2.3 and 4.2.4 of Chapter 4.

From sections 4.2.3 and 4.2.4 we have

$$Q = \frac{\pi^3}{\alpha^3} \frac{(x_B T_c)^2}{} \frac{(\mu+1)}{(2\mu+1)} \left[ \int_{E_{c2'min}}^{\Delta E=0} M_{BF}^2 \; I_{ub}^2 \; e^{\frac{\mu}{\mu+1} \frac{(E_{c2'} - E_{c1})}{x_B T_c}} \; e^{-\frac{(2\mu+1)}{(\mu+1)} \frac{(E_{c2} - E_{v1'})}{x_B T_c}} ds_{CON}(E_{c2'}) \; dE_{c2'} \right.$$

$$\left. \int_{\Delta E=0}^{\infty} M_{BF}^2 \; I_{ub}^2 \; e^{-(E_{c2'}-E_{c2})/x_B T_c} \left( - \frac{(E_{c1}+E_{c2}-E_{v1'}-E_{c2'})}{x_B T_c} \frac{(2\mu+1)}{(\mu+1)} + 1 \right) ds_{CON}(E_{c2'}) \; dE_{c2'} \right. \qquad \text{A4.12}$$

With $ds_{CON}$ and $M_{BF}^2 \; I_{ub}^2$ constant the remaining $E_{c2'}$ integrals are now straight forward, and give after some rearrangement

$$Q = \frac{\pi^3 (x_B T_c)^3}{\alpha^3} M_{BF}^2 \; I_{ub}^2 \; ds_{CON}(E^+_{c2min}) \; e^{-(E_{c2'min}-E_{c1})/x_B T_c}$$

$$\left[ \frac{1}{\mu} \; e^{-\frac{E_{max}}{x_B T_c}} - \frac{(\mu+1)^2}{(2\mu+1)^2 \mu} \; e^{\frac{2\mu+1}{(\mu+1)} \frac{\Delta E_{max}}{x_B T_c}} \right] \qquad \text{A4.13}$$

The same result as A4.11.

ie

$$\int \Phi(\gamma X + \frac{B}{X})\ e^{(\gamma^2-\mu)X^2}\ X\ dX$$

$$= \frac{1}{2(\mu-\gamma^2)} - \frac{1}{2\sqrt{\mu}\ (\sqrt{\mu}+\gamma)} \quad \exp\ [-2(\beta\gamma + \beta\sqrt{\mu})]$$

A4.17

Now considering the $\Delta E$ negative case

$$I \equiv \int_0^\infty \left[1 - \Phi(gX - \frac{b}{X})\right] e^{(g^2-\mu)X^2}\ X\ dX$$

$$= \int_0^\infty \left[1 + \Phi(-gX + \frac{b}{X})\right]\ e^{(g^2-\mu)X^2}\ X\ dX$$

A4.18

$$= \frac{1}{2(\mu-g^2)} + \int_0^\infty \Phi(-gX + \frac{b}{X})\ e^{(g^2-\mu)X^2}\ X\ dX$$

A4.19

Using A4.17

$$I = \frac{1}{2(\mu-g^2)} + \frac{1}{2(\mu-g^2)} - \frac{1}{2\sqrt{\mu}\ (\sqrt{\mu}-g)} \quad \exp\ (-2(-bg + b\sqrt{\mu}))$$

Now take $\sqrt{\mu} = g + \delta$ so $\mu = g^2 + 2g\delta + \delta^2$

$$I = \frac{1}{(2g\delta+\delta^2)} - \frac{1}{2(g+\delta)\delta} \exp\ (-2b\delta)$$

A4.20

**APPENDIX 4 PART 2 - A USEFUL FORMULA FOR THE ΔE NEGATIVE INTEGRATION IN PART 1**

When ΔE is negative a non standard integration result must be used, and this is now derived.

From G+R we have the result

$$\int_0^\infty \left[1 - \Phi\left(\gamma X + \frac{B}{X}\right)\right] e^{(\gamma^2-\mu)X^2} X \, dX$$

$$= \frac{1}{2\sqrt{\mu}\,(\sqrt{\mu}+\gamma)} \exp\left[-2(\beta\gamma + \beta\sqrt{\mu})\right] \qquad \text{A4.14}$$

Now considering just $\int_0^\infty e^{(\gamma^2-\mu)X^2} X \, dX$ and substituting $Y = X^2$

$$\int_0^\infty \frac{1}{2} e^{(\gamma^2-\mu)Y} dY = \left[\frac{e^{(\gamma^2-\mu)Y}}{2(\gamma^2-\mu)}\right]_0^\infty$$

$$= \frac{-1}{2(\gamma^2-\mu)} \quad \text{if } \mu > \gamma^2$$

A4.15

$$= \frac{1}{2(\mu-\gamma^2)}$$

thus

$$\frac{1}{2(\mu-\gamma^2)} - \int \Phi\left(\gamma X + \frac{B}{X}\right) e^{(\gamma^2-\mu)X^2} X \, dX$$

$$= \frac{1}{2\sqrt{\mu}\,(\sqrt{\mu}+\gamma)} \exp\left[-2(\beta\gamma - \beta\sqrt{\mu})\right]$$

A4.16

$$I = \frac{1}{2g\delta}\left(1 + \frac{\delta}{2g}\right) - \frac{1}{2g\delta}\left(1 + \frac{\delta}{g}\right)\exp(-2b\delta) \qquad \text{A4.21}$$

$$I = \frac{1}{2g\delta}\left(1 - \frac{\delta}{2g} + \frac{\delta^2}{4g^2} \ldots\right) - \frac{1}{2g\delta}\left(1 - 2b\delta + 2b^2\delta^2 - \frac{\delta}{g} + \frac{2b\delta^2}{g} + \frac{\delta^2}{g^2} \ldots\right)$$

A4.22

So letting $\delta \to 0$

$$I = \frac{1}{4g^2} + \frac{b}{g} \qquad \text{A4.23}$$